INVESTIGATION OF THE SYNERGY BETWEEN ALZHEIMER'S DISEASE AND EPILEPSY THROUGH DATA-DRIVEN MOLECULAR NETWORKS

Anna Harutyunyan

ORCID: 0000-0002-6165-5639

Student ID: 1035378

Submitted in total fulfilment for the degree of Doctor of Philosophy

March 2023

Department of Medicine, Royal Melbourne Hospital

Faculty of Medicine, Dentistry and Health Sciences

The University of Melbourne

Embrace the wisdom of age and experience with humility, yet possess the courage to reject such wisdom, if it ever becomes an impediment to progress…

-A.H.

ABSTRACT

Overview: In the recent years, a bi-directional association between Alzheimer's Disease (AD) and epilepsy has been observed, with AD-like cognitive impairments often presenting in epilepsy patients, and high rates of epileptic seizures seen in a sub-set of AD patients. These seizure-prone AD patients reportedly show accelerated cognitive decline and more aggressive disease progression compared to those without seizures. The mechanism and primary mode of action of this association remains unknown, although a synergistic interaction has been proposed. The general aim of this doctoral research was to investigate the electrical and molecular properties of the above-mentioned pathophenotypes and elucidate the mechanisms underlying the potential synergy between AD-like amyloid pathology and epileptiform activity, and their role in accelerated cognitive decline.

Introduction and literature review: The introductory sections of Chapter 1 provide an overview of the current literature on epilepsy and Alzheimer's Disease, focusing on pathophysiological mechanisms commonly implicated in both syndromes. The subsequent sections discuss several benchmark studies that first reported on the increased co-occurrence of seizures among AD patients, followed by a critical review of the most prominent as well as recently emerged hypotheses that aim to provide mechanistic insight into the nature of the proposed bi-directional association between AD and acquired epilepsy. The concluding sections provide a gentle introduction into the emerging field of network medicine, systems-based analysis, interrogation methods of high-throughput biological data and the general framework of computational models and methodology that was implemented throughout this work.

Experimental chapters: The first and second experimental chapters aim to characterize the molecular signature of a brain affected by amyloid pathology and seizures. Utilizing proteomic and metabolomic data from two collaborative studies as well as publicly available transcriptomic data, Chapter 2 describes the molecular signature of human AD and that of most widely used mouse models of AD, while Chapter 3 captures the molecular profile of well-established rat models of genetic (GAERS) and acquired (post SE) epilepsies. Informed by the insight gained from Chapters 2 and 3, the third experimental chapter (Chapter 4) aimed to capture the shared molecular signature associated with AD and temporal lobe epilepsy (TLE) – the most common type of epilepsy comorbid with AD. A hypothesis-free, systems-level

approach was used to characterize the pathophysiological state of each disease on a molecular level by constructing data-driven gene coexpression networks representing the respective pathologies. The topology and architecture as well as the preservation of functional gene modules between the two networks were compared through network preservation analysis, identifying two clusters of synaptic reorganization and signalling-associated genes as highly preserved between AD and TLE. The fourth and final experimental chapter (Chapter 5) aims to investigate the mechanism and potential mediators of the bi-directional relationship between amyloid pathology and epilepsy by examining the effect of recurrent seizures on hallmark features of AD pathology such as amyloid plaque deposition and cognitive performance. RNA sequencing and bioinformatic analysis of mouse hippocampal tissue was conducted in order to investigate the molecular mechanisms of synergy between recurrent seizures and already-present AD pathology as well as identify key mediators of accelerated disease progression, which could serve as promising targets for intervention.

Discussion and conclusions: Informed by computational analysis from chapters 2, 3 and 4, and reinforced by experimental evidence from chapter 5, the final chapter of this thesis (Chapter 6) provides a synthesis of the newly gained insights into the strong synergistic nature of the relationship between amyloid pathology and recurrent seizures. A subsequent extensive review of the most current molecular neuroscience research facilitated interpretation of our results, leading to the proposal of a "dual-pathology" disease model for epilepsy and AD. In this paradigm, the synergistic self-propagating interaction between epileptiform activity and amyloid pathology defines a distinct subpopulation of "dual-pathology" patients, characterized by faster disease progression and more severe cognitive decline. Furthermore, I describe specific cellular pathways mediating the synergy between amyloid pathology and recurrent seizure activity and introduce a mechanistic framework underlying the chain of events through which this synergy leads to accelerated cognitive deterioration. Each step in this framework or chain of events is reinforced by a benchmark proof-of-concept study published in leading peer-reviewed journals and which, with the exception of the most recent 2022-2023 studies, have been independently replicated by other research groups. The concluding sections of this chapter emphasize the utility of integrating phenotypic and electroencephalographic data from *in vivo* studies with high-throughput "omics" data into network-based computational models for a holistic examination of pathophysiological mechanisms underlying complex diseases and identification of novel therapeutic targets.

DECLARATION

This is to certify that:

i. this thesis comprises only my original work, except where indicated in the Preface,

ii. due acknowledgement has been made in the text and figure legends to all other material used,

iii. the thesis is fewer than 100,000 words in length, exclusive of tables, figures, bibliographies and appendices.

Signed: *Anna Harutyunyan*

PREFACE

This PhD work was conducted in collaboration with our colleagues at Monash University Central Clinical School and Alfred Hospital. Chapters 3 and 4 of this thesis are based on published articles listed in the table below, of which I am the sole primary author and have contributed towards more than 50% of the work. The contributions of all co-authors are detailed in the table below.

Chapter 2 (unpublished material not submitted for publication)

The transcriptomic data constituting the basis for the analyses described in Chapter 2 was sourced from a publicly available repository (Gene Expression Omnibus, (Clough & Barrett, 2016)) with accession numbers and corresponding publications listed in the main text.

Chapter 3 (published material included)

The proteomic and metabolomic data constituting the basis for the analyses described in Chapter 3 was generated from two large collaborative studies jointly created by Dr. Pablo Casillas Espinosa and Prof. Terence O'Brien. In all experiments involving GAERS animals, the live animal work was conducted by Pablo Casillas Espinosa with assistance from Zahra Ali. In experiments involving post-SE-TLE rats, the live animal work was conducted by Pablo Casillas Espinosa with assistance from Cristal Li and Emma Braine. The automatic seizure detection algorithm described in section 3.2.4. was developed by Rui Li. Additionally, this chapter includes parts of my original work, that have been incorporated into a collaborative publication by Pablo Casillas Espinosa, which is currently under review. In all instances, the reported results, including all figures and text were generated by me.

Chapter 4 (published material included)

The transcriptomic data constituting the basis for the analysis described in this chapter and the corresponding publication was sourced from a publicly available repository (Gene Expression Omnibus, (Clough & Barrett, 2016)) with accession numbers and corresponding publications listed in the main text.

Chapter 5 (unpublished material not submitted for publication)

The findings reported in this chapter will serve as the basis for a publication which is currently in preparation and will be submitted to *Cell Systems*. All findings were generated by me, including the *in vivo* and *in vitro* experiments, data analysis, creation of figures and graphs, interpretation of results and writing of the original manuscript.

Publication title	Citation	GR % contribution	Co-author contributions
Chapter 3 An integrated multi-omic network analysis identifies seizure-associated dysregulated pathways in the GAERS model of absence epilepsy	Published (A. Harutyunyan et al., 2022)	>70% methodology, software, formal analysis - metabolomics, proteomics (with assistance from Debbie Chong) integrated multi-omic network analysis, statistical analysis of behavioural data, figure preparation, interpretation of results, writing and editing of the original manuscript	Debbie Chong: input towards proteomics analysis, input towards manuscript; Rui Li: EEG data analysis; Anup D. Shah: technical consulting (proteomics and metabolomics); Zahra Ali: assistance with live animal experiments; Cheng Huang: technical consulting (proteomics); Christopher K. Barlow: raw data acquisition and technical consulting (metabolomics), input towards methods section of the manuscript; Piero Perucca, Terence J. O'Brien and Nigel C. Jones: expertise and consulting (GAERS model, absence epilepsy); Ralf Schittenhelm: input towards conceptualisation, technical consulting (proteomics); Alison Anderson: conceptualisation, supervision, expertise towards software and methodology, interpretation of results, review and editing of manuscript, co-senior author; Pablo Casillas-Espinosa: conceptualisation, funding acquisition, supervision of live animal work, review and editing of manuscript, co-senior and corresponding author
Chapter 4 Network preservation analysis reveals dysregulated synaptic modules and regulatory hubs shared between Alzheimer's Disease and temporal lobe epilepsy	Published (Harutyunyan, Jones, Kwan, & Anderson, 2022)	>90% conceptualization, methodology, data mining, formal analysis, figures, interpretation of results, writing and editing of the original manuscript	Nigel C. Jones: review and editing of the manuscript; Patrick Kwan: review and editing of the manuscript; Alison Anderson: provided expertise regarding methodology, conceptualization and interpretation of results, senior and corresponding author
Chapter 5 Investigating the synergy between amyloid pathology and recurrent seizures in the 5xFAD model of Alzheimer's Disease	Manuscript in preparation	>90% conceptualization, *in vivo* and molecular experiments, imaging, RNAseq and network analysis, interpretation of results, writing the original manuscript	Samantha L.W. Warren: assistance with microscopy/imaging; Alison Anderson: conceptualization, supervision, expertise in RNAsequencing, interpretation of results; review and editing of manuscript; Patrick Kwan: conceptualization, supervision, review and editing of manuscript Nigel C. Jones: conceptualization, supervision, review and editing of manuscript

PUBLICATIONS AND CONFERENCE PROCEEDINGS

Published articles and manuscripts

Harutyunyan A, Jones NC, Kwan P, Anderson A. Network Preservation Analysis Reveals Dysregulated Synaptic Modules and Regulatory Hubs Shared Between Alzheimer's Disease and Temporal Lobe Epilepsy. *Frontiers in Genetics*. 2022;13.

Harutyunyan A, Chong D, Li R, Shah AD, Ali Z, Huang C, et al. An Integrated Multi-Omic Network Analysis Identifies Seizure-Associated Dysregulated Pathways in the GAERS Model of Absence Epilepsy. *Int J Mol Sci.* 2022;23(11).

Harutyunyan A, Warren S.L.W, Anderson A, Jones NC, Kwan P. The role of immediate early genes and complement system in synergistic pathology of epilepsy and Alzheimer's Disease. **In preparation.*

Dejakaisaya H, **Harutyunyan A,** Kwan P, Jones NC. Altered metabolic pathways in a transgenic mouse model suggest mechanistic role of amyloid precursor protein overexpression in Alzheimer's disease. *Metabolomics*. 2021;17(5):42.

Casillas-Espinosa PM, Anderson A, **Harutyunyan A,** Li C, Lee J, Braine EL, et al. Disease-modifying effects of sodium selenate in a model of drug-resistant, temporal lobe epilepsy. *Elife.* 2023;12.

Platform presentations and published abstracts

Harutyunyan A, Anderson A, Kwan P, Jones NC. The synergistic relationship between Alzheimer's Disease and recurrent seizures is mediated by dysregulated gliosis and reactivation of immediate-early genes. 35th International Epilepsy Congress, Dublin, Ireland, 2023

Harutyunyan A, Anderson A, Kwan P, Jones NC. The synergistic relationship between Alzheimer's Disease and recurrent seizures is mediated by neuroinflammation and dysregulated astrogliosis. Workshop on Neurobiology of Epilepsy (WONOEP), Kildare, Ireland, 2023

Harutyunyan A, Warren SLW, Anderson A, Kwan P, Jones NC. Kindling-induced expression of immediate early genes is associated with increased seizure severity and

neuroinflammation in 5xFAD model of Alzheimer's Disease. MDHS Graduate Research Symposium, Parkville, Australia, 2022

Harutyunyan A, Anderson A, Kwan P, Jones NC. The role of immediate early genes and complement system in synergistic pathology of epilepsy and Alzheimer's Disease. Students of Brain Research (SOBR) annual symposium, Melbourne, Australia, 2022

Harutyunyan A, Casillas-Espinosa PM, Kwan P, Jones NC, Anderson A. Integrated multi-omic analysis of epileptic rats identifies disease modules and therapeutic targets. Asian and Oceanian Epilepsy Congress, Japan, 2021 ***awarded best presenter prize***

Chong D, **Harutyunyan A,** Shah A, Perucca P, Jones N, Schittenhelm R, et al. Proteomic analysis of a rat model of genetic generalised epilepsy with absence seizures. *Epilepsia.* 2021;62:93. International Epilepsy Congress, 2021

Harutyunyan A, Casillas-Espinosa PM, Jones NC, Anderson A. Integrative multi-omic approaches for identification of seizure-associated modules. Translational Neurogenetics Conference, Melbourne, Australia, 2021

Harutyunyan A, Anderson A, Kwan P, Jones NC. Network View of Disease. Epilepsy Society of Australia virtual meeting, 2020

Harutyunyan A, Anderson A, Kwan P, Jones NC. Gene coexpression network analysis reveals commonly dysregulated inflammatory modules in Alzheimer's Disease and temporal lobe epilepsy. Monash University Graduate Research Symposium, Melbourne, Australia, 2019

Poster presentations

Harutyunyan A, Anderson A, Warren SLW, Kwan P, Jones NC. The role of immediate early genes and complement system in synergistic pathology of epilepsy and Alzheimer's Disease: insights from a dual- pathology mouse model. Society for Neuroscience, Washington DC, United States of America, 2023

Harutyunyan A, Anderson A, Kwan P, Jones NC. The synergistic relationship between Alzheimer's Disease and recurrent seizures is mediated by dysregulated gliosis

and reactivation of immediate-early genes. American Epilepsy Society Annual Meeting, Orlando, FL, United States of America, 2023

Harutyunyan A, Anderson A, Kwan P, Jones NC. Kindling-induced expression of immediate early genes is associated with increased seizure severity and neuroinflammation in Alzheimer's Disease. 13th FENS Forum of Neuroscience, Paris, France, 2022

Harutyunyan A, Anderson A, Kwan P, Jones NC. The synergistic relationship between Alzheimer's Disease and recurrent seizures is mediated by reactivation of immediate-early genes. Epilepsy Melbourne annual meeting, Melbourne, Australia, 2022

Harutyunyan A, Anderson A, Kwan P, Jones NC. Characterizing the molecular signature of epilepsy in Alzheimer's Disease. Epilepsy Society of Australia Virtual Conference, 2021 ***awarded special commendation for best poster***

Chong D, **Harutyunyan A,** Li, R, Shah A, Perucca P, Jones N, Schittenhelm R, O'Brien TJ, Anderson A, Casillas-Espinosa PM. A Systems Biology Approach to Interrogate the Molecular Pathways Underlying Absence Epilepsy. American Epilepsy Society virtual meeting, 2021

Dejakaisaya H, **Harutyunyan A,** Kwan P, Jones NC. Metabolomics profiling of the brain revealed potential mechanisms associating Alzheimer's disease to higher seizure susceptibility in mice. Epilepsy Society of Australia virtual meeting, 2020

Harutyunyan A, Kwan P, Jones NC, Anderson A. Epilepsy in Alzheimer's Disease. Students of Brain Research Symposium, Melbourne, Australia, 2019

AWARDS

2023: Epilepsy Society of Australia Travel Fellowship

2022: High Commendation Award for MMI optical microscopy image competition

2022: MDHS Graduate Student Support Grant

2021: Best Platform Presentation Award, Asian & Oceanian Epilepsy Congress, ILAE

2021: ILAE Epilepsy Congress Bursary

2021: Special Commendation Award for best poster, Epilepsy Society of Australia

2020: AusBiotech Student Scholarship

2020: European Molecular Biology Laboratory travel grant, EMBL Australia

2019: Melbourne Research Scholarship

2019: Melbourne International Fee Remission Scholarship

ACKNOWLEDGEMENTS

I acknowledge the Traditional Owners of the land on which this research was conducted, the Boon Wurrung peoples of the Yaluk-ut Weelam clan, and pay my respects to the Elders, past and present.

I acknowledge and offer my gratitude to all those who made this PhD journey possible.

First of all, my dear supervisors for the guidance and support I received during the last four years.

Nigel and Patrick – for giving me the opportunity to undertake my PhD at the best university of Australia, welcoming me into your team, and being in my corner during difficult times. Thank you for your wisdom and patience.

Alison – for having all the answers, the support and encouragement, and most of all – the long and inspiring scientific discussions, which shaped a huge part of this work. Your dedication to the purest form of scientific enquiry is inspiring.

The Bioinformatics Melbourne team and The Data Fluency team at Monash University for helping with my journey from a biochemist into a bioinformatician.

Epilepsy and Behaviour Lab members and collaborators: Juliana Castro, Gabi Dezsi, Matt Hudson and Pablo Casillas – for valuable training and guidance.

Former colleagues and mentors, Walter Gonzalez, Tarciso Velho and Luis Sanchez – for training me in top calibre surgical, histological and molecular techniques, the result of which are the beautiful microscopy images in this thesis. Carlos Lois and my first research mentor Jenna Craig, for teaching me the importance of exact precision in research work, and that cutting corners is not an option.

My fellow students and friends – my "Friday Night Madness" mates Jeff, RX, Janine, Jenn and my work wife Sam – you all made this journey so much more fun, and I will cherish our friendship always.

My family: Oreo and Biscuit, for being the best emotional support, Fahad and Fawad, for always bringing me food and making those long lockdown months bearable. Mom – for fiercely fighting, when I myself couldn't, for my right to a world-class education, Dad – for instilling in me the qualities of a true scientist and inventor. You made me who I am, and I will forever be grateful. Ծնորհակալ եմ:

Lastly, a couple of pep talks:

For the exhausted PhD student, who might years from now read this thesis as an example for their own – you got this! I hope you are as excited about your PhD as I am for mine! If you are overwhelmed, remember the strange years of 2020-2021, and remind yourself that while we sat alone under lockdowns, armies of researchers and academics, just like me and you, were working day and night to save billions of people from Covid19. And you know what? They succeeded! So never forget that the work you do is valuable and essential.

And finally, because I am positive that I'll go back and read my PhD thesis probably more than once - for my future self:

Look how far you've made it! If you ever doubt your abilities, be reminded that learning is your superpower. If in the future, academia is still as brutal, you'll face many rejections. In moments of weakness, when feelings of inadequacy try and break your resolve, remember, that you are the intellectual descendant of visionaries, and that you owe it to them, and all those who were robbed of their chances, to see this through. When faced with rejections you try to seek an easy way out, or sell out, remember, that researchers like you save millions of lives and it is up to you to have the wisdom and be where you are needed. Remember that very few people are equipped with the unique set of skills, knowledge and the cognitive architecture to wield it, so it is your duty to not waste it. If not you, then who?

So do, or do not, there is no try!

Dedicated to Rima "Mnatsakanovna" Harutyunyan (1933-2020), the original Dr. Harutyunyan, a dedicated physician and surgeon, a truly fierce Pusheen, whose brilliance saved many young lives, including my own.

Table of Contents

LIST OF FIGURES AND TABLES

Figures

Tables

CHAPTER 1

ALZHEIMER'S DISEASE AND EPILEPSY: A CRITICAL REVIEW OF THE LITERATURE

1.1 Alzheimer's Disease

Alzheimer's disease (AD) is the most common form of dementia and is characterised by a chronic and progressive loss of memory, changes in personality and deficits in specific cognitive domains. With the increase in life expectancy and aging population, AD is enroute to become the second leading cause of death globally, predicted to affect around 130 million people by 2050. In Australia and several other high-income countries (England, Wales, Scandinavia) dementia including AD is already the leading cause of death for women and people aged over 85 (Australian Bureau of Statistics 2019, UK office for National Statistics 2018). In 1906 professor Alois Alzheimer first described AD as "a peculiar disease", referring to then mysterious, and now – infamous, plaques and tangles, that he observed in the brain of his patient Auguste, but was unable to determine whether they were the root cause of her disease, or merely a by-product (Alzheimer, Forstl, & Levy, 1991). More than a century later, with dementia epidemic looming over the globally aging population, the question regarding the role of amyloid beta in the pathophysiology of AD remains as relevant as ever, though without a definitive answer. Nevertheless, amyloid plaques and their main component, the Aβ peptides, are the most described pathological hallmarks of AD, with the long-awaited encouraging results from a phase 3 clinical trial of anti-amyloid antibody (van Dyck et al., 2022) and its subsequent approval by the FDA, we are closer than ever towards the first disease-modifying treatment for AD. The immense efforts towards development and testing of amyloid clearing agents that lead to this breakthrough were largely motivated by the amyloid cascade hypothesis, originally proposed by Hardy and Higgins (Hardy & Higgins, 1992). This hypothesis established the neurotoxic aggregates of amyloid beta (Aβ) – a fragment of amyloid precursor protein (APP), as the root cause for pathology development, thus defining the conceptual landscape of Alzheimer's research for decades, following its publication in 1992. In this linear causality paradigm, specific mutations at the cleavage sites of APP result in its amyloidogenic cleavage by β and γ-secretases, leading towards the accumulation of Aβ inside the neurons as well as in the extracellular space, and its subsequent aggregation into protofibrils and amyloid plaques (Figure 1.1).

The amyloid cascade hypothesis also provides a mechanism by which amyloid pathology is linked to the formation of the second pathological hallmark of AD – the intracellular neurofibrillary tangles (NFT). In 1976, utilizing the most advanced electron microscopy and biochemical technique of the time, Robert Terry and colleagues characterized the structure of NFT, describing them as a "twisted tubule" or a "strange double-helical filament" similar to DNA (Wisniewski, Narang, & Terry, 1976). From the subsequent studies it was evident that these NFT are accumulations of aggregated tau protein. Tau is a microtubule associated protein, coded by the MAPT gene, which, under normal physiological conditions acts as a stabilising structure of microtubule, thus facilitating intracellular transport pathways. Pathological hyperphosphorylation of tau causes it to detach from the microtubules, thereby destabilizing the cytoskeleton and disrupting normal intracellular transport. The hyperphosphorylated tau forms filamentous aggregates, which accumulate inside the neurons as the infamous neurofibrillary tangles, resulting in the breakdown of normal cellular processes and subsequent death of neurons.

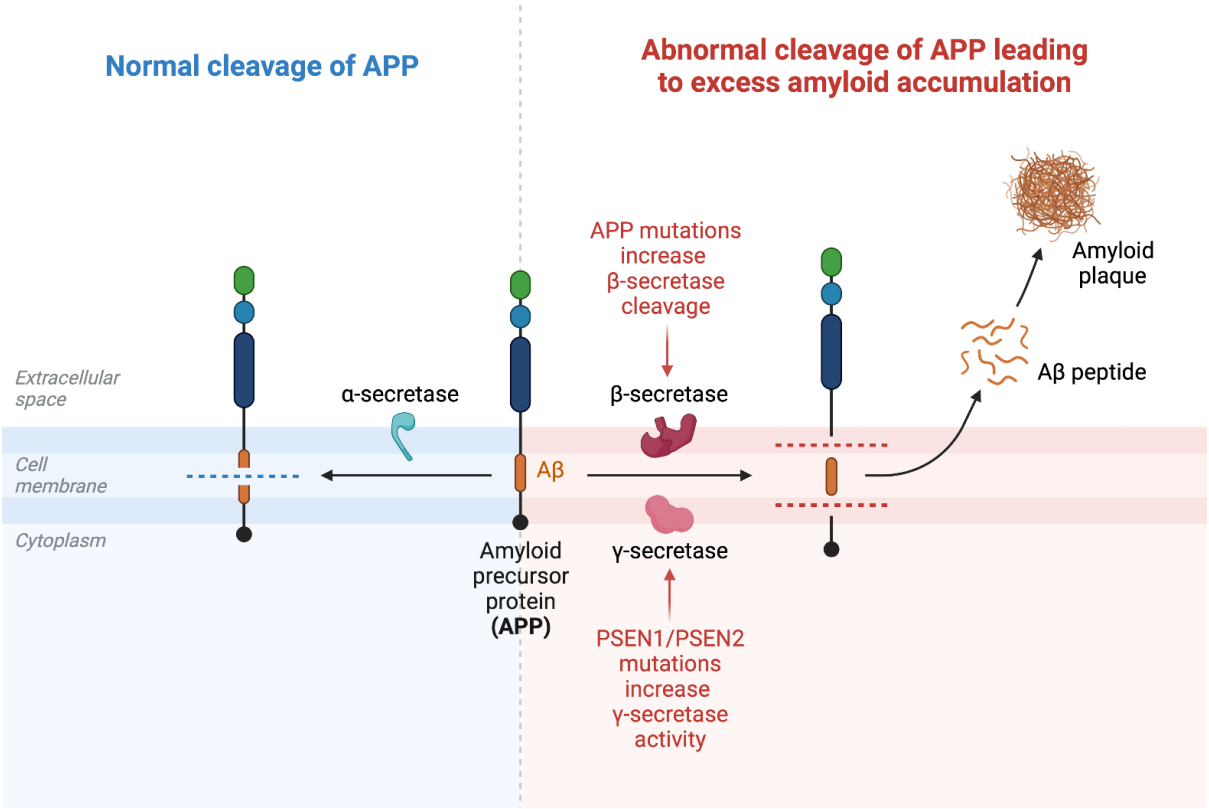

Figure 1.1 Amyloid precursor protein processing by secretases. A summary depiction of amyloidogenic (abnormal) and non-amyloidogenic cleavage of amyloid precursor protein (APP). This abnormal cleavage result in the formation of a sticky neurotoxic A-beta which then gets accumulated as plaques in the extracellular space. *The figure was created with Biorender.com*

The amyloid cascade hypothesis provides an elegant and self-evident model which describes the chain of events underlying familial or early onset Alzheimer's disease (FAD or EOAD). However, the majority (over 99%) of AD cases are sporadic in nature and don't involve any mutations in the APP gene or its cleavage enzymes. This sporadic type of AD, which is also referred to as late-onset AD (LOAD), still features amyloid deposition, synaptic loss and cognitive impairments seen in patients with autosomal dominant mutations, but usually presents later in life. Several earlier gene-wide association studies (GWAS) identified the e4 allele of apolipoprotein E as a strong risk factor for developing sporadic AD, while possession of the e2 allele seems to be protective against AD (Saunders et al., 1993; Strittmatter et al., 1993). Apoe, an important apolipoprotein, has been primarily studied for its role transporting cholesterol and other fats within the brain and the periphery.

While amyloid plaque deposition and neurofibrillary tangles correlate with cognitive impairment, there have been several reports of amyloid plaques and NFT present in the post-mortem brains with no evidence of cognitive impairment (Forman et al., 2007). Moreover, studies have reported cognitive improvement in AD models as a response to various treatments but without any effect on amyloid load, suggesting it is unlikely that amyloid plaques *per se* cause cognitive deterioration and an alternative or parallel mechanism mediates synaptic function underlying the cognitive symptoms associated with AD. In light of this evidence, in addition to the earlier "traditional" pathophysiology mechanisms such as the amyloid cascade and tauopathy, several recent hypotheses have been proposed, each attempting to offer mechanistic understanding of the complex pathophysiology and the systemic changes in the brain caused by AD. Among others, neuroinflammation, oxidative stress, excitotoxicity, metabolic and mitochondrial dysfunction are suggested to have key roles in AD pathogenesis (Akiyama et al., 2000; Grundke-Iqbal et al., 1986; Hardy & Higgins, 1992). While there is evidence supporting each of these hypotheses, there is increasing realization that interplay between multiple genetic and environmental factors is likely involved.

1.2. Epilepsy and seizure disorders

The epilepsies are a heterogeneous group of chronic neurological conditions characterised by recurrent spontaneous seizures and often associated psychiatric and cognitive symptoms (Orrin Devinsky et al., 2018). They are estimated to affect over 50 million people of all age groups worldwide and make up 0.5% of the global burden of disease (Beghi et al., 2019; World Health Organisation, 2019). Although many patients achieve seizure control or even seizure freedom, a substantial number of patients require a combination of medications, resective surgery or neuromodulation devices, and close to one-third of epilepsy patients continue to have uncontrolled seizures (Orrin Devinsky et al., 2018). The debilitating direct effects of seizures such as accidents and injuries are often compounded by indirect effects such as epilepsy-related neuropsychiatric comorbidities, leading to significant reduction in the overall quality of patients' life. Owing to advances in modern medicine and decades of collaborative research effort, our understanding of seizures and their aetiology has evolved from the regrettable notions of the patients "being possessed" towards understanding of the various genetic and environmental causes and processes involved in generation of seizures (ictogenesis) and transformation of normal neural circuits into epileptic circuits (epileptogenesis). A continuously updated list of seizure classification and relevant definitions is maintained by the international league against epilepsy (ILAE) which also provides a detailed framework for diagnosis of seizures, epilepsies and epilepsy syndromes (Scheffer et al., 2017). Figure 1.2. summarizes the current ILAE classification of seizure and epilepsy types and aetiologies.

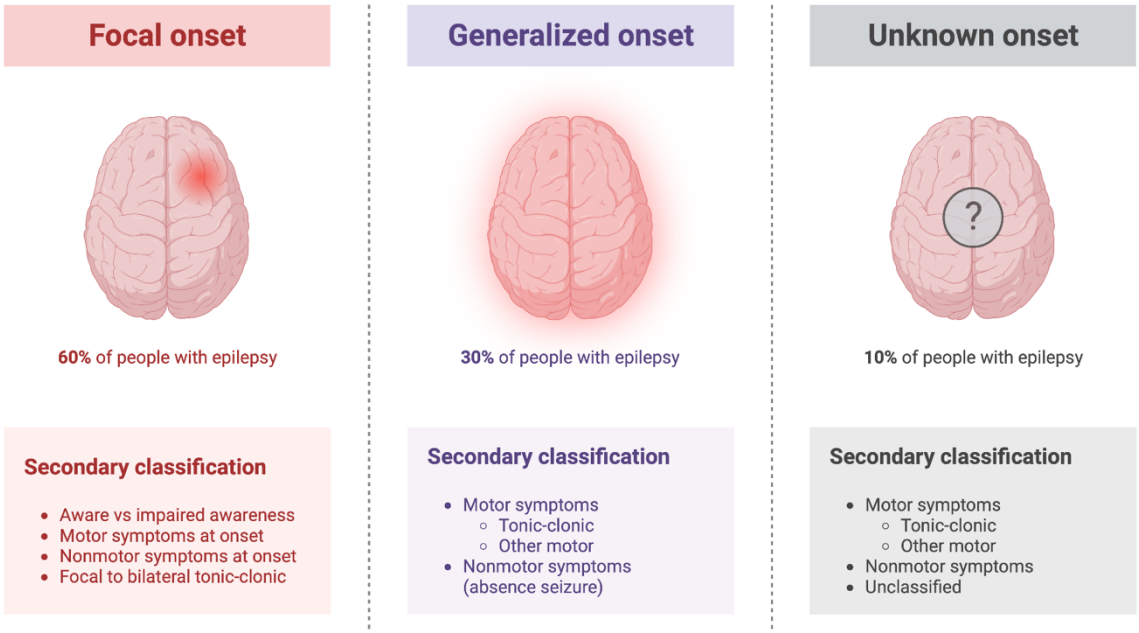

Figure 1.2 The basic ILAE 2017 operational classification of seizure types as described in (Fisher et al., 2017) *Figure created with BioRender.com*

1.3. Epilepsy in AD: bi-directional association between amyloid pathology and seizures

1.3.1. Evidence from clinical studies

In the recent years, a bi-directional association between Alzheimer's Disease and epilepsy has been observed, with AD-like cognitive impairments often presenting in epilepsy patients, and increased rates of epileptic seizures reported in AD patients. Notably, non-convulsive epileptiform activity has been identified in over 40% of patients with sporadic AD (K. A. Vossel et al., 2016). Various transgenic mouse models of AD also show spontaneous epileptiform and seizure activity and increased susceptibility to chemically and electrically induced seizures (Bezzina et al., 2015; Palop et al., 2007; Tanila et al., 2019; Ziyatdinova et al., 2016). Importantly, there is solid evidence indicating that co-occurrence of epileptiform activity with AD-like pathology is associated with faster disease progression and more severe cognitive decline (K. A. Vossel et al., 2016; K. A. Vossel, Tartaglia, Nygaard, Zeman, & Miller, 2017). Epileptiform activity, which is defined as spikes and sharp waves in the EEG, is commonly detected in the temporal brain regions of AD patients (K. A. Vossel et al., 2016). Consequently, temporal lobe epilepsy (TLE) is generally recognized as the subtype of epilepsy most commonly comorbid with AD (Scharfman, 2012), with the two diseases having overlapping risk factors, as well as electrophysiological, neuropsychiatric and neuroimaging (functional magnetic resonance imaging, fMRI) commonalities. Traumatic brain injury, inflammation, aging and stroke are risk factors for both AD and TLE (Hauser & Annegers, 1991; Hauser, Morris, Heston, & Anderson, 1986; Hesdorffer, Hauser, Annegers, Kokmen, & Rocca, 1996). Additionally, the traditional hallmarks of AD such as amyloid plaques, neurofibrillary tangles and hippocampal sclerosis have been reported in TLE patients (Davidson et al., 2011; Mackenzie & Miller, 1994; Tai et al., 2016; Thom et al., 2011).

A very recent study has investigated the temporal lobe tissue from 19 drug-resistant TLE patients and found increased expression and phosphorylation of APP, upregulation of APP-cleaving enzymes ADAM10 and BACE1 and their cleavage product Aβ42 and increased expression and hyperphosphorylation of two tau isoforms (Gourmaud et al., 2020).

While there is no shortage of novel hypotheses and elegantly conceived review articles (Palop & Mucke, 2010; Romoli, Sen, Parnetti, Calabresi, & Costa, 2021; K. A. Vossel et al., 2017) attempting to elucidate the mechanistic link between seizures, AD pathology and cognitive deterioration, there are substantial uncertainties regarding the cause-effect relationships

between epileptiform activity and amyloid pathology. First, epileptiform activity and seizures are observed in early as well as late stages of AD, therefore, it is challenging to determine if the early undetected epileptiform discharges and subsequent circuit modifications increase the risk of developing AD, or the already-present AD pathology renders the neuronal circuits hyperexcitable, thereby increasing the patients' susceptibility to seizures. Furthermore, the reports on the increased prevalence of dementia and seizures in the context of epilepsy and Alzheimer's disease diagnoses, respectively, vary considerably, ranging from 3-fold increase in the risk of developing seizures all the way to 87-fold increase in the context of early onset AD (Amatniek et al., 2006). This variation could be attributed to the varying clinical diagnostic criteria for dementia diagnosis, the small size of available cohort-based EEG studies, and lack of standardized comprehensive neuropsychological assessment (Dun et al., 2022; Huang, Fu, Li, & Peng, 2022; Miranda & Brucki, 2014; B. Zhao et al., 2021; N. Zhao et al., 2022). Additionally, there seems to be inherent heterogeneity within the AD cohort, where only a subset of patients develop seizures. Several systematic review and meta-analysis studies have attempted to pool the seizure incidence data from the small AD cohort studies. In 2022 alone, at least five systematic reviews investigating the prevalence of epilepsy/seizures in AD patients have been published – all coming to analogous conclusions that the available clinical data is scarce and a large number of the studies are not directly comparable due to the lack of standardized diagnostic criteria for cognitive impairment, "epileptiform" activity and/or seizures (Dun et al., 2022; Huang et al., 2022; B. Zhao et al., 2021; N. Zhao et al., 2022).

Fortunately, in the last two years, this lack of vital clinical data has been somewhat attenuated with the publication of several large scale, multi-centre population-based studies (Banote, Håkansson, Zetterberg, & Zelano, 2022; Habeych, Falcone, Dagar, Ford, & Castilla-Puentes, 2021; Schnier, Duncan, Wilkinson, Mbizvo, & Chin, 2020; Vöglein et al., 2020), as well as randomized clinical trials involving anti-seizure drugs (K. Vossel et al., 2021) and long-term EEG studies (Horvath et al., 2021), which provide critical insight into the nature of this "bi-directional" relationship between seizures and amyloidosis. One of these studies involving over 20,745 individuals (10,527 with AD diagnosis and 10,218 cognitively intact controls) established that seizures in AD are highly recurrent (>70% recurrence rate, within <8 months) and are associated with more severe cognitive impairment (Vöglein et al., 2020). Furthermore, subclinical epileptiform activity seems to correlate well with the rate of cognitive decline among patients with AD (Horvath et al., 2021). Another 2022 study looking at CSF biomarkers

in a large (>18,000 individuals) cohort of AD patients with or without seizures demonstrated that, compared to those without seizures, the subpopulation of AD patients who did develop seizures had biochemically more severe disease profile, evidenced by increased concentrations of total tau and p-tau, and reduced concentration of Amyloid beta 1-42 in the CSF (Banote et al., 2022). The above clinical evidence argues that epileptiform activity is more relevant in the context of AD progression than previously recognized. Importantly, this suggests that in addition to differing clinical prognosis and EEG profile, the subpopulation of AD patients presenting with seizures also has a distinct cognitive and biochemical profile (Banote et al., 2022). Accordingly, at least for this subgroup of epilepsy-prone AD patients, the accelerated cognitive deterioration is the inevitable consequence of disease progression and is likely precipitated by the synergistic interaction between AD pathology and recurrent seizures.

Understanding the mechanism and the key mediators of the synergistic interaction between hyperexcitability and AD pathology would allow for identification of specific biomarkers and aid with more accurate diagnosis of this subtype of AD. While the treatment against amyloid pathology is still in preliminary stages, there are a number of effective next-generation anti-epileptic drugs that have been shown to improve spatial memory and executive function in patients with AD and epileptiform activity (K. Vossel et al., 2021). If the early hyperexcitability and subclinical epileptiform activity are the main drivers of cognitive decline and further neuroinflammation and synaptic degeneration, early diagnosis and anti-seizure treatment could slow down disease progression and delay cognitive deterioration.

1.3.2. Evidence from mouse models

Generation of rodents that model aspects of various human conditions advanced medical research by leaps and bounds by allowing the understanding and treatment of numerous diseases. According to Alzheimer Research Forum (alzforum.org) there are 189 rodent models of AD as of year 2020. The vast majority (180) of them are mouse models, with some strains being utilized more than others (Table1.1). A lot of these models are genetic i.e. they harbor one or more of the mutations in amyloid precursor protein (APP), tau protein, presenilins: enzymes that process APP, apolipoproteins E2, E3, E4 with various promotors and knock-in or knock-out combinations. Some of these mutations such as APP and PSEN1 appear to be causative and were identified in families that develop familial or early onset AD. Others, like variations in apolipoproteins are risk factors and have been identified through large GWAS studies. Based on the mutation type, promotor and background strain, the severity and temporal

progression of pathology development differs between mouse models, with some lines developing amyloid plaques as early as at two months of age, while some lines don't develop them at all, or after 12 months of age (Table 1.1).

Model	Gene	Mutation	Pathology
3xTg	**APP, PSEN1, tau**	**APP(Swe), PS1(M146V), MAPT(P30IL)**	**Extracellular Aβ deposits by 6 m.o., plaques and tangles, synaptic dysfunction**
5xFAD	**APP, PSEN1**	**APP(Swe, Fl, Lon), PS1(M146L, L286V)**	**Intracellular accumulation of Aβ, plaques at 2 m.o., gliosis, synapse degeneration, neuronal loss**
APP/PS1	**APP, PSEN1**	**APP(KM670,671NL), PS1(L166P)**	**Amyloid plaques in neocortex at 1.5 m.o., in hippocampus at 3-4 m.o., phosphorylated tau**
Tg2576	**APP**	**APP(Swe)**	**Amyloid plaques at 12 m.o., astrogliosis, microgliosis**
J20	**APP**	**APP(Swe, In)**	**Amyloid plaques, dystrophic neurites, synaptic loss**
TgCRND8	**APP**	**APP(Swe, In)**	**Amyloid plaques at 3 m.o., neurotic pathology at 5 m.o., astrogliosis, microgliosis**
rTg4510	**tau**	**MAPT(P301L)**	**Tangle-like inclusions at 4 m.o., neuronal loss in CA1, forebrain atrophy at 10 m.o.**

Table 1.1 Summary of the most widely used transgenic mouse models of Alzheimer's Disease

In line with clinical observations, many AD models also display increased seizure susceptibility and aberrant EEG activity, compared to healthy controls. Several in vivo experiments involving transgenic mouse lines (APdE9, Tg2576, ArcticAPP, hAPPJ20, rTg4510) that model age-dependent amyloid accumulation and tauopathy reported increased susceptibility to electrically and chemically induced seizures, as well as epileptiform activity (Bezzina et al., 2015; B. F. Corbett et al., 2013; B. F. Corbett et al., 2017; Hazra et al., 2016; Ziyatdinova et al., 2016), frequent unprovoked seizures (C. H. Fu et al., 2019; Minkeviciene et al., 2009), reduced expression of inhibitory markers and decreased resting membrane potential of neocortical pyramidal cells (Minkeviciene et al., 2009). The extracellular plaque depositing APP/PS1 double transgenic line harbouring APPswe and PS1dE9 mutations is one of the most investigated transgenic mice in AD research. Multiple research groups have observed spike-trains (Papazoglou et al., 2016), epileptiform spikes (Reyes-Marin & Nunez, 2017), spontaneous seizures (Ziyatdinova et al., 2011) and increased sensitivity to proconvulsant agents such as PTZ in APP/PS1 mice. Additionally, the expression of inhibitory markers and

resting membrane potential of neocortical pyramidal cells were reported to be decreased in the APP/PS1 (Minkeviciene et al., 2009). Another line that robustly develops amyloid plaques at early stages is the hAPPJ20 line, which was shown to have spontaneous seizures, mossy fibre sprouting and depletion of NMDA and AMPA receptors in the dentate gyrus (Palop et al., 2007). The abundance of the currently available lines of transgenic mice carrying different APP-related mutations provide a useful system of controlled environment and known variables to determine which form(s) of amyloid product (full-length APP, AICD, Aβ oligomers, senile plaques, etc.) mediate the observed circuit hyperexcitability phenotypes.

1.4. Effect of amyloid pathology on neuronal excitability and synaptic transmission

Cognitive deterioration is the inevitable consequence of AD, however it is important to note that impairment in cognitive function such as failure to recall encoded memories, may not simply be the consequence of neuronal death, but rather the result of impaired synaptic transmission (Selkoe, 2002). Indeed, synaptic loss is the best correlate and predictor of cognitive decline in AD-affected brains (Terry et al., 1991), however, the exact mechanism underlying this process is not fully elucidated. Given the central role of APP and its cleavage products in AD pathology, it is reasonable to propose the involvement of one or more amyloid products in increasing neuronal excitability and thereby resulting in seizure-induced synaptic dysfunction and subsequent cognitive deterioration. A question arises then, which form of amyloid product is the major mediator of hyperexcitability? The following paragraphs discuss the involvement of above-mentioned amyloid products in causing circuit hyperexcitability, epileptiform activity and seizure-induced synaptic dysfunction in the context of recent evidence from in vitro and in vivo studies.

1.4.1. Soluble Amyloid beta

Using epileptiform spikes and discharges on the EEG as a measure of circuit excitability, several recent studies involving different transgenic AD mouse models demonstrated that the concentration of soluble Aβ oligomers is the best determinant of circuit hyperexcitability. Accordingly, a study by Palop et al, utilised several models of transgenic APP mice displaying varying concentrations of Aβ, ranging from minimal (hAPP-I5), to moderate (hAPP-J9/FYN) to severe (hAPP-J20, hAPP-ARC48), found evidence of comparable hyperexcitability only in the lines with soluble Aβ fragments (hAPP-J9/FYN, hAPP-J20 and hAPP-ARC48), but not in the hAPP-l5 - a transgenic mouse that overexpresses a wild-type human APP, but has no

elevated Aβ levels or any plaque deposition (Mucke et al., 2000; Palop et al., 2007). Similarly, another study involving chronic EEG monitoring of APParc and APPswe/PS1dE9 mice demonstrated that increased epileptiform activity correlated with higher soluble Aβ production (Ziyatdinova et al., 2016). Notably, APParc mice displayed less frequent discharges compared to APPswe/PS1dE9, despite them expressing more mutant human APP. While the APPswe/PS1dE9 mice present with dense Aβ plaques at 6 months of age and show increased levels of soluble Aβ oligomers compared to APParc line, the APParc mice demonstrate higher APP overexpression, but reduced production of soluble Aβ as the arctic mutation resides within the Aβ sequence and does not affect β-secretase cleavage. (Papazoglou et al., 2016; Reyes-Marin & Nunez, 2017; Ziyatdinova et al., 2011). This line of evidence suggests that the increased concentration of Aβ peptide and not the mutated APP itself, is likely responsible for increased excitability.

While Aβ production is a normal consequence of cellular metabolism, the pathogenic association of the newly-cleaved soluble Aβ fragments with the lipid raft structures of the plasma membrane results in its intracellular accumulation and aggregation into neurotoxic oligomers and fibrils, which are thought to be the key mediators of synaptic loss and neuronal dysfunction. Published literature agrees that Aβ has acute effect on synaptic function and can inhibit hippocampal long-term potentiation (Walsh et al., 2002), however the reports on the mechanisms and direction of this effect are controversial. Several earlier electrophysiological studies involving bath application of Aβ to organotypic slices and cell culture reported increase in synaptic activity and excitability of neurons (Minkeviciene et al., 2009), while others suggest synaptic depression (Kamenetz et al., 2003). This inconsistency implies that the neuro-modulatory effect of Aβ depends on its concentration and oligomeric state as well as the type of neuron in question. The soluble oligomeric species of Aβ can bind to a wide range of ion channels and neurotransmitter receptors such as N-methyl-D-aspartate receptors (NMDAR), nicotinic acetylcholine receptors (nAChR), as well as various other ligands expressed both on the surface of neurons and glia, triggering the activation of downstream signalling pathways (Shankar et al., 2007). For instance, at low picomolar presynaptic concentrations Aβ acts as a positive synaptic regulator, reportedly potentiating synaptic transmission, while at the same time, at higher (nanomolar) postsynaptic concentrations it is a negative regulator, causing synaptic depression (Abramov et al., 2009; Palop & Mucke, 2010). Additionally, Aβ has been

suggested to block glutamate reuptake from synaptic cleft, thus resulting in glutamate spill-over and subsequent excitotoxicity (Lei et al., 2016).

1.4.2. APP overexpression-related indirect mechanisms

While increased APP production and dense core amyloid plaques may not directly affect neuronal excitability, there are several indirect mechanisms through which these amyloid products can lead to hyperexcitability and neuronal loss. One mechanism through which APP overexpression may indirectly disrupt the excitatory/inhibitory balance is through β-secretase cleavage. The activity and protein level of β-secretase – one of the enzymes that cleave APP is reportedly increased in patients with AD (Fukumoto, Cheung, Hyman, & Irizarry, 2002). This enzyme also cleaves NaVβ2 – a subunit of a voltage gated sodium channel NaV1.1 (Wong et al., 2005). The phenotype associated with loss-of-function mutations in this channel range from febrile seizures to severe myoclonus. It has been observed in several transgenic AD and BACE1-null mice that there is increased β-secretase-dependent cleavage of NaVβ2, leading to NaV1.1 being retained inside the cell, thus resulting in reduced sodium current due to decreased surface levels of NaV1.1 (B. F. Corbett et al., 2013; D. Y. Kim, Gersbacher, Inquimbert, & Kovacs, 2011; Verret et al., 2012). These studies conclude that Navβ2 and its correct processing is essential for normal expression and function of NaV1.1, and loss of VGSC at random sites could compromise the ability of action potential generation. Since NaV1.1 is prominently expressed in Parvalbumin expressing (PV) inhibitory interneurons, decreased sodium current due to inadequate number of NaV1.1 channels will result in reduced inhibitory input and overall increase in excitability of the larger network. Fast-spiking PV expressing basket cells generate high-frequency oscillations in gamma range, which reflects their inhibitory input onto excitatory pyramidal neurons. Disruption in gamma oscillatory power due to inadequate interneuron function results in network hypersynchrony (Cardin et al., 2009; Y. Wang et al., 2010). A study by Verret and colleagues utilised the hAPPJ20 mice to demonstrate that hypersynchronous activity was more likely during reduced gamma oscillatory activity, which suggested that gamma activity is a modulator of hyperexcitability and epileptiform activity. Furthermore, they established that the disruption of gamma oscillatory activity and subsequent circuit hypersynchrony is causally linked to the dysfunction in NaV1.1, as it was found that when the deficit in NaV1.1 activity was rescued, the inhibitory input was restored, leading to a reduction in epileptic activity in hAPPJ20 mice (Verret et al., 2012).

Based on the evidence from the above-mentioned studies it is reasonable to hypothesize the following chain of events that lead to network hypersynchrony in hAPP transgenic mice: overexpression of mutant human APP causes an increase in β-secretase-dependent cleavage of NaVβ2 subunit of NaV1.1 on PV interneurons, and a subsequent reduction of inhibitory input. Reduced inhibitory input renders the circuit hyperexcitable, while reduced gamma oscillatory power allows for hypersynchrony of the neuronal network and ultimately the emergence of epileptiform activity.

1.4.3. Neuroinflammation

Another mechanism by which amyloid products lead to hyperexcitability and synaptic dysfunction is through triggering neuroinflammatory response cascades (Canevari, Abramov, & Duchen, 2004; T. Kim et al., 2013). Chronic neuroinflammation is a hallmark of AD pathology, and is an early event during disease progression (Cappellano et al., 2013). Several epidemiological studies have shown that patients who have been receiving long-term anti-inflammatory treatment show decreased risk of developing AD compared to age-matched controls, however, the attempts to reverse neurodegeneration and cognitive decline in late stages of AD using anti-inflammatory agents have failed so far (Breitner, 1996; Breitner et al., 1995; Jaturapatporn, Isaac, McCleery, & Tabet, 2012; Stewart, Kawas, Corrada, & Metter, 1997).

Microglia, the resident immune cells of the nervous system, have been shown to be key players in sustaining chronic neuroinflammation and inducing neuronal dysfunction in the context of AD pathology. These cells have two general functions: physically destroying the intruders by engulfing them; and releasing inflammatory cytokines in order to recruit more microglia to mount an innate immune response. Fibrillar aggregates of amyloid beta have been shown to bind to a multitude of microglial receptors including CD36, TLR4 and TLR6, inducing activation of inflammasomes and classical complement pathway (S. Chen, Frederickson, & Brunden, 1996) and triggering phagocytic clearance (Heneka et al., 2015; S. Liu et al., 2012). Upon interaction with fibrillar amyloid beta, microglia recognize it as danger associated molecular pattern (DAMP) and become “reactive” to facilitate phagocytic clearance. This process is generally referred to as “reactive microgliosis” and is characterized by changes in cell morphology and surface markers as well as secretion of proinflammatory cytokines including IL-1β, TNF- α, IL-6 and upregulation of toll-like receptors. The released

inflammatory cytokines recruit more microglia to the vicinity of amyloid plaque to form a "protective barrier" by surrounding the plaque (Condello, Yuan, Schain, & Grutzendler, 2015).

In addition to activating inflammatory cascades, cytokines also control the permeability of the blood-brain barrier (BBB), regulate the expression of genes involved in neurotransmission and synaptic plasticity, and modulate receptor coupled ion channels and voltage gated ion channels: therefore, chronic neuroinflammation and excessive production of proinflammatory cytokines may alter neuronal excitability and have detrimental effects on synaptic and neuronal health (Vezzani & Viviani, 2015). For example, the classic pro-inflammatory cytokine IL-1β which is induced after brain injury, has been shown to have proconvulsant effects, while its receptor antagonist supresses seizures (Vezzani et al., 1999). The production of active IL-1β is controlled by the NLRP3 inflammasome, which, upon activation, cleaves pro IL-1β and pro-IL-18 into their active state. It is important to note that fibrillar Aβ alone can activate the inflammasome (S. Liu et al., 2012; Tejera et al., 2019; Venegas et al., 2017) as it can be recognized as a PAMP/DAMP and is able to bind to TLRs. As a result of excess amyloid deposition, prolonged activation, aging-related DNA damage and oxidative stress some microglia may become less responsive to anti-inflammatory cytokines such as IL-10, IL-4 and TGF- β and start producing excess amount of proinflammatory cytokines (Block, Zecca, & Hong, 2007). This microglial neurotoxicity more recently referred to as "disease associated microglia" contributes towards faster disease progression. Indeed, older patients when exposed to immune challenge, experience significantly prolonged inflammatory response, have increased expression of IL-1β and higher risk of developing cognitive impairments and depression (Penninx et al., 2003; Wofford, Loehr, & Schwartz, 1996).

Similar to microgliosis, astrogliosis is signified by astrocytes transforming into active astrocytes, leading to changes in the functions and morphology of each astrocyte (Habib et al., 2020). Evidence from mouse models of AD indicates that reactive astrogliosis results in impairment of normal astrocytic function, leading towards emergence of "disease associated astrocyte" populations and reduced ability of astrocytes to uptake glutamate (Mathur et al., 2015; Olsen et al., 2018; Söllvander et al., 2016). Since glutamate is the most abundant excitatory neurotransmitter in the brain, the decrease in the rate of glutamate uptake from the synaptic cleft and its extracellular accumulation may increase the overall neuronal excitability, subsequently causing glutamate excitotoxicity (Perea et al., 2016).

1.5. Network view of disease

Over the past decades advances in medicine, biotechnology and genetics have enabled us to define biological systems at the molecular level by integrating high-throughput transcriptomic, proteomic and metabolomic data from the same cell population or tissue and generating groups of genes and biological pathways associated with particular states of the system (Barabási & Oltvai, 2004). This has enabled the construction of data-driven networks of genes and proteins that provide framework for understanding the molecular basis of complex diseases by comparing the signature network attributes of normal and dysfunctional states (Y. Chen et al., 2008; Schadt, Friend, & Shaywitz, 2009). Viewing disease as a result of elaborate interplay of cellular pathways – much like a network, accounts for the intricacy and complexity of human biology, as it assumes that perturbations in a single node of this network have the potential of affecting the entire module it belongs to. This system or network approach is proving to be powerful in biomarker discovery in cancer research due to its multiple advantages over the traditional linear causality model approach, which fails to fully account for the complex web of interactions of gene products and key regulators (Lehmann et al., 2011; Nagrath et al., 2007). To take it a step further, this *in silico* method could be used to redefine disease, moving from "collection of symptoms" to "differentially wired or perturbed gene network" thus also changing the way we think about diagnosis and personalized medicine.

1.5.1. Transcriptomics and high throughput sequencing

The above-mentioned network approach to biomedical research has been fuelled by the data generated through high throughput technology such as transcriptomics, proteomics and metabolomics. Diseases as dysfunctional states are associated with altered gene expression which can be captured by gene expression profiling via microarray or RNA-seq technology and performing a differential gene expression analysis of the mRNA in a given tissue (Z. Wang, Gerstein, & Snyder, 2009). Comparison of transcriptomes allows for identification of differentially expressed genes as a result of treatment or disease, or between different types of cells and tissues. In addition to novel technology such as nCounter by NanoString (Goytain & Ng, 2020) that directly quantifies the number of mRNA molecules in the sample, microarray and RNA-sequencing are the two widely used high-throughput methods for gene expression analysis. High throughput transcriptomics is unbiased compared to quantitative PCR, that probes a pre-selected list of genes, as it is able to probe virtually every known transcript at once. While microarray technology is more affordable and has revolutionized transcriptomics, RNA-

seq is more sensitive, able to detect post-transcriptional modifications and doesn't require previous knowledge on the sequence of the transcript, which is why it is considered the gold standard for discovery research (Hoeijmakers, Bartfai, & Stunnenberg, 2013; Raz et al., 2011).

1.5.2. Pathway enrichment analysis

Differential gene expression analysis is a powerful method of comparing the variations in gene transcripts between groups. It has been instrumental in identifying numerous new biomarkers for numerous diseases ranging from various cancers to neurodegenerative and cardiovascular diseases (Han, Xue, Tao, & Zhu, 2019; Lu & Thum, 2019; Mihaly et al., 2013; X. Pang et al., 2017). However, when there are hundreds or thousands of genes differentially expressed between two groups, it becomes challenging to make biologically relevant conclusions from the analysis results. A more meaningful understating of the pathology would entail capturing changes in relevant biological pathways and their interaction. Pathway enrichment analysis addresses this issue by summarizing the large gene list into a smaller list of more easily interpretable biological pathways. Most pathway enrichment analysis methods involve a statistical test that determines if the genes in a given set are overrepresenting any pathway more than what is expected by chance (Reimand et al., 2019). These pathways are then assigned an enrichment score and can be put in an enrichment map, which is a network graph, where nodes represent pathways and the edges connecting the nodes represent commonalities in the composition of the pathway.

1.5.2. Gene coexpression network analysis

High throughput sequencing and differential expression analysis are invaluable for determining the relative abundance of every single transcript in a given tissue and identifying transcripts that are orders of magnitude more or less abundant compared to housekeeping genes. However, small changes in the expression of a large number of genes may be overlooked. Genes do not operate in isolation, neither do they change their expression without any consequence to the rest of the members of the given biological pathway. Thus, it is not sufficient to find a differentially expressed gene or a group of genes, in order to characterize a disease. A growing body of evidence suggests that complex diseases such as diabetes result from small but consistent changes in the expression of many genes rather than large, obvious defects in a few genes (Grimes, Potter, & Datta, 2019; Michael R. Johnson et al., 2015; Mukherjee, Klaus, Pricop-Jeckstadt, Miller, & Struebing, 2019; B. Zhang et al., 2013). Gene coexpression network analysis addresses this issue by interrogating the expression pattern of all genes in the

given transcriptome. Gene coexpression networks are undirected graphs, where the nodes are genes and the edges reflect the Pearson correlation coefficient between any pairs of genes. The nodes in the network are connected by an edge if the two genes have similar expression pattern i.e. they are overexpressed or underexpressed together (Lee, Hsu, Sajdak, Qin, & Pavlidis, 2004).

In 2005 Zhang and Horvath introduced the concept of weighted gene coexpression networks (Zhang & Horvath, 2005), where coexpression measure of gene pairs is converted into a connection weight in the representative network graph. Since then, weighted gene coexpression network analysis (WGCNA) has been implemented in R programming environment (Langfelder & Horvath, 2008) and became one of the most widely utilized and validated frameworks for gene coexpression analysis, with over 14,000 citations of the WGCNA R package since its publication in 2008. Weighted gene coexpression networks can be hierarchically clustered into highly connected groups of genes called modules, and further examined using graph theoretical measures. Since genes involved in the same biological pathways tend to have similar expression pattern, these highly connected modules represent functionally related cellular functions and can be cell-type specific. The topology of two networks can then be compared using differential network analysis in order to capture similar connectivity, which in turn, reflects the overlap in biological pathways implicated in the conditions the networks are associated with (Langfelder & Horvath, 2007). On the other hand, differentially connected networks may indicate changes in the underlying cellular activity, or perturbation. Centrality measures such as degree centrality and betweenness centrality can be explored to identify the highly connected nodes within the perturbed gene modules, which could be important regulators and provide valuable insight in the groups of genes that are relevant to the mechanism of perturbation (Figure 1.3).

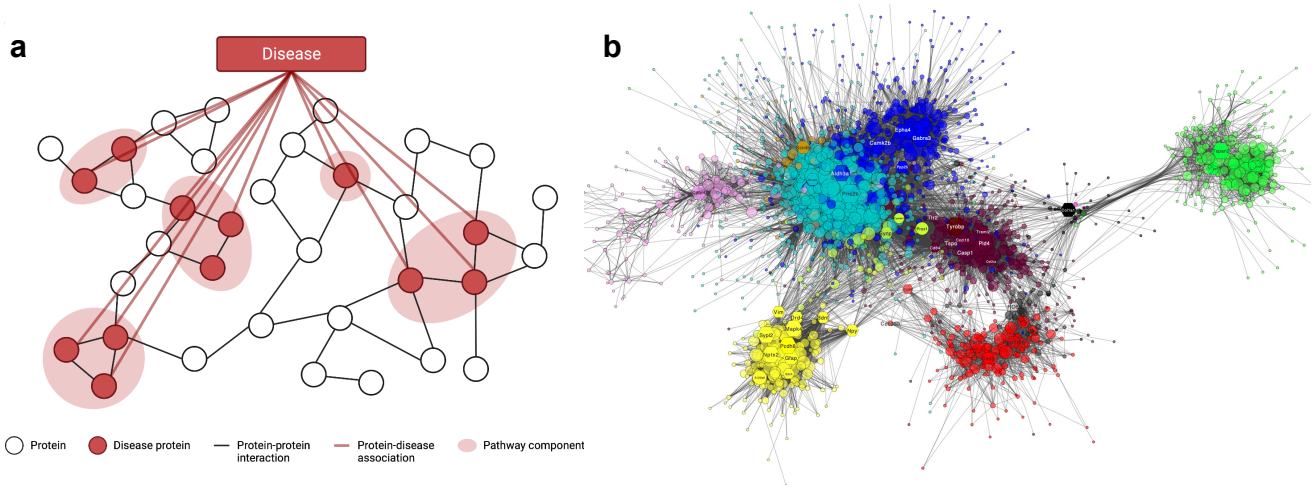

Figure 1.3 Biological networks. a. A disease interactome mapping protein-protein interactions around known disease proteins. b. Gene coexpression network depicting colour-coded functional modules.

Because of the interconnected nature and complexity of biological networks, it can be difficult to see diseases as independent from one another at the molecular level. Different disease-related modules can overlap so that perturbations in one disease module can have an effect on the presentation of the other. This network-based dependency between pathophenotypes has led to the concept of the human diseasome (Figure 1.3). It represents disease graph networks where nodes represent diseases and edges between them represent different molecular relationships among disease-associated cells. Understanding the links between diseases can help us not only understand how different phenotypes are related at the molecular level but also why certain diseases occur together. The rapidly growing field of network medicine offers insights that could lead to new approaches to disease prevention, diagnosis and treatment. The use of diseasome-based methods could aid in drug discovery, especially when it comes to molecularly related diseases such as AD and epilepsy.

1.6. Research aims

It is increasingly evident that epileptiform activity is more prevalent in AD patients than previously recognized. Further, the presence of epileptiform activity predicts faster cognitive decline in AD, and it could promote accelerated disease progression through not yet fully known mechanisms. Thus, the overall aim of this PhD thesis was to explore the molecular links between pathways that could mediate the common electroencephalographic and behavioural phenotypes seen in the context of AD and epilepsy pathologies. The four experimental chapters included in this work utilise network-based computational methods, and specifically aim to:

1) characterise the molecular signature of human AD and that of most widely used mouse models of AD (Chapter 2)
2) characterise the molecular signature of the brain which presents with pathophysiology seen in in two distinct models of epilepsy: the post-status epilepticus model of temporal lobe epilepsy and the GAERS model of absence epilepsy (Chapter 3)
3) investigate the shared molecular signature of AD and temporal lobe epilepsy by identifying commonly dysregulated pathology-specific gene modules which could explain the correlated incidence of the two diseases (Chapter 4)
4) investigate the mechanism and potential mediators of the bi-directional relationship between amyloid pathology and epilepsy by examining the effect of recurrent seizures on hallmark features of AD pathology such as amyloid plaque load and cognitive performance (Chapter 5).

CHAPTER 2

THE MOLECULAR SIGNATURE OF ALZHEIMER'S DISEASE: INSIGHT FROM HUMANS AND ANIMAL MODELS

2.1. Introduction

Alzheimer's is a complex disease, probably a combination of more than one dysregulated biological pathway or mutation, however, it is possible to extract enough gene expression information in order to construct a representative group of dysregulated genes and biological pathways that describe the pathology with reasonable accuracy. This model can then be used to identify molecules for pharmacological targeting. In turn, the development of these targeted therapeutic agents largely relies on the translatability of the mechanisms and their mode of action from mouse models to humans. There are over 150 genetic mouse models of Alzheimer's disease, each mimicking one or more of the rare mutations implicated in familial Alzheimer's disease. However, the vast majority of human AD cases are sporadic in nature, with no common single mutation at play. While it is hard to model sporadic AD in animals, increasing affordability of high throughput technology, open access databases and approaches are giving rise to new investigative options. With the dramatic reduction in the cost of whole transcriptome analysis and a huge number of publicly available microarray and RNAseq data, it is now possible to combine the results of several experiments in a meta analysis for increased statistical power and reproducibility, as well as integrate transcriptomic and metabolomic profiles of various models to evaluate the extent of similarity and translatability of biological pathways and mechanisms between mouse models and humans. Therefore, the initial step of this PhD was to characterise the molecular signatures of human sporadic (late onset) AD and that of most widely used mouse models of AD. The two sets of transcriptomes would then be compared in an attempt to identify a model with most similar molecular signature to that of human AD pathology.

2.2. Methods

2.2.1. Datasets

In order to generate a reliable and representative gene coexpression signature of a disease, large datasets with more than 30 samples are needed. To characterize the molecular signature of AD, a publicly available large microarray dataset of post-mortem brain tissue from Late Onset

Alzheimer's Disease (LOAD) patients and non-demented subjects from the Harvard Brain Tissue Resource Centre (GSE44770) was used. This dataset was contributed by Zhang et al., who in a 2014 study identified TYROBP as a key regulator in LOAD using causal probabilistic Bayesian and gene co-expression networks (B. Zhang et al., 2013). The dataset includes prefrontal cortex samples from 129 AD and 101 non-demented control individuals. The expression matrix was downloaded from NCBI Gene Expression Omnibus (Clough & Barrett, 2016) on 10/08/2019 via GEOquery R package, filtered for low abundancy genes and the probe annotations were mapped to Entrez IDs (G. Zhou et al., 2019). Variance stabilizing and quantile normalizations were performed, followed by differential expression analysis using Limma R package (RStudio version 3.6). The differentially expressed genes were then ranked based on fold change and a Gene Set Enrichment Analysis (GSEA) (Subramanian et al., 2005) based on the KEGG database was performed using the NetworkAnalyst 3.0 tool (G. Zhou et al., 2019).

2.2.2. Weighted gene coexpression network analysis

A weighted gene coexpression network was constructed using the filtered and normalized expression matrix. Briefly, a correlation matrix was constructed from the Pearson correlation values of all genes. A series of soft thresholding values were used to determine the optimal power at which the correlation matrix fit the scale-free topology model, i.e. when the characteristcs of the network are independent of its size. The expression matrix reached a 90% fit to scale-free topology at ß=12, a soft threshold power recommended by creators of WGCNA R package for datasets containing more than 40 samples. An adjacency matrix was then constructed reflecting the pair-wise correlation coefficients between all annotated genes. The correlation network was then built based on the adjacency matrix, where each node corresponds to a single gene, and the edges between the nodes represent the correlation between the expression level of the given gene across all samples. The gene modules were then identified through hierarchical clustering and functionally annotated through pathway enrichment analysis. Hubs were determined by identifying the member gene with highest connectivity in each module.

2.2.3. Functional annotation and enrichment analysis

In order to determine the functional significance of the detected modules we performed a pathway enrichment analysis of the genes constituting each module using the g:Profiler online tool (Reimand et al., 2016). Some of the larger modules rendered over several hundred significantly enriched Gene Ontology and KEGG pathways. Since the Gene Ontology database

has a hierarchical order, we clustered the terms lower in hierarchy into their representative "parent" terms using a similarity threshold of 90% (Supek, Bosnjak, Skunca, & Smuc, 2011).

2.3. Results

Because the AD and NDC samples came from the same study, this facilitated a direct comparison of gene expression between these samples (Figure 2.1). A total of 4426 differentially expressed genes were identified between the AD and NDC samples (FDR<0.05, Log2(FC)>1). Pathway enrichment analysis of underexpressed and overexpressed genes revealed overall downregulation of genes involved in synaptic transmission, axonogenesis, transport, and metabolic (mitochondrial, aerobic respiration) systems, and upregulation of genes involved in apoptotic, inflammatory and innate immune systems in AD samples compared to non-demented controls. Our differential expression analysis results agree with the previous report associated with this dataset (B. Zhang et al., 2013).

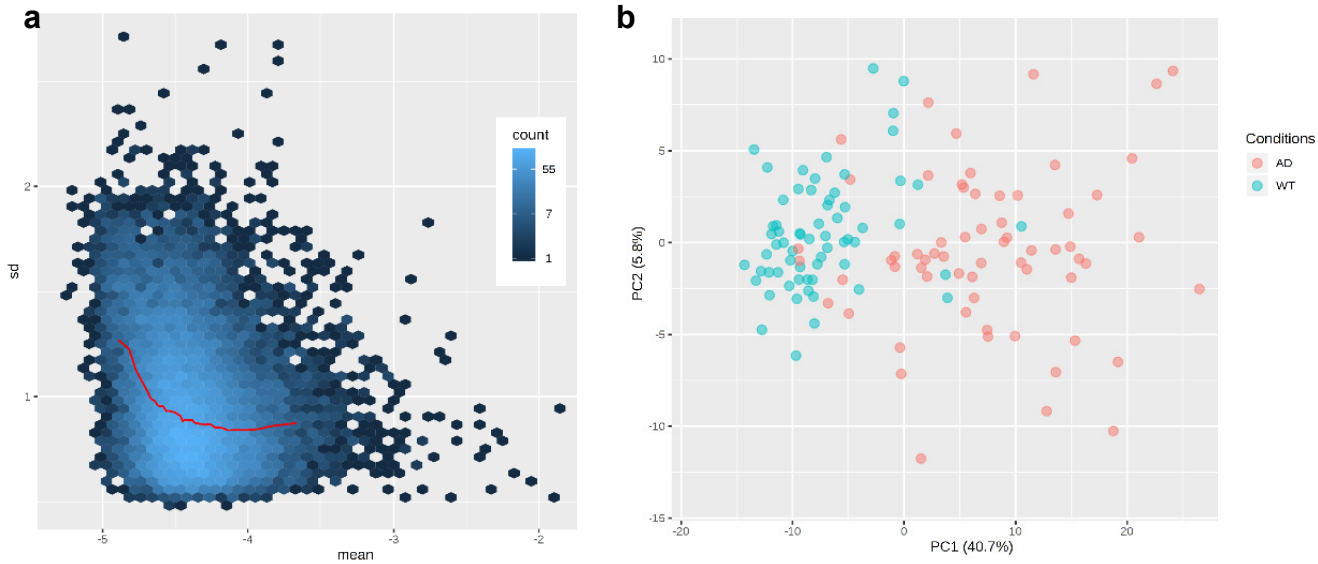

Figure 2.1 Quality control and preprocessing of expression data a. Mean vs Standard Deviation plot of gene expression values. b. Principal component analysis between LOAD (AD) and non-demented control (WT) samples.

After filtering and probe annotation, 14707 genes were included in the AD coexpression network. WGCNA identified 10 modules, ranging from 27 to 2897 nodes in size (Figure 2.2, Table 2.1). The same 10 modules could be identified independently of WGCNA in the Steiner-Forest zero-order network, demonstrating that the gene modules identified by the WGCNA algorithm are robust and have functional significance. We functionally annotated these modules based on the member genes and named them based on the most enriched pathways in the top hierarchy level (Table 2.1). Not surprisingly, when cross-referenced with the KEGG

pathway database, the genes constituting the largest module rendered the "Alzheimer Disease" pathway amongst the most significantly enriched (FDR=1.531 x10-11).

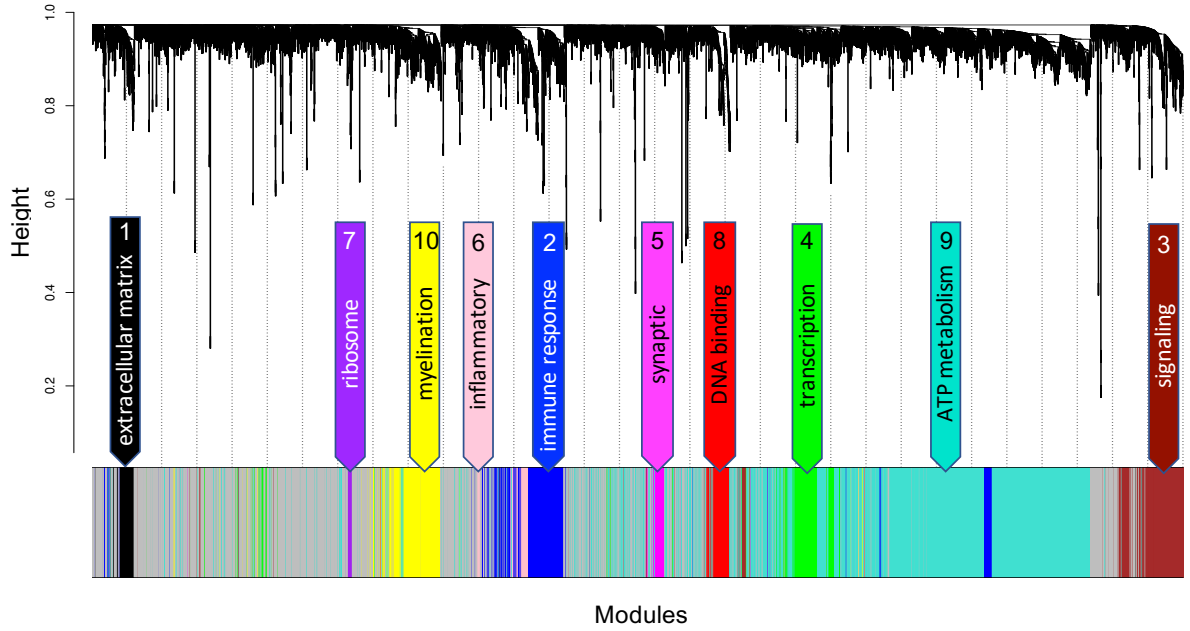

Figure 2.2. Hierarchical cluster dendrogram of AD network. WGCNA identified 10 modules of coexpressed genes labelled by colour. Each branch (vertical line) corresponds to one gene. The colour rows below the dendrogram indicate module membership. The modules are functionally annotated and named based on the enriched GO pathways of the member genes. The grey module (partially not shown) contains genes that have no specific module assignment i.e. the expression pattern of these genes does not show sufficient variability.

Module	Functional annotation	Size	Hub gene
Green (4)	**transcription**	**370**	**SMG5**
Blue (2)	**immune response**	**576**	**TNFRSF1B**
Brown (3)	**signalling**	**487**	**DPEP3**
Yellow (10)	**myelination**	**455**	**FA2H**
Red (8)	**DNA binding**	**170**	**CABP5**
Magenta (5)	**synaptic**	**109**	**DNM1**
Pink (6)	**inflammatory**	**121**	**DOCK2**
Turquoise (9)	**ATP metabolism**	**2897**	**NSF**
Black (1)	**extracellular matrix**	**123**	**DSP**
Purple (7)	**ribosome**	**27**	**RPL27AP6**

Table 2.1. Functional annotation, number of member genes and hub genes of AD coexpression modules. The annotation of a given module was determined based on the most significantly enriched pathways associated with the genes comprising the module. The node with most connections within each module was identified as the hub gene of the module.

A cortex-specific gene coexpression network was visualized using the differentially expressed genes as seed nodes in the NetworkAnalyst 3.0 web-based environment. NetworkAnalyst cross-references the TCSBN database for tissue-specific coexpression of genes. The resulting network contained 7530 nodes and 105632 edges, which is too large to analyze in a meaningful way. To address this issue, a zero-order subnetwork was extracted via Prize-collecting Steiner Forest algorithm, resulting in a highly connected network of 2569 nodes and 30239 edges (Table 2.2). Ten large modules were identified using the WalkTrap algorithm. These modules were analogous to those identified by WGCNA algorithm. The nodes of highest degree centrality and betweenness centrality are listed in Table 2.2.

Gene	Degree	Description	Gene	Betweenness	Description
PGM2L1	250	Phosphoglucomutase 2	**CFLAR**	570286	CASP8 And FADD Like Apoptosis Regulator
GABBR2	234	GABA type B receptor subunit 2	**LAMA5**	557022	Laminin Subunit Alpha 5
DLGAP1	192	DLG associated protein 1	**PLP2**	400454	Proteolipid Protein 2
ATL1	191	Atlastin GTPase 1	**SOGA2**	313429	Microtubule Crosslinking Factor 1
CALM3	190	Calmodulin-3	**DOPEY2**	259965	DOP1 Leucine Zipper Like Protein B
PRKCB	179	Protein kinase C beta	**STXBP5L**	245985	Syntaxin Binding Protein 5
KCNQ5	173	VG potassium channel subfamily Q	**MAML2**	238340	Mastermind-Like Protein 2
ITFG1	173	Integrin alpha FG	**GRIK2**	190839	Glutamate Receptor 6
MAP7D2	169	MAP7 domain containing 2	**FGFR1**	180769	Fibroblast Growth Factor Receptor 1
MOAP1	166	Modulator of apoptosis 1	**KDM6B**	177434	Lysine Demethylase 6B

Table 2.2. Top 10 nodes in AD coexpression network with highest degree centrality (left) and betweenness centrality (right).

Centrality measures can be a good indication of the prominence of the given gene, which, when put in context with its function helps identify key regulators (Koschutzki & Schreiber, 2008). These hub genes have known protein-protein interaction (PPI) with a large number of genes, thus their dysregulation may have a ripple effect on the larger gene-group, and the biological pathway.

One advantage of the NetworkAnalyst tool is the ability to integrate expression values of genes to zero order gene coexpression network, which allows to visualize the upregulated and downregulated modules of genes with functional enrichment information at the same time. When visualizing the composition of the two largest modules, which account for over 70% of all genes in the network, a distinct expression pattern is evident: the largest module (Module 9, turquoise, Figure 2.3) consists of mostly downregulated genes involved in synaptic systems including ion channels and their subunits, axon guidance, neurotransmitters and their receptors, ion transport, GABAergic, glutamatergic and serotonergic synapses, while the second-largest module (Module 2, blue, Figure 2.4) consists of mostly upregulated genes involved in inflammatory cascades, cytokine signaling and apoptosis. Functional enrichment analysis of these upregulated nodes revealed strong enrichment in KEGG inflammatory pathways such as PI3K-Akt, MAPK, TNF, NK-kappa B signalling pathways. When cross-referencing the Gene ontology terms, cell activation and proliferation, angiogenesis and cell adhesion processes appear to be enriched. Chord diagrams in Figure 2.3 and Figure 2.4 represent the most significantly enriched pathways and corresponding genes of Module 9 and Module 2, respectively, after hierarchical pathway clustering with similarity threshold of 85%.

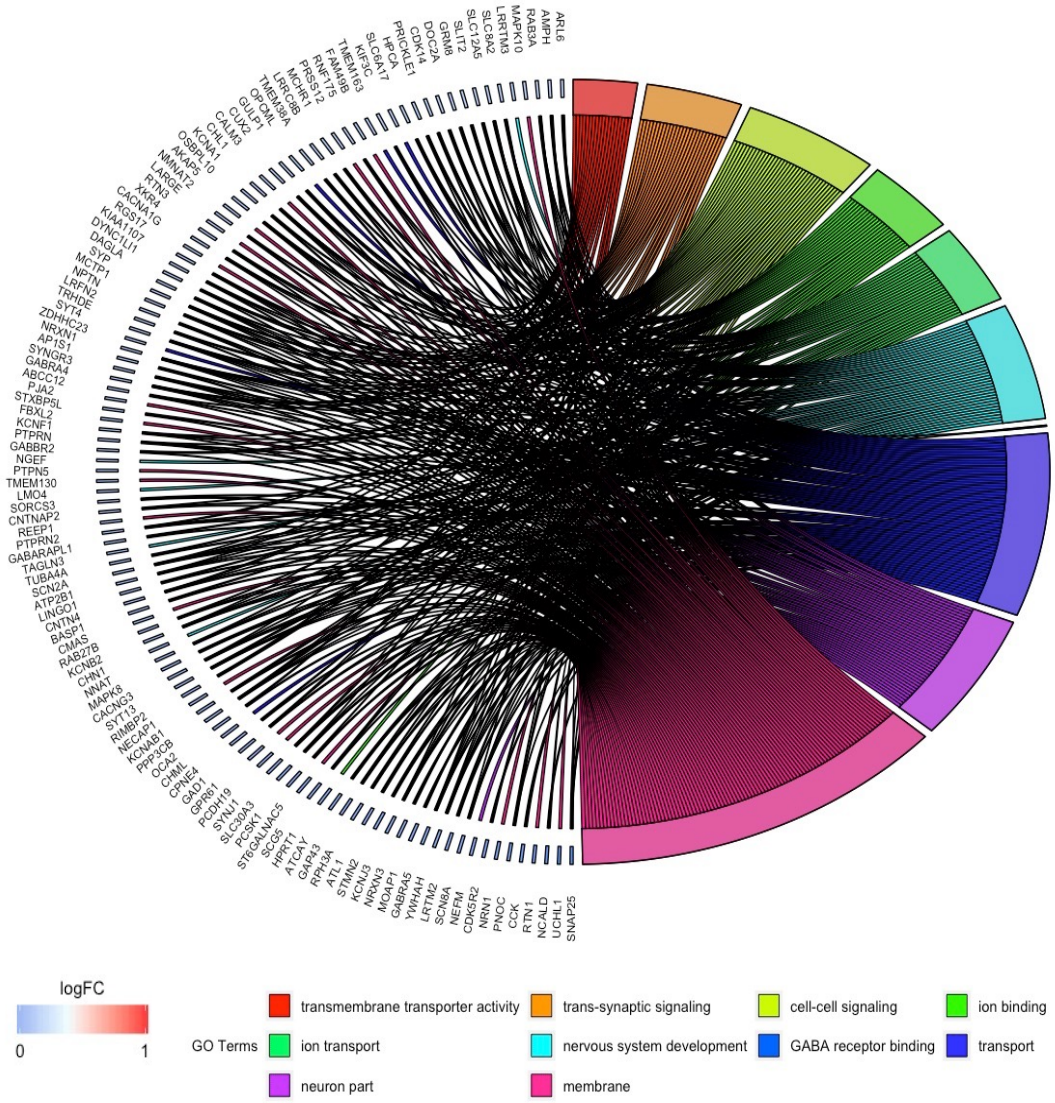

Figure 2.3. **Functional enrichment of genes in Module 9 of LOAD coexpression network.** The Gene Ontology Biological Process terms were hierarchically clustered into parent terms (similarity threshold 85%).

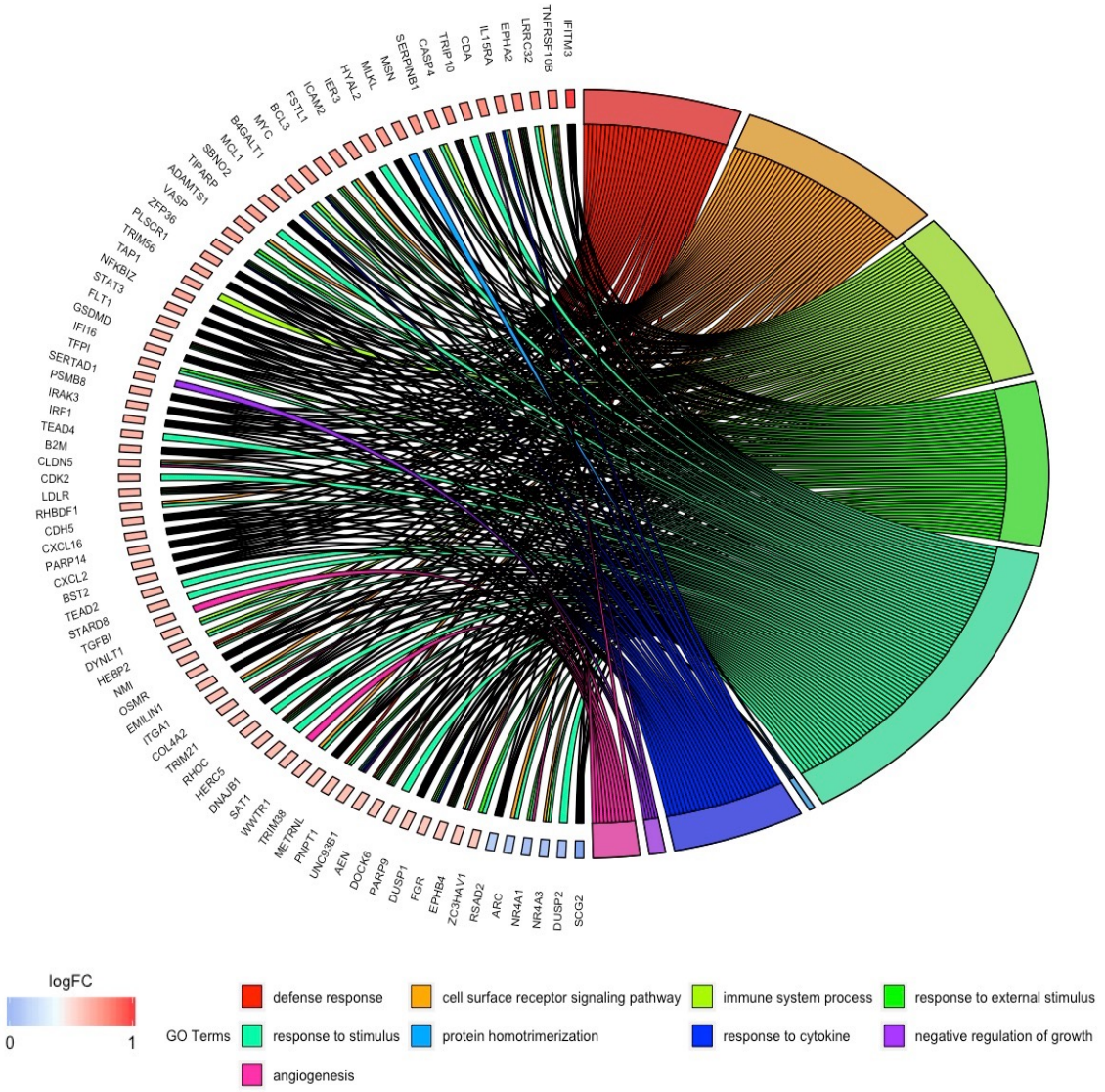

Figure 2.4. Functional enrichment of genes in Module 2 of LOAD coexpression network. The Gene Ontology Biological Process terms were hierarchically clustered into parent terms (similarity threshold 85%).

In order to construct a transcriptomic signature of AD mouse models we compiled publicly available gene expression datasets from most widely used transgenic mouse models. Briefly, a systematic search of gene expression profiling data was conducted in the NCBI Gene Expression Omnibus with keywords Alzheimer's Diseases [all synonyms] and mouse [all synonyms]. The microarray expression sets from all available AD mouse models (n=17) were downloaded. Only datasets which had more than 5 transgenic samples and respective non-transgenic controls were included. In the interest of increasing statistical power and robustness of the transcriptomic signature, for each mouse model, individual microarray datasets from

several experiments (provided they involved mice of comparable age and analysed the same brain region) were combined. Only models with at least three available raw datasets were included in the analysis (n=4, Table 3). ComBat algorithm within the SVA R package was used to correct the expression matrices for experiment-specific batch effects. A gene-level meta-analysis with random effect model was then conducted for each group, and a combined effect size for each differentially expressed gene was calculated. A pathway enrichment analysis was then performed for all 4 models based on each DEG list. In order to identify mouse models with most transcriptomic overlap with human AD, we calculated the percentage of overlap between the homolog genes found to be differentially expressed in the human brain with LOAD and the brain of the given mouse model (Table 2.3). Additionally, an overrepresentation analysis (ORA) was conducted for each list of DEG to identify the fold change distribution of the underlying genes constituting each significantly enriched pathway. The DEG's and enriched pathways of APP/PS1, Tg4510 and 5xFAD mouse lines had substantial overlap with those of human LOAD featuring robust inflammatory signature and neurotransmission systems (Figure 2.5). Similar to findings from human data, immune system and inflammation related pathways were significantly enriched in all 4 mouse models.

Model name, mutation	Age (months)	Total # datasets	Total # samples	Total # DE genes	Overlap mouse/ human	Top enriched GO pathways
APP/PS1 (APPSwe, PSEN1)	5-6 mo	3	62	**833**	33.9%	Chemokine signaling MAPK signaling TNF signaling
Tg2576 (APPSwe)	10-12 mo	6	74	**10**	18%	Steroid metabolism
Tg4510 (MAPT tauP301L)	4-6 mo	4	78	**2447**	24.6%	Regulation of action potential Cytokine production
5xFAD (APP(Swe, Fl,Lon), PSEN1(M146L, L286V))	3-5 mo	4	17	**392**	36.5%	Activation of MAPK activity Regulation of action potential Acute inflammatory response

Table 2.3. A summary of mouse models used in the meta-analysis and results from gene expression profiling. The percent overlap between mouse and human is the percentage of homolog genes found to be differentially expressed in the human brain with LOAD and the brain of the given mouse model.

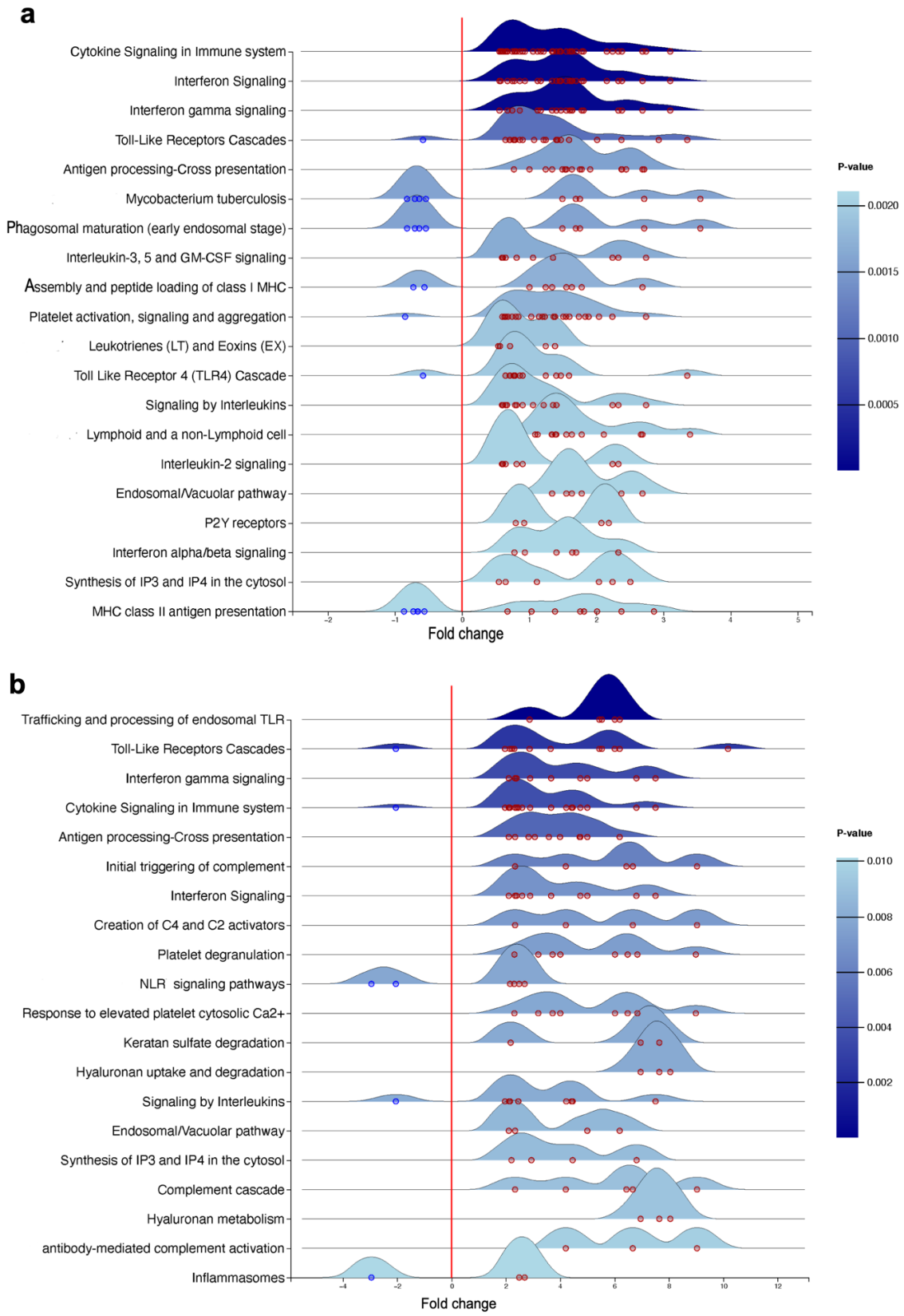

Figure 2.5. Ridgeline charts of top 20 significantly enriched Reactome gene sets in a) APP/PS1 and b) 5xFAD mouse models calculated via GSEA. The X-axis corresponds to the fold change magnitude and direction (up or down regulation) for corresponding Reactome pathways shown on Y-axis. The circles at the base of each ridge represent the differentially up- or downregulated genes that constitute the given pathway.

2.4. Discussion

The attempts of developing therapeutic agents that combat the progression of AD largely rely on the translatability of the mechanisms and the mode of action from mouse models to humans. However, pre-clinical models do not always resemble the spectrum of human disease, especially in the case of a heterogeneous and multifactorial one such as AD. These inter-species differences (i.e., between mice and humans) motivated efforts to develop more relevant pre-clinical models, leading towards generation of over 150 genetic mouse models of Alzheimer's disease, each mimicking one or more of the rare mutations in the amyloid precursor protein and/or the enzymes that cleave it, resulting in abnormal processing and aggregation of amyloid plaques. While no single preclinical model truly recapitulates the temporal evolution and the cognitive and neuropsychiatric features of AD pathology as seen in human patients, due to the diversity of the available transgenic lines and the variety of pathology they represent, there is an opportunity to dissect the distinct facets of the pathophysiological mechanisms that lead to neurodegeneration and cognitive decline in the setting of AD. The four mouse models investigated in this study differ substantially, and thus each of them is better suited for studying a different aspect of AD pathology. Based on our results, we conclude that on a systems level, the 5xFAD mouse has the most overlap with the human molecular signature of AD, as its transcriptome demonstrated the highest number of DE genes and enriched pathways overlapping with those from human LOAD samples, therefore we selected the 5xFAD line as a relevant AD model to be used in the subsequent studies of this PhD work.

CHAPTER 3

INVESTIGATING THE MOLECULAR SIGNATURE OF EPILEPSY: A MULTI-OMIC STUDY

3.1. Introduction

The most common type of epileptiform activity that AD patients experience are referred to as complex partial seizures, or silent seizures, which are usually non-convulsive episodes of impaired awareness and unresponsiveness, in some ways similar to absence seizures seen in generalized childhood absence epilepsies.

To explore the potential molecular links between pathways that could mediate the common electroencephalographic and behavioural phenotypes seen in the context of AD and absence epilepsy, Chapter 3 aims to characterize the molecular signature of a brain that is chronically hyperexcitable but does not harbour any amyloid-related mutations. To this end, the well-established GAERS model of absence epilepsy was utilized. Additionally, given that absence seizures involve thalamocortical regions and generally bypass the hippocampus, while the seizures seen in AD patients are reported to have focal onset and involve the hippocampal circuits, we also investigated the molecular signature of a brain presenting with hippocampal onset focal seizures seen in mesial temporal lobe epilepsy (mTLE) by utilizing the post status epilepticus model of mTLE.

3.1.1 Absence epilepsy

Absence epilepsy syndromes, including childhood absence epilepsy and juvenile absence epilepsy, are grouped under the genetic generalised epilepsy (GGE) umbrella by the latest classification of the International League Against Epilepsy (ILAE) (Scheffer et al., 2017). While some GGE cases have been linked to a single causal gene, the vast majority are presumed to have a polygenic architecture (Reid, Berkovic, & Petrou, 2009; Reid, Jackson, Berkovic, & Petrou, 2010). This assumption is supported by observations that most patients with GGE do not have a strong family history of epilepsy and that siblings of affected individuals have an 8% risk of developing epilepsy, which is lower that the risk expected for a recessive (25%) or dominant (50%) inherited trait (Mullen, Berkovic, & the, 2018; Perucca, Bahlo, & Berkovic, 2020).

The pathophysiological changes leading to absence epilepsy have been studied in various animal models (Coenen & van Luijtelaar, 2003; Crunelli & Leresche, 2002). One of the most utilised and validated is the Genetic Absence Epilepsy Rats from Strasbourg (GAERS) model, derived by selective inbreeding of Wistar rats that expressed spontaneous absence-type seizures accompanied by generalised spike and wave discharges on EEG recordings (Marescaux, Vergnes, & Depaulis, 1992; Powell et al., 2014; Vergnes et al., 1982). The GAERS model shares many behavioural characteristics and pharmacological response profile to anti-seizure medication to human absence epilepsy (Danober, Deransart, Depaulis, Vergnes, & Marescaux, 1998; Devinsky, Schein, & Najjar, 2013; Marks et al., 2016; Vergnes et al., 1982). Absence epilepsy involves diffuse, bilateral cerebral regions (Depaulis & Charpier, 2018) and predominantly presents in children and adolescents (Depaulis & Charpier, 2018) and as such, resective epilepsy surgery is unable to be conducted on these individuals. Therefore, human tissue collection from living individuals for research is challenging. To this end, animal models, such as the GAERS, are especially important to aid the investigation of novel targeted therapy development and have high potential to elucidate the molecular changes underlying disease development.

3.1.2. Temporal lobe epilepsy

Accounting for almost half of the drug-resistant epilepsies, temporal lobe epilepsy (TLE) is the most common form of drug-resistant epilepsy in adults, and is frequently accompanied by disabling neuropsychiatric and cognitive comorbidities (B. Hermann, Seidenberg, & Jones, 2008; B. P. Hermann et al., 2000; Kwan, Schachter, & Brodie, 2011; Sharma et al., 2007; Tellez Zenteno, Patten, Jetté, Williams, & Wiebe, 2007). TLE is generally recognized as the subtype of epilepsy that has the most overlap in its pathophysiology with AD (Scharfman, 2012). In addition to electrical abnormalities and cognitive impairment, AD and TLE share pathological features such as amyloid deposition (Mackenzie & Miller, 1994), tau pathology (Tai et al., 2016; Thom et al., 2011) and hippocampal sclerosis (Davidson et al., 2011). To uncover pathology-related molecular pathways in chronic TLE, we used the well-validated kainic acid (KA) post-status epilepticus (SE) model of TLE, where animals develop resistance to drug treatment, as well as the behavioral, cognitive and sensorimotor comorbidities analogous to human drug-resistant TLE (P. M. Casillas-Espinosa et al., 2019; Thomson et al., 2020).

3.1.3. Multi-omic approach

Integrative systems-level analyses have shown to facilitate more complete investigation and comprehensive understating of complex biological systems and heterogeneous diseases like epilepsies. Nevertheless, many previous studies aiming to characterise the molecular profile of various epilepsy models have generally been constrained to a few molecules, or single "omes" such as the genome (Pablo M. Casillas-Espinosa et al., 2017) or proteome (Danış et al., 2011; Yuce-Dursun, Danis, Demir, Ogan, & Onat, 2014). These single layer studies are limited to only providing details on the dysregulated genes/proteins without any indication about potential inter-layer interactions, which are especially pertinent to complex diseases such as epilepsy (Schadt, 2009). Identifying causative genetic markers is challenging due to polygenic architecture of the GGEs. Additionally, numerous changes can occur after initial gene expression, such as epigenetic modifications, that can influence downstream protein expression and the function of larger network of biological pathways (Gibney & Nolan, 2010). Thus, the proteome and the metabolome can better reflect the observed phenotype, as they provide snapshots of all processes that are underway at any given time (Horgan & Kenny, 2011). At present, there is a lack of studies investigating changes at these two levels in the context of absence epilepsy. We envisaged that integration of these layers would enable the discovery of coherent molecular signatures, and identify cellular mechanisms and changes, not present at an earlier stage of molecular expression, that are more relevant to disease development.

Biological systems respond to multiple inputs that vary simultaneously and interact with each other in multiple ways, forming complex molecular networks. As such, the use of systems biology and network theory methodology to model and characterise these networks can elucidate the emergent behaviour of the system. Over the past decade, there has been growing support and evidence for changing the scientific paradigm of disease diagnosis and treatment from "single gene – single disease" to a more holistic systems approach, wherein groups/modules of genes (as well as gene products and metabolites) and the biological pathways they represent define the pathology. Network approaches have been used to identify these "disease modules", study the pathophysiology mechanisms in a wide range of fields (Bell et al., 2011; Ciriello et al., 2015; Dejakaisaya, Harutyunyan, Kwan, & Jones, 2021; Bin Zhang et al., 2013), and uncover molecular relationships between apparently distinct disease phenotypes (Anna Harutyunyan et al., 2022). Their utility in investigating epilepsy pathology has also been demonstrated (M. R. Johnson et al., 2015; Oliver et al., 2014). Here, we aimed to: a) gain insight into the biological pathways that drive the electrical and behavioural

abnormalities seen in absence epilepsy and temporal lobe epilepsy and b) to identify the molecular signature associated with seizures in the GAERS and post-SE-TLE models. To this end, we conducted behavioural analysis and electroencephalographic (EEG) profiling of GAERS and post-SE-TLE rats in relation to their respective control groups, followed by mass spectrometry-based proteomic and metabolomic analysis of the brain tissue from both pairs of groups. Given that absence epilepsy is a disorder of corticothalamic networks (Snead, 1995), we selected the somatosensory cortex (SCx) and thalamus, key regions in this network, for proteomic and metabolomic analyses. Conversely, since TLE is characterized with hippocampal-onset seizures, we investigated the hippocampus and SCx tissue of post-SE-TLE animals.

Utilizing basic statistical techniques for multisensor data merging and the framework of weighted correlation network analysis, we integrated the data from two molecular layers into multi-omic networks, which were then clustered into modules of highly correlated proteins and metabolites. We then assessed the correlation of these protein-metabolite modules to behavioural and seizure outcomes from the GAERS and post-SE-TLE rats, with the aim of identifying modules showing strong correlation with the seizure and behavioural phenotypes associated with absence epilepsy and TLE.

3.2 Materials and Methods

3.2.1. Animals

All procedures were approved by the Alfred Research Alliance Ethics Committee and adhered to the Australian code for the care and use of animals for scientific purposes. All animals where individually housed with alternating 12-hour cycles of light and dark (lights on at 07:00h). Food and water were provided *ad libitum* for the whole duration of the study. For absence epilepsy study, twenty-four-week-old male GAERS and non-epileptic control (NEC) rats were used. For TLE study, eleven-week-old male Wistar rats were used.

3.2.2. Modified kainic acid-induced post-status epilepticus experimental protocol

To generate chronic TLE phenotype, a repeated low dose kainic acid (KA) administration protocol was used (Bhandare et al., 2017; P. M. Casillas-Espinosa et al., 2019). Rats were intraperitoneally injected with an initial dose of KA 7.5 mg/kg, and continuously monitored for behavioural seizures (Racine, 1972). If no continuous seizure activity was observed, another i.p. dose of 5 mg/kg followed by 2.5 mg/kg doses of KA were administered up to a maximum of 20 mg/kg (Brady et al., 2019). An animal was eliminated from the experiment if it didn't

show a stable self-sustained SE after a maximum KA dose. Shams were handled identically but received saline injections instead of KA. After four hours of sustained SE, as evaluated by visual confirmation of behavioural seizures, the animals were given diazepam (5 mg/kg/dose) to stop the SE (Bhandare et al., 2017; P. M. Casillas-Espinosa et al., 2023; P. M. Casillas-Espinosa et al., 2019). Nine weeks after the induction of SE the animals underwent electrode implantation surgery.

3.2.3. EEG Electrode Implantation Surgery

Twenty-four-week-old male GAERS (n=6) and NEC (n=6) rats, along with twenty-week-old post-SE-TLE (n=5) and Sham (n=5) rats underwent EEG electrode implantation surgery under aseptic technique as previously described (Pablo M. Casillas-Espinosa et al., 2017; Pablo M. Casillas-Espinosa, Sargsyan, Melkonian, & O'Brien, 2019). Briefly, animals were anesthetized with isoflurane (Ceva isoflurane, Piramal Enterprises Limited, India), the fur was shaved from the skull and a single midline incision was made on the scalp (Casillas Espinosa et al., 2015). Four burr holes were drilled through the skull without penetrating the dura, one on each side of the frontoparietal region (AP: ±1.7; ML: -2.5), and one on each side of the temporal region, (AP: ±5.6; ML: left 2.5) anterior to lambda. Epidural stainless-steel screw recording electrodes (EM12/20/SPC, Plastics One Inc) were screwed into each hole. Ground and reference epidural stainless-steel screw electrodes were implanted on each side of the parietal bone above the cerebellum. The recording electrodes were fixed in position using self-curing dental cement (VX-SC1000GVD5/VX-SC1000GMLLQ, Vertex, Australia). The incision was sutured, and buprenorphine was administered intraperitoneally (0.05 mg/kg, Indivior Australia).

3.2.4. EEG Acquisition and analysis

Animals were connected to the EEG acquisition system 10 days after electrode implantation surgery using cables (M12C-363, Plastics One Inc, Australia) that allowed free movement around the cage (P. M. Casillas-Espinosa et al., 2019). EEG recordings were acquired continuously for 24 hours using Profusion 3 software (Compumedics, Australia), unfiltered and digitized at 512Hz. An automatic detection algorithm developed by our group was used to detect and quantify seizures (Rui Li, 2021). The detection algorithm decodes the frequency spectrum power of the EEG data, one of the most important characteristics of spike-wave discharge (SWD) patterns. The SWDs detection module, composed of graph neural network and recurrent neural network, aggregates information across both the brain connectivity network and EEG temporal sequence. After automatic detection was performed, the total

number and duration of SWDs along with average SWD duration were computed. An EEG recording was defined as a seizure if the SWD had an amplitude 3-times the baseline with a frequency of 7-12 Hz and a duration of more than 0.5 seconds (Pablo M. Casillas-Espinosa et al., 2017; Pablo M. Casillas-Espinosa et al., 2019).

3.2.5. Behavioural Tests

To evaluate the behavioural comorbidities reported in GAERS and TLE rats, we used the widely validated open field test (OFT) and sucrose preference test (SPT) as previously published (P. M. Casillas-Espinosa et al., 2023; P. M. Casillas-Espinosa et al., 2019; Jones et al., 2008). Additionally, since hippocampal- based memory impairments were reported in TLE, we subjected the post-SE-TLE rats to the novel object recognition (NOR) and novel placement object (NPO) tests to assess their spatial memory performance. All tests were performed in a light-controlled (~110 lux), closed, quiet and clean room between 9 am and 5 pm. Animals had at least one hour to acclimatize to the room prior to testing. Testing was performed in a blinded manner to strain. The OFT is a 100 cm diameter circular arena, with an inner circle arena of 66 cm in diameter. For each test, the rat is placed gently into the centre of the field and its behavioural activity filmed from above for 10 minutes. The distance travelled, and the entries and time spent in the inner circle were objectively assessed from the video feed using Ethovision software (Version 3.0.15, Noldus, Netherlands) (P. M. Casillas-Espinosa et al., 2019; Johnstone et al., 2015; Jones et al., 2008). The SPT was performed 48 hours after OFT completion. Animals remained in their home cage throughout the testing period. One hour before testing, animals were given up to 0.5 ml of 2% sucrose to familiarise them to the taste. Animals were then presented with two bottles, one filled with tap water and the other with 2% sucrose solution for 24 hours (P. M. Casillas-Espinosa et al., 2019). Bottle position was randomized to avoid position preference (P. M. Casillas-Espinosa et al., 2019; Jones et al., 2008; Sarkisova, Midzianovskaia, & Kulikov, 2003). Total fluid intake and percentage preference for sucrose were recorded.

3.2.6. Tissue Preparation

Animals were anesthetised using 5% isoflurane and subsequently euthanised via 150 mg/kg pentobarbitone sodium intraperitoneal injection (Lethabarb, Virbac, Australia). The thalamus and SCx were rapidly harvested, snap frozen in liquid nitrogen and stored at -80^{0}C. Approximately 30mg of tissue was cryogenically pulverized using a 12-well biopulverizer

(BioSpec Products, OK USA Part number 59012MS) according to manufacturer's instructions. The biopulverizer and pestles were cooled in liquid nitrogen. Frozen samples were added to a well and pulverized by sharply striking the pestle four to five times with a mallet. Powdered tissue was transferred into a cold Eppendorf tube. Resulting tissue was split into two portions for proteomic and metabolomic analysis.

3.2.7. Proteomic analysis using LC-MS/MS

30mg of tissue from each region was processed. Powdered samples were lysed in 4% SDS, 100 mM Tris (pH8.1, 95°C, 10 minutes) and sonicated. Lysate was cleared by centrifugation (16,000 g, 10 minutes) and protein concentration was determined using Pierce™ BCA Protein Assay Kit (Thermo). Equal amount of protein was denatured and alkylated using Tris(2-carboxyethyl)-phosphine-hydrochloride and 2-Chloroacetamide (final concentration of 10 mM and 40 mM, respectively), and incubated (95°C, 5 minutes). Proteins were precipitated using chloroform/methanol followed by sequencing grade trypsin digestion (37°C, overnight, enzyme to protein ratio of 1:100). Digestion was stopped by adding formic acid (concentration of 1%). Peptides were cleaned with BondElut Omix Tips (Agilent) and concentrated in a vacuum concentrator prior to MS analysis.

Using a Dionex UltiMate 3000 RSLCnano system equipped with a Dionex UltiMate 3000 RS autosampler, samples were loaded via an Acclaim PepMap 100 trap column (100 µm x 2 cm, nanoViper, C18, 5 µm, 100å; Thermo Scientific) onto an Acclaim PepMap RSLC analytical column (75 µm x 50 cm, nanoViper, C18, 2 µm, 100å; Thermo Scientific). Peptides were separated by increasing concentrations of 80% ACN/0.1% FA at a flow of 250 nl/min (158 minutes) and analyzed with QExactive HF mass spectrometer (Thermo Scientific) operated in data-independent acquisition (DIA) mode. Sixty sequential DIA windows (isolation width: 10 m/z) were acquired (375 - 975 m/z) (resolution: 15.000; AGC target: 2e5; maximum IT: 9 ms; HCD Collision energy: 27%) following a full ms1 scan (resolution: 60.000; AGC target: 3e6; maximum IT: 54 ms; scan range: 375-1575 m/z). Acquired DIA data were evaluated in Spectronaut 13 Laika (Biognosys) using in-house spectral library derived from the same brain samples. Multi-dimensional scaling was undertaken to identify outliers. Differential expression analysis was conducted using R Studio (version 1.2.5033) and R's (version 3.6.3) limma package on log-transformed intensity values (Ritchie et al., 2015).

3.2.8. LC-MS Untargeted Metabolomic analysis

Remaining pulverized frozen tissue was weighed by transferring to a fresh eppendorf tube and 20 µL of extraction solvent (2:6:1 $CHCl_3$:MeOH:H_2O v/v/v, internal standards: 2 µM CHAPS, CAPS, PIPES and TRIS) (0°C) per mg of tissue was immediately added. The mixture was briefly vortexed before sonication in an ice-water bath (10 minutes) followed by centrifugation (20,000xg, 4°C, 10 minutes). Supernatant was transferred to a MS vial for analysis. A Dionex RSLC3000 UHPLC coupled to a Q-Exactive Orbitrap MS (Thermo) was used. Samples were analysed by hydrophilic interaction liquid chromatography (HILIC) following a previously published method (Stoessel et al., 2016). The chromatography utilized a ZIC-p(HILIC) column 5µm 150 x 4.6 mm with a 20 x 2.1 mm ZIC-pHILIC guard column (both Merck Millipore, Australia) (25 °C). A gradient elution of 20 mM ammonium carbonate (A) and acetonitrile (B) (linear gradient time-%B: 0 min-80%, 15 min-50%, 18 min-5%, 21 min-5%, 24 min-80%, 32 min-80%) was utilized. Flow rate was maintained at 300 µL/min. Samples were kept in the autosampler (6°C) and 10 µL was injected for analysis. MS was performed at 35,000 resolution, operating in rapid switching positive (4 kV) and negative (−3.5 kV) mode electrospray ionization (capillary temperature 300°C; sheath gas flow rate 50; auxiliary gas flow rate 20; sweep gas 2; probe temp 120°C). Samples were randomised and processed in a single batch with intermittent analysis of pooled quality-control samples to ensure reproducibility and minimise variation. For accurate metabolite identification, a standard library of ~300 metabolites were analysed before sample testing and accurate retention time for each standard was recorded. This standard library also forms the basis of a retention time prediction model used to provide putative identification of metabolites not contained within the standard library (Darren J. Creek et al., 2011). Acquired LC-MS/MS data was processed in an untargeted fashion using open source software IDEOM, which initially used *ProteoWizard* to convert raw LC-MS files to *mzXML* format and *XCMS* to pick peaks to convert to *.peakML* files (D. J. Creek, Jankevics, Burgess, Breitling, & Barrett, 2012). *Mzmatch.R* was subsequently used for sample alignment and filtering (Scheltema, Jankevics, Jansen, Swertz, & Breitling, 2011). IDEOMwas utilised for further data pre-processing, organisation and quality evaluation (D. J. Creek et al., 2012). Raw peak intensity values of metabolites which passed the RT error check were included in the final data matrix for statistical analysis. Peak intensity values were log-transformed, quantile normalized and unit-variance scaled to achieve normal distribution. Principal component analysis was conducted to identify and remove outliers prior to further statistical analysis. To identify differences in metabolite abundance between strains, the fold

changes of each metabolite were calculated and compared via unpaired t-test between the groups. For both proteomics and metabolomics, p-values associated with the t-tests were corrected for multiple comparisons using the Bejamini-Hochberg method, and significance threshold was set to FDR<0.05 (Benjamini & Hochberg, 1995).

3.2.9. Multi-omic data integration and Weighted Gene Co-expression Network Analysis (WGCNA)

To integrate proteomic and metabolomic data for network analysis, we unit-variance scaled and concatenated the normalized data into a single matrix for each cerebral region. Unit-variance scaling uses standard deviation as the scaling factor, thus, the resultant integrated data can be analysed based on correlations (Jackson, 1991). Correlation-based multi-omic networks were then constructed by employing the framework of WGCNA. An adjacency matrix was constructed reflecting the pairwise Pearson correlations between all detected proteins and metabolites across all samples in each dataset. Correlation networks for each brain region were built based on respective adjacency matrices. In these networks, each node corresponds to a single molecule and the edges between nodes represent the correlation between the relative abundance of the given metabolite/protein across all samples. An average linkage hierarchical clustering algorithm was employed to identify metabolite/protein modules (arbitrarily labelled by colour). Central regulatory hubs were determined for each module by identifying the node with highest degree centrality (largest number of connections to other nodes) and most significant correlation to the first principal component associated with the module. For each network, the correlation of modules to the experimental groups (GAERS vs NEC, TLE vs Sham), seizure phenotype and cognitive performance was assessed through Pearson correlation. To assess overlaps in module composition of the networks representing each cerebral region, a cross-tabulation based approach was employed to generate contingency tables reporting the number of overlapping proteins/metabolites (Langfelder, Luo, Oldham, & Horvath, 2011). Overlap significance (whether the number of overlapping proteins/metabolites is larger than expected by chance) was assessed through Fisher's exact test.

3.2.10. Enrichment analysis

Enrichment analysis was carried out using various publicly available web tools and packages implemented in the R/RStudio environment. For single-omics enrichment analysis, MetaboAnalyst 5.0's quantitative enrichment analysis module was used (Z. Pang et al., 2021) for metabolomic data and the PADOG (Pathway Analysis with Down-weighting of Overlapping Genes) module of Reactome (Fabregat et al., 2018; B. Jassal et al., 2020) was

used for proteomic data. To functionally annotate the protein-metabolite modules identified by WGCNA we employed the joint pathway analysis module of MetaboAnalyst 5.0 (Z. Pang et al., 2021). This analysis uses both proteins and metabolites in a single query and is based on weighted data integration to address the issue of genes/proteins overwhelming the integrated pathway analysis results due to significantly different sizes of genomic/transcriptomic and metabolomic pathway databases.

3.3. Results - Absence epilepsy study (GAERS)

3.3.1. Behavioural testing and electroencephalography (EEG) recordings confirm epileptic phenotype in the GAERS group.

EEG analysis showed that twenty-four-week-old male GAERS experienced on average, around 200 seizures in the 24-hour EEG period, each lasting for ~7 seconds on average (Figure 3.1.a), while the age and sex matched NEC rats did not display any seizures (Figure 3.1 a, b, c). Behavioural testing also confirmed that the GAERS exhibited increased anxious behaviour, measured by the open field test (OFT). Compared to the NECs, the GAERS had decreased number of entries ($p=0.037$) and time spent in the centre of the open field ($p=0.008$) (Figure 1d). Further, the GAERS also showed a decreased preference for sucrose compared to NECs ($p=0.026$, Figure 3.1.e), which is indicative of anhedonic-like behaviour.

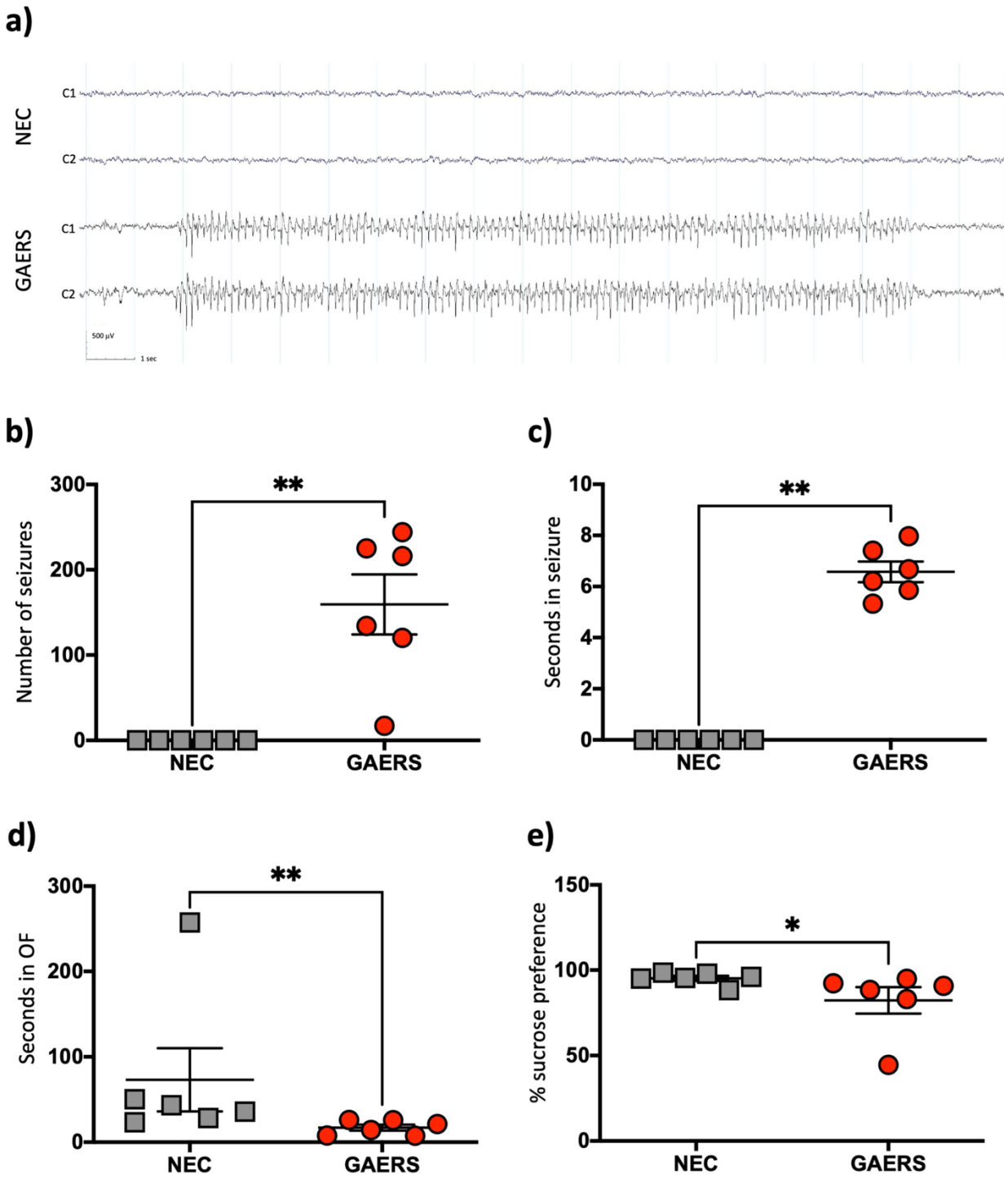

Figure 3.1. The EEG profile, seizure and behavioural outcomes observed in GAERS and NEC groups. (a) A recorded example of the characteristic EEG trace of the GAERS and NEC rats. (b-e) A t-test was used for all comparisons, data shown as mean with SEM, significance indicated with an asterisk (*) at $p<0.05$; (b) The number of seizures observed for individual rats. (c) The average time spent in seizures for individual rats. (d) The amount of time spent in the centre of the open field. (e) The percentage of sucrose preference.

3.3.2. Proteomic analysis identifies various differentially expressed proteins in the GAERS group.

We used untargeted proteomics to identify differentially expressed proteins in GAERS and NEC rats. In the SCx, 102 differentially expressed proteins were identified. From these, 55 proteins were found to be upregulated in GAERS compared to NEC, while 47 were downregulated (Figure 3.2a). In the thalamus, 123 proteins were identified as differentially expressed (Figure 3.2.b), with 74 upregulated and 49 downregulated in GAERS compared to the NEC. The top 10 differentially expressed proteins in the SCx and thalamus are listed in Table 1 and Table 2, respectively. Amongst the differentially expressed proteins, 53 were common between the two cerebral regions (Figure 3.2.c). Pathway Analysis with Down-weighting of Overlapping Genes (PADOG) indicated upregulation of pathways involved in oxidation and metabolism/clearance of neurotransmitters and their precursors in both brain regions (Figure 3.2. d, e).

3.3.3. Metabolomic analysis identifies differentially abundant metabolites and significantly enriched metabolic pathways in the GAERS group.

Similar to proteomics, untargeted metabolomics data were acquired using high-resolution mass spectrometry (MS) from the same brain regions of GAERS and NEC. After initial filtering and normalization, 897 metabolites were included in the statistical analysis (criteria: Fold-change > 1.5; FDR<0.05). In the SCx, 57 metabolites were found to have significantly different abundance between strains, amongst which 27 showed a decrease and 30 showed an increase in GAERS (Figure 3.3.a). In the thalamus, 45 metabolites had significantly different abundance, with 23 decreased and 22 increased in GAERS compared to NEC (Figure 3.3.b). Amongst the differentially abundant metabolites, 29 were common between the two cerebral regions (Figure 3.3.c). Metabolite set enrichment analysis (MSEA) showed significant enrichment in several amino acid metabolic pathways, galactose metabolism, glycolysis, and lysine degradation in both brain regions (Figure 3.3.d, e).

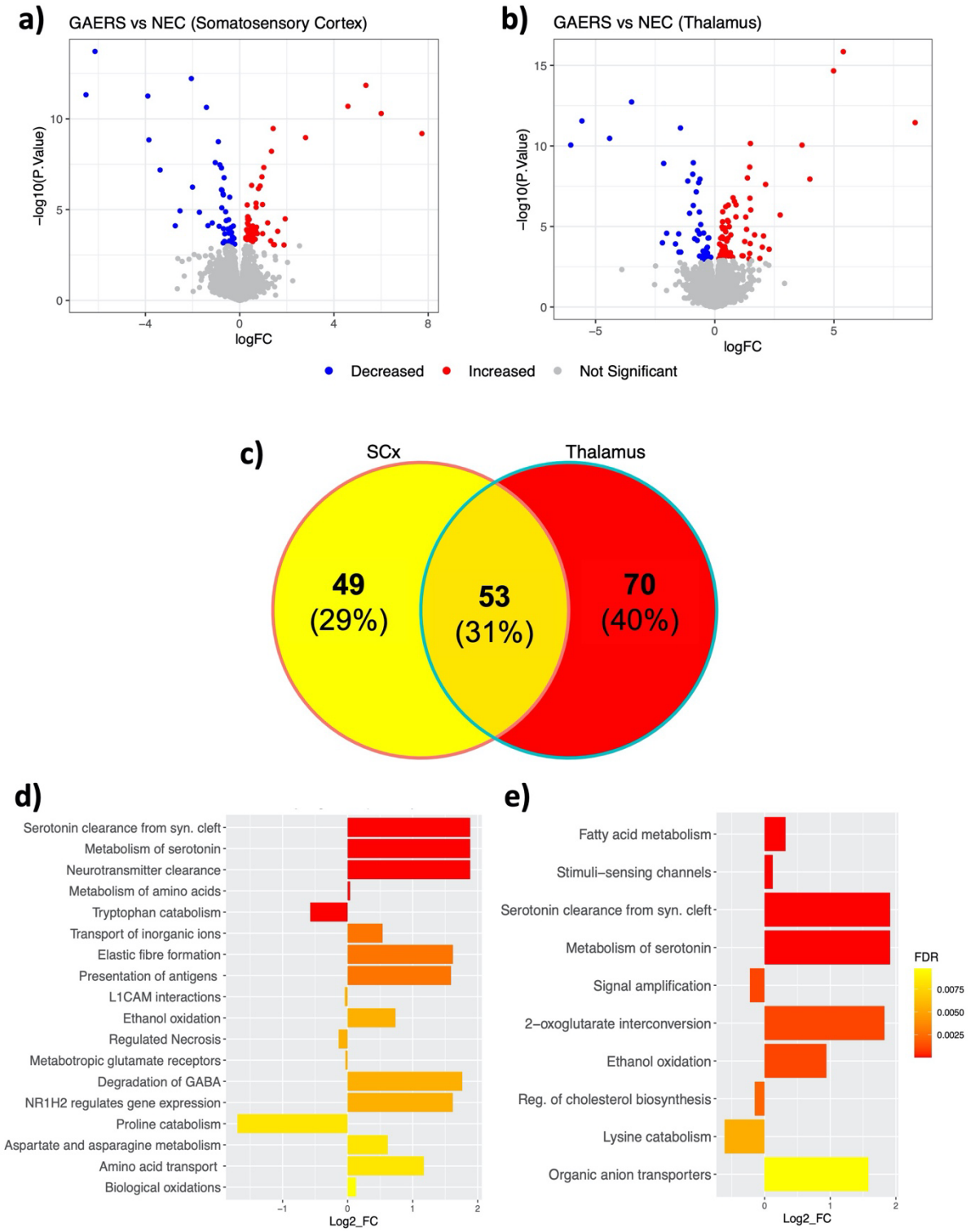

Figure 3.2. Proteomic profiling of the somatosensory cortex (SCx) and thalamus of GAERS compared to NEC. Top: Volcano plots showing the changes in the abundance of all quantified proteins (log_2FC, x-axis) and their statistical significance ($-log_{10}$(q value), y-axis) in GAERS relative to NEC in the **(a)** SCx and **(b)** thalamus. The upregulated proteins in GAERS compared to NEC are shown in red and downregulated proteins are in blue. **(c)** Venn diagram showing the differentially expressed proteins that are region-specific or common between SCx and thalamus of GAERS. Bottom: Differentially regulated pathways identified in the **(d)** SCx and **(e)** thalamus of GAERS, based on the PADOG analysis. The log_2FC (x-axis) indicates the direction of regulation ($log_2FC>0$ upregulated, $log_2FC<0$ downregulated) of the whole pathway in GAERS relative to NEC.

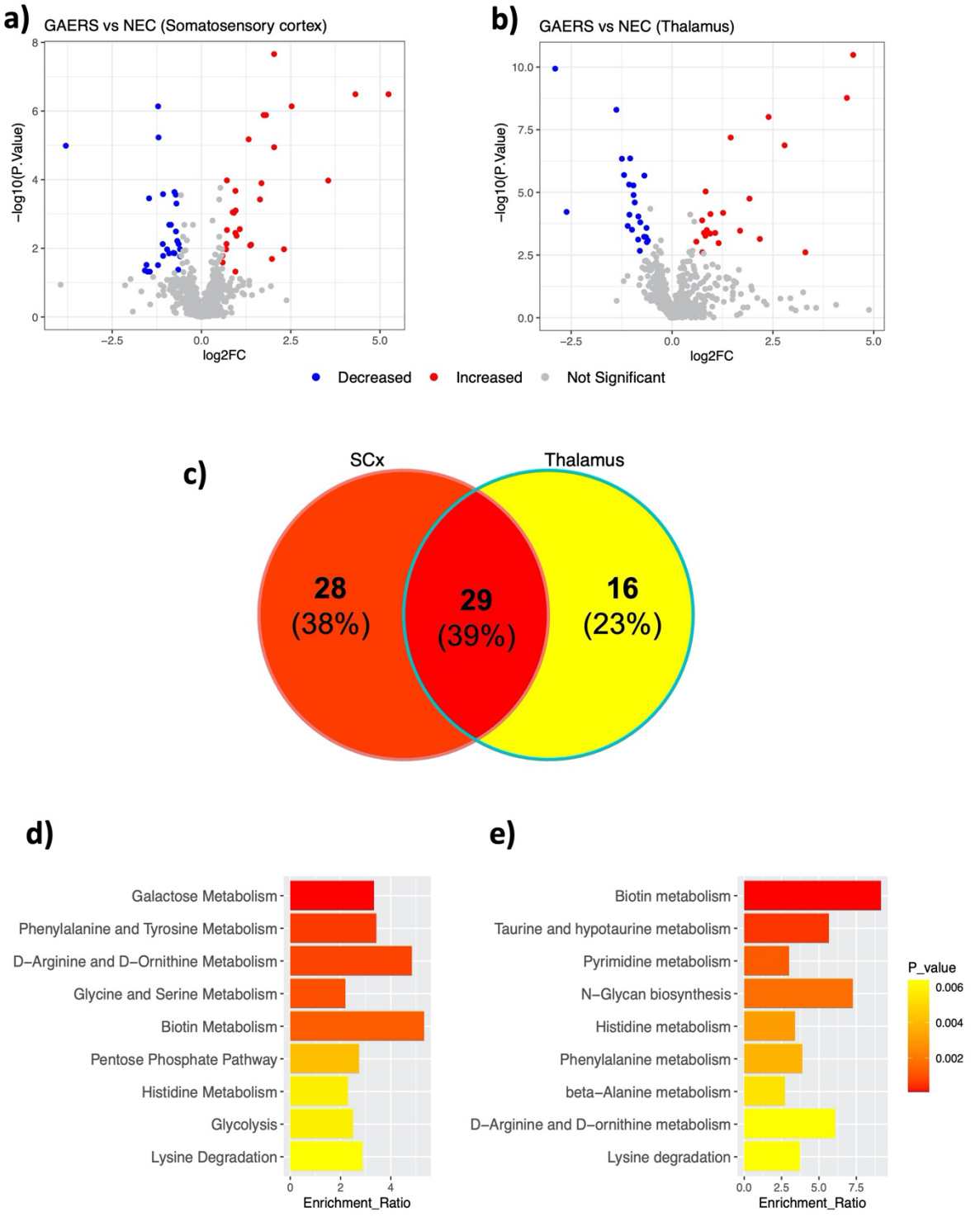

Figure 3.3. Metabolomic profiling of the SCx and thalamus of GAERS compared to NEC. Top: Volcano plot of the –Log10(Pvalue) vs Log2FC of all identified metabolites in GAERS relative to NEC in the **(a)** somatosensory cortex and **(b)** thalamus with the metabolites showing increased abundance in GAERS compared to NEC in red and those with decreased abundance in GAERS compared to NEC in blue. **(c)** a Venn diagram showing the differentially abundant metabolites that are region-specific or common between SCx and thalamus of GAERS. Bottom: The enriched pathways identified in the **(d)** SCx and **(e)** thalamus of GAERS, based on the metabolite-set enrichment analysis (MSEA).

3.3.4. Modules with varying correlations to GAERS and seizure phenotype identified in the multi-omic networks from SCx and thalamus

To represent the proteome and metabolome of GAERS and NEC in the context of a network, we leveraged the general framework of Weighted Gene Coexpression Network Analysis (WGCNA) to integrate the proteomic and metabolomic datasets into two multi-omic correlation networks, each representing the respective brain region. In these networks, each node corresponds to a single molecule (metabolite/protein) and the edges between nodes represent the correlation between the relative abundance of the given molecule across all samples. A hierarchical clustering algorithm identified 22 distinct protein-metabolite modules of various size, density and connectivity (Figure 3.4.a, c) in both SCx and thalamic networks. Each module of the given network was uniquely annotated by colour. We then assessed the correlation strength of each module to the strain (GAERS vs NEC), various seizure parameters and behavioural outcomes from rats in both groups. In the SCx network, the Blue module showed the strongest and most significant (PCC=1, $p=2x10^{-10}$) correlation with the GAERS strain. It also showed strong correlation to longer average seizure duration (PCC=0.98, $p=1x10^{-7}$) and higher seizure frequency (PCC=0.81, p=0.003) (Figure 3.4.b). This module is functionally enriched for multiple pathways, including 'aminoacyl-tRNA biosynthesis', 'ABC transporters', and 'protein digestion and absorption'. Glutathione S-transferase mu 1 (Gstm1) was identified as the central regulatory hub of this module. Gstm1 is one of the top upregulated proteins in SCx (FC=4.6, FDR=1.8E-8). It is noteworthy that with the exception of three proteins, all of the differentially expressed proteins identified in the SCx, regardless of expression levels, belong to the Blue module. This suggests that the concerted action of these proteins and their coregulation is drastically altered in the brain of GAERS compared to NECs. WGCNA analysis of the thalamic datasets revealed 22 modules (Figure 3.4. c, d). Again, there was one module that was highly correlated with the GAERS (PCC=1, $p=1x10^{-12}$). It was strongly correlated with longer average duration (PCC=0.98, $p=2x10^{-8}$) and higher frequency of seizures (PCC=0.83, $p=9x10^{-4}$). This module, co-incidentally also labelled Blue, was enriched for numerous pathways implicating synaptic signalling and plasticity, and the metabolism of various neurotransmitters and amino acids. Interestingly, several significantly enriched thalamic pathways including: 'lysine degradation', 'ABC transporters', and 'aminoacyl-tRNA biosynthesis', were also significantly enriched in the SCx. Aldehyde dehydrogenase 2 family member (Aldh2) was found to be the central hub of this module. Aldh2 is one of the top upregulated proteins in the thalamus of GAERS (FC=5.4, FDR=7.34x10-13)

and is involved in the metabolism of aldehydes produced by lipid peroxidation such as ethanol and 4-hydroxy-2-noneal (4-HNE) (C.-H. Chen, Ferreira, Gross, & Mochly-Rosen, 2014).

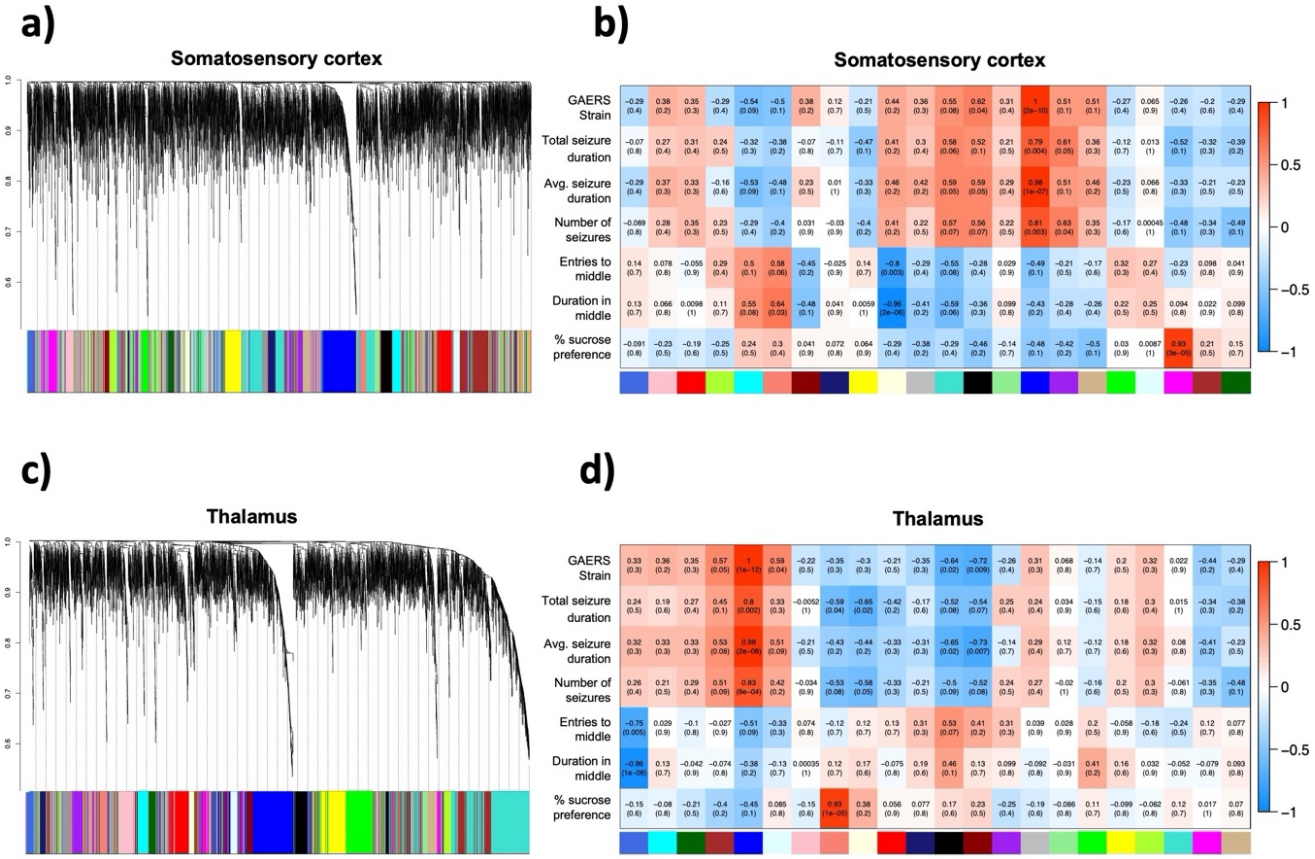

Figure 3.4. WGCNA of integrated multi-omic data from somatosensory cortex and thalamus. Left: Hierarchical cluster dendrogram of **a)** SCx and **c)** thalamic correlation networks. Each vertical line in the dendrogram represents a single protein/metabolite, with the arbitrarily assigned colour of their respective modules at the bottom. Right: Heatmap of all modules (x axis) identified via WGCNA in **b)** SCx and **d)** thalamus and their corresponding Pearson correlation to phenotypic traits (y axis). Each block in the heatmap shows the direction (red: positive, blue: negative), strength (top coefficient) and significance (in brackets) of the Pearson correlation of the given module to the GAERS strain, seizure parameters, and behavioural outcomes.

3.3.5. Seizure-associated modules show overlap in SCx and Thalamus

To disentangle the region-specific and global signatures associated with the GAERS, we conducted an overlap analysis between all 22 modules from both cerebral regions to reveal common proteins and metabolites constituting each SCx and thalamic module. Notably, the most significant ($p=3.9x10^{-46}$) overlap with 189 proteins/metabolites was between the GAERS-associated Blue modules from the respective SCx and thalamic networks (Figure 3.5.a). Joint pathway analysis of the overlapping proteins/metabolites revealed enrichment in several pathways, with “lysine degradation” and “Aminoacyl-tRNA biosynthesis” as the most significantly enriched (FDR=0.0073, Figure 3.5.b). Since the Blue modules in both networks show strong correlation with seizures, anxious and anhedonic-like behaviour - all of which are

characteristic of absence epilepsy, we conclude that these modules are the most significant determinants of the molecular signature associated with the absence seizure phenotype the GAERS exhibit. Therefore, our subsequent analyses focus on these two modules.

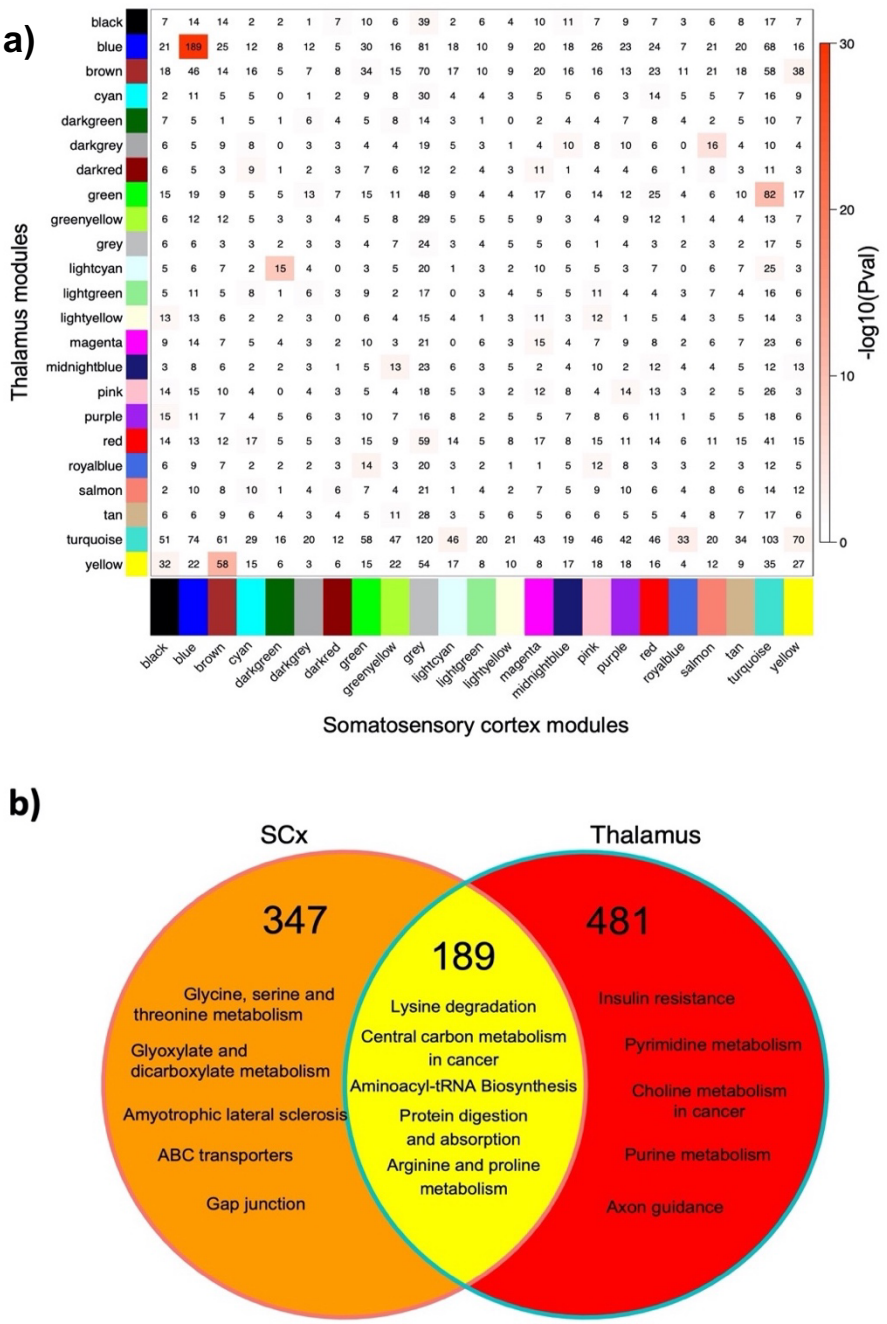

Figure 3.5. The overlap between cortical and thalamic modules. (a) A contingency table of overlapping proteins/metabolites between all pairs of cortical (X axis) and thalamic (Y axis) modules. Each block in the table shows the number of overlapping proteins+metabolites in the intersection of corresponding cortical and thalamic modules. The table is colour-coded with -log10 of the P value associated with the Fisher exact test. **(b)** A Venn diagram depicting the enriched pathways as determined by the joint pathway enrichment analysis of the region-specific and common/overlapping proteins+metabolites from the seizure-associated Blue modules. The diagram is colour-coded with the number of region-specific and common proteins+metabolites in the two Blue modules.

3.3.6. Quantitative enrichment analysis of the seizure-associated modules identifies various differentially regulated pathways

To identify specific seizure-associated dysregulated pathways, we carried out quantitative enrichment analysis on the proteins comprising the seizure-associated Blue modules in both the SCx and thalamus. Using the PADOG (Pathway Analysis with Down-weighting of Overlapping Genes) module of Reactome database (Fabregat et al., 2018; B. Jassal et al., 2020) we identified over 700 differentially regulated pathways in both cerebral regions. The top upregulated pathways in the GAERS were involved in synthesis, transport and clearance of neurotransmitters, synaptic signalling, and oxidative processes (Figure 3.6.a, b). Conversely, the pathways that were downregulated in the GAERS compared to the NEC were involved in lysine catabolism, GTPase cycle, breakdown of galactose and glycogen, necrosis regulation and the innate immune system (Figure 3.6.a, b).

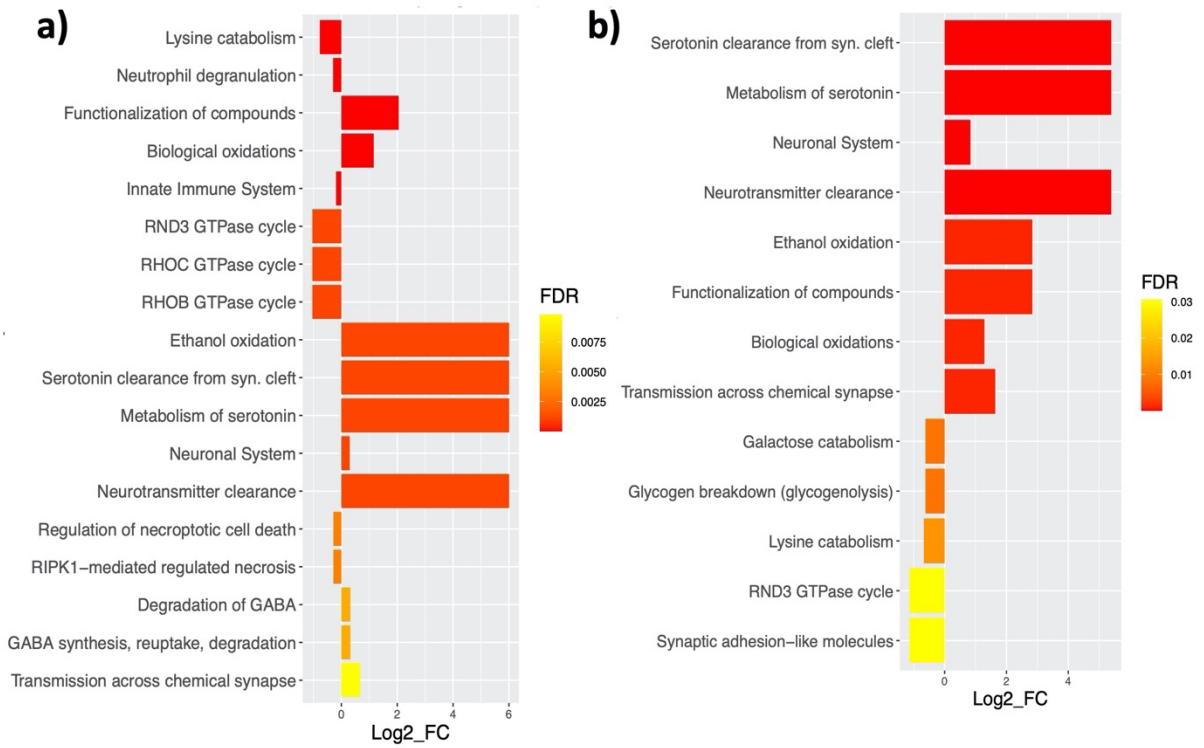

Figure 3.6. Enrichment analysis of proteins from seizure-associated Blue modules. Differentially regulated pathways in the Blue module from **(a)** the SCx and **(b)** thalamus identified via PADOG analysis. Significance threshold was set to FDR<0.05. The log_2FC (x-axis) indicates the direction of regulation ($log_2FC>0$ upregulated, $log_2FC<0$ downregulated) of the whole pathway in GAERS relative to NEC.

3.4. Results – Temporal lobe epilepsy study (TLE)

3.4.1. Proteomic analysis identifies differentially expressed proteins in post SE-TLE rats.

In the same manner as in GAERS study, untargeted proteomics and metabolomics analyses were carried out in the somatosensory cortex and hippocampus of post-SE-TLE and sham groups using the methodology described in sections 3.2.1-3.2.8 to identify potential markers of TLE in the hippocampal and cortical proteome and metabolome of post-SE rats. A total of 5615 and 5538 proteins were identified and quantified across all samples in the somatosensory cortex and hippocampus, respectively, considering a false discovery rate (q-value) cut-off of 1%. Differential expression analysis between post-SE-TLE and sham groups revealed 14 proteins in the hippocampus and 20 proteins in the somatosensory cortex to be significantly different across experimental conditions (Figure 3.7). Among the top upregulated proteins in the somatosensory cortex of post-SE-TLE rats were signal transduction proteins (Gnal, Chgb), gliosis markers (GFAP, Bmerb1) and heat-shock proteins (Hspha2, Hsph1). Astrogliosis markers were also upregulated in the hippocampus (GFAP and Vim) along with cell stress-related proteins (Hspa2, Itgb1, Map3k4).

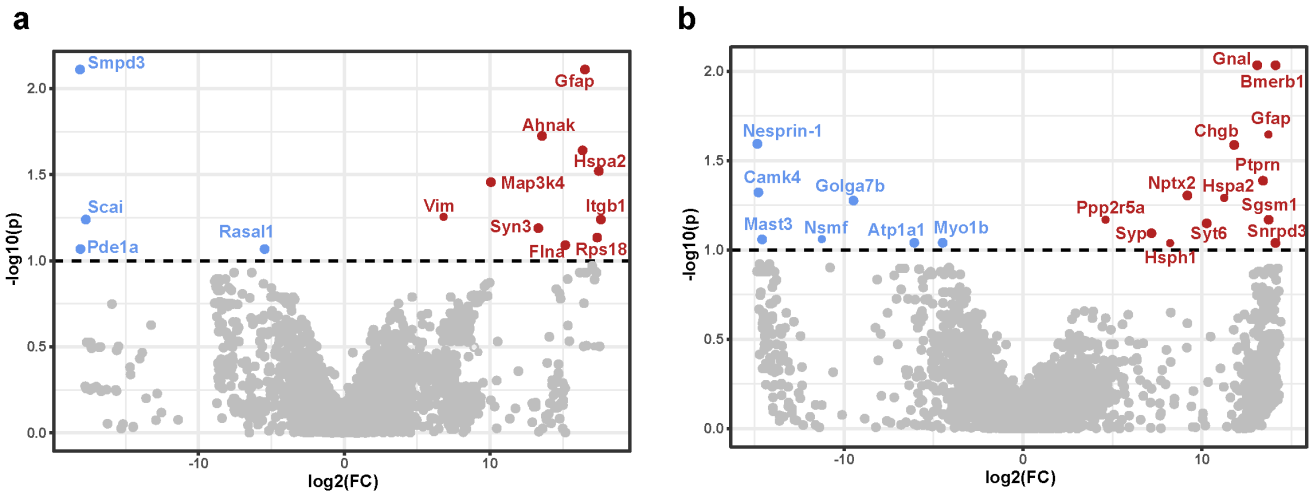

Figure 3.7. Differential expression analysis of all detected proteins in a. hippocampus and b. somatosensory cortex of post-SE-TLE rats compared to shams. Red marks proteins with significantly increased abundance, and blue marks proteins with decreased abundance. Significance threshold was set to FDR< 0.05, Fold Change > 2.

3.4.2. Integrative network analysis identifies discrete protein-metabolite modules correlated with TLE

Using the methodology described in section 3.2 we integrated the untargeted multi-omics (proteomics and metabolomics) datasets with the behavioural and EEG data (seizure severity, cognitive and sensorimotor outcomes) to investigate protein-metabolite groups/pathways correlated with the post-SE-TLE phenotype. Weighted correlation network analysis identified 20 and 17 protein-metabolite modules, respectively, in the hippocampal and cortical multi-omic datasets. Several protein-metabolite modules showed significant positive and negative correlations with the TLE group and EEG/behavioural traits (Figure 3.8), representing distinct proteomic responses to TLE pathology. Each module was labelled based on its principal biology identified via joint pathway enrichment analysis (described in section 3.2.10).

In the hippocampal network, the *focal adhesion* (navy), *endocytosis* (black), *syndecan interactions* (gray), *proteasome* (green) and *neuron projections* (salmon) modules were significantly positively correlated with TLE phenotype. In the somatosensory cortex correlation network, the *vesicle transport* (green), *RNA transport* (purple) and *endomembrane system* (gray) modules were significantly correlated with the TLE group and seizure frequency (Figure 3.8b). Additionally, the *vesicle transport* and *endomembrane system* modules are negatively correlated with hippocampus-dependent memory performance, as measured by the novel object placement test. In both brain regions synaptic signalling-related modules show a robust trend towards downregulation. Specifically, the *trans-synaptic signalling* modules in both SCx and Hippocampal networks as well as cortical *long term potentiation* (red), *ABC transporters* (black) and hippocampal *circadian entrainment* (magenta) modules are negatively correlated to TLE group.

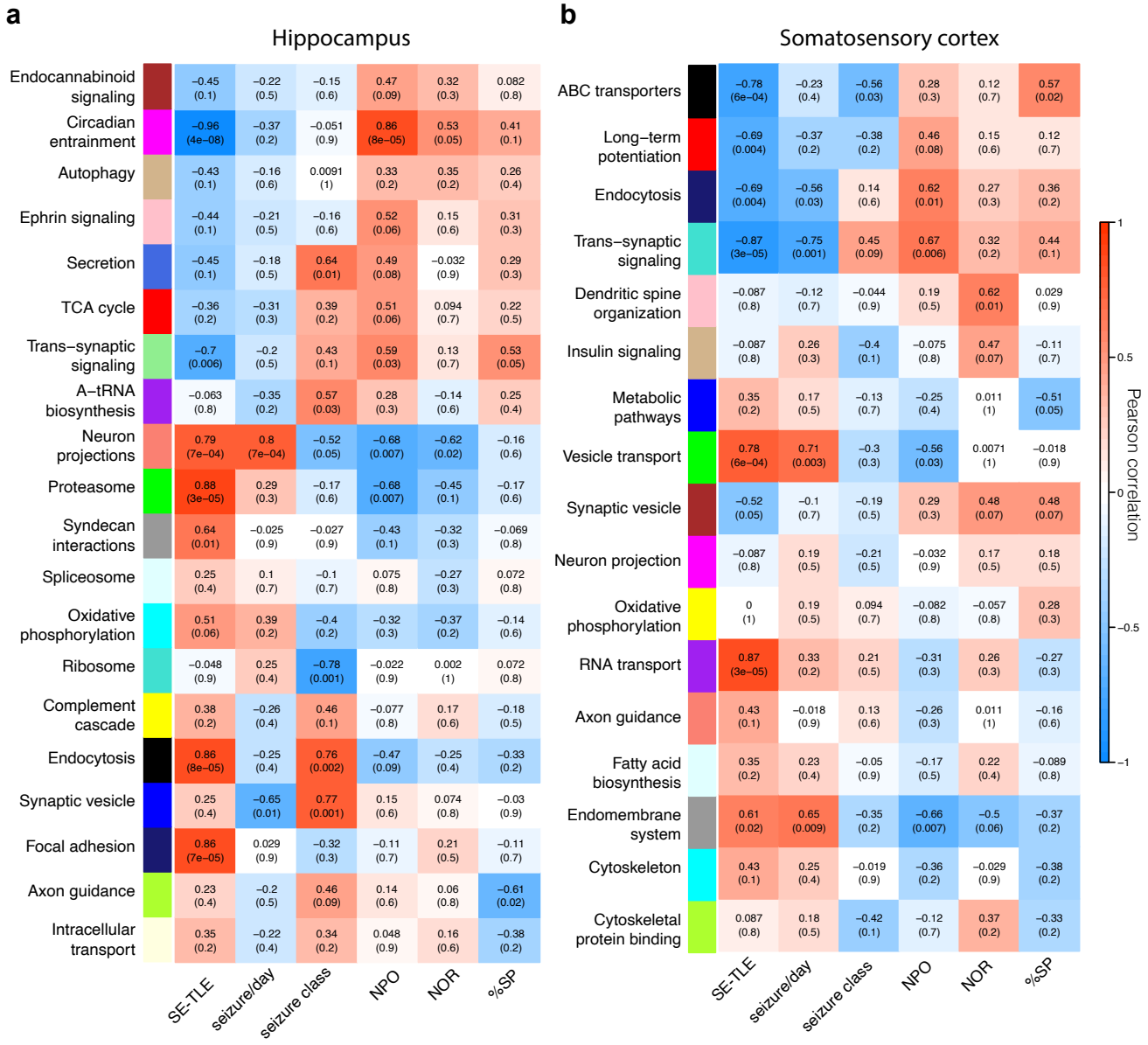

Figure 3.8. Module-trait correlation heatmap. The relationship of protein-metabolite modules (in the Y axis) with measured clinical traits (X axis) in the **a.** hippocampus and **b.** somatosensory cortex of post-se-TLE rats. Each square block shows the Pearson correlation coefficient (PCC) of each module with the clinical traits as well as the associated P value in brackets. The PCC values range from -1 to 1, depending on the strength and direction of the correlation.

3.5. Discussion

Dimension reduction is crucial for hypothesis generation to elucidate pathological mechanisms and changes in biological pathways as a response to treatment. To identify epilepsy associated disease modules, we performed a network medicine integration of our untargeted/targeted multi-omics datasets and phenotypic outcomes (seizures and behavior) to evaluate the correlation coefficients of single modules between the different treatment groups and phenotypic traits. By mapping significant genes/proteins together with metabolites to biological pathways, the network integration allowed for reduction in experimental and biological noise and higher confidence levels, thereby generating potential new disease modules that show a strong relationship with epilepsy phenotype. In this study, we demonstrate the utility of a network-based, integrative multi-omics approach to interrogate the molecular signatures associated with absence epilepsy and TLE.

In the TLE study, upon closer examination of the biological pathways that each protein-metabolite module annotates to, we found that the majority of the modules in both hippocampal and cortical TLE networks (Figure 3.8) fall into two categories: they are either pathology related, or homeostatic. For example, the hippocampal *neuron projections* (Figure 3.8a, salmon) module is positively correlated to epilepsy phenotype, more frequent and severe seizures, and is enriched for cardiomyopathy disease ontology terms, which have been shown to be associated with several epilepsy syndromes (O. Devinsky et al., 2018; Gilchrist, 1963; Naggar, Lazar, Kamran, Orman, & Stewart, 2014; Stöllberger, Wegner, & Finsterer, 2011; Surges & Sander, 2012). In contrast, the *circadian entrainment* module (Figure 3.8a, magenta) is negatively correlated to TLE phenotype, and shows positive correlation towards homeostatic behaviours as measured by NPO, NOR and sucrose preference tests. This suggests that the proteins and metabolites (as well as the cellular pathways they are involved in) that constitute the "healthy state" operate in a concerted fashion in a healthy brain but are lost in the setting of TLE.

In the absence epilepsy/GAERS study traditional linear analysis of single-omics data provided large lists of differentially abundant proteins and metabolites, however, when the two omics layers were integrated into a network along with behavioural and EEG data relevant to the disease phenotype, a single distinct protein-metabolite module that defines the molecular signature of absence seizures was identified in each brain region. The strong correlation of

these two Blue modules (Figure 3.4) with the GAERS strain and more frequent seizures in both the SCx and thalamic correlation networks provide further support for its association with epilepsy and identify it as a "seizure-associated disease module". Interestingly, almost all of the differentially expressed proteins and a large number of differentially abundant metabolites identified were represented in the seizure-associated Blue module in both regions. Overlap analysis of SCx and thalamic multi-omic networks revealed that the two seizure-associated modules have a large number of proteins and metabolites in common, and share numerous enriched pathways, indicating potential global mechanisms affected across both brain regions in epileptic animals. By conducting a joint pathway enrichment analysis which uses both proteins and metabolites in a single query, we generated a smaller list of enriched pathways which were further investigated. Additionally, we conducted quantitative pathway analysis (PADOG) through Reactome resource, which indicated the direction (upregulated vs downregulated) of changes in the significant pathways. Reactome and PADOG were preferred over other pathway analysis types and resources due to several advantages. Firstly, Reactome is a manually curated database and thus, the included pathways have all been experimentally verified (Bijay Jassal et al., 2020). Secondly, the PADOG method addresses the issue of exaggerated significance assigned to genes/proteins which appear in a large number of pathways by assigning more weight to those that are gene set-specific. Thus, if the gene sets that are highly specific to the seizure-associated pathways are differentially regulated, it is more likely that these pathways are truly relevant to absence epilepsy pathology.

The majority of differentially regulated pathways from the seizure-associated modules indicate an increase in synaptic transmission and metabolism of neurotransmitters. Given the increased synchrony in neuronal firing in the context of absence epilepsy, these results are expected. However, the most notable characteristic feature of the molecular signature associated with GAERS elucidated by our analyses is the dysregulation of the lysine degradation pathway. Lysine degradation is the top commonly enriched pathway in the SCx and thalamus of the GAERS (Figure 3.5.a). Mainly localised to mitochondria, lysine degradation provides substrates such as glutamate and acetyl-CoA for downstream metabolic cascades (Leandro & Houten, 2020). Currently, there are no links between absence epilepsy and lysine degradation dysregulation, however, perturbations in this pathway have been linked to pyridoxine-dependent epilepsy (PDE) (Leandro & Houten, 2020; van Karnebeek et al., 2012). Specifically, genetic mutations affecting ALDH7A1 activity (which is involved in cerebral lysine

catabolism) have been identified as the genetic cause of PDE (van Karnebeek et al., 2012). ALDH7A1 is part of the aldehyde dehydrogenase superfamily that includes ALDH2 – the central regulatory hub of the thalamic seizure-associated module. Several of the substrates generated through lysine degradation are necessary for synthesis of Glutathione (GSH) – a tripeptide consisting of glutamate, cysteine and glycine (Glu-Cys-Gly). Glutathione is an important anti-oxidant in the mammalian brain that protects cells from damaging effects of free radicals by conjugating with various reactive oxygen species and electrophiles (Meister, 1988). The conjugation of glutathione is catalysed by Glutathione-S transferases (GSTs) – a family of phase II detoxification enzymes which includes GSTM1, the regulatory hub of the seizure associated module in the SCx (Oakley, 2011; Townsend & Tew, 2003). According to our metabolomic data, the concentration of GSH (Glu-Cys-Gly) is significantly decreased (Log2FC=-2.3, FDR=0.038) in the thalamus of GAERS, and shows a trend towards decrease in SCx (Log2FC=-0.13, FDR=0.2). The reduced concentration of GSH in both the SCx and thalamus hint towards a potential perturbation of oxidative stress balance in absence epilepsy. We postulate that in response to dysregulated lysine catabolism and increased oxidative burden, a compensatory "rewiring" of the downstream signalling pathways occurs in the GAERS brain, which is modulated by Aldh2 and Gstm1 – the regulatory hubs of the seizure associated modules. This is further supported by our findings that Aldh2 and Gstm1 were among the top differentially expressed proteins in the GAERS strain. We speculate that on one hand, due to downregulated lysine catabolism and accumulation of L-lysine, there is a compensatory increase in aldehyde dehydrogenase activity mediated by Aldh2. On the other hand, due to increased synchronisation of neuronal firing and shortage of GSH, there is higher oxidative burden and accumulation of ROS in the GAERS brain, which leads to compensatory increase in glutathione-S-transferase (GST) activity, mediated by Gstm1 and other GSTs. While no association between GSTM1 and absence epilepsy has previously been identified, individuals with drug-resistant epilepsy and a defect in GSTM1 enzymatic activity have increased levels of lipid peroxidation markers, compared to non-epileptic controls and epileptic individuals with normal GSTM1 activity (C.-S. Liu & Tsai, 2002). Oxidative stress is widely recognized as a contributor of epileptogenesis (Patel, 2018; Pearson-Smith & Patel, 2017), and while we have recognised it as a defining feature of the molecular signature of absence epilepsy, oxidative stress could be both the cause and the consequence of pathophysiology development.

It has been shown previously that modularity is a conserved property of biological systems and the cellular functions are carried out by highly connected modules of genes, proteins and metabolites (Oldham, Horvath, & Geschwind, 2006; Oldham et al., 2008). These functional modules tend to be extremely heterogeneous, wherein the majority of the nodes have relatively few connections with other nodes, while a few "hub" nodes are highly connected and therefore are considered important regulators of the given module (Ravasz, Somera, Mongru, Oltvai, & Barabasi, 2002). Gstm1 and Aldh2 were identified as the regulatory hubs of the seizure-associated module in the SCx and thalamus of GAERS, and therefore have the potential of influencing the larger molecular network they regulate, making them potential biomarkers of absence epilepsy and promising candidates for pharmacological manipulation.

It is important to note that most of the biological pathway databases used in this study were curated using information gleaned from human studies. As such, their translatability to a rat model of epilepsy is assumed, but not verified. However, due to the lack of available databases utilising information obtained from rodent studies, these databases represent the best available resource, as they are continuously updated with the most relevant and accurate information available. While the results obtained from this study were promising, to the best of our knowledge, many of these pathways and molecules have not been described in the context of absence epilepsy. Therefore, further experimental validation is necessary to establish these pathways and associated proteins and metabolites as being implicated in absence epilepsy. Overall, our study identifies novel pathways and regulatory hubs with strong potential as candidate biomarkers and treatment targets for drug repurposing and development.

CHAPTER 4

DYSREGULATED SYNAPTIC MODULES IDENTIFIED BETWEEN ALZHEIMER'S DISEASE AND TEMPORAL LOBE EPILEPSY: A NETWORK PRESERVATION STUDY

Alzheimer's Disease and Epilepsy are complex diseases, that likely involve combinations of more than one dysregulated biological pathway or mutation. It is, however, possible to extract enough gene expression information from affected tissues in order to construct a representative network of gene groups and biological pathways that describe the pathology of these conditions with reasonable accuracy. Therefore, we aimed to gain insight into the underlying pathophysiological mechanisms potentially shared between epilepsy and AD patients by exploiting the emerging high throughput and computational methodologies. A hypothesis-free, systems-level approach was used to characterize each pathology on a molecular level by constructing data-driven gene coexpression networks representing AD and temporal lobe epilepsy – the most common type of epilepsy comorbid to AD.

4.1. Introduction

In the past 50 years, it has become apparent that there is increased prevalence of epileptic seizures in patients with AD compared to the general population (Hauser et al., 1986; Hesdorffer et al., 1996; McAreavey, Ballinger, & Fenton, 1992; Volicer, Smith, & Volicer, 1995; K. A. Vossel et al., 2013), but only recently have there been well-designed studies attempting to understand this link (Miranda & Brucki, 2014; K. A. Vossel et al., 2017). A 2006 study reported that patients with AD have ~10-fold increased risk of developing seizures, with early onset or familial AD patients having as high as 87-fold higher risk (Amatniek et al., 2006). These patients show more severe cognitive impairment (McAreavey et al., 1992) and rapid disease progression (Volicer et al., 1995). In AD patients, epileptiform activity is commonly detected in temporal brain regions (K. A. Vossel et al., 2016), and temporal lobe epilepsy (TLE) is generally recognized as the subtype of epilepsy that has the most overlap in its pathophysiology with AD (Scharfman, 2012). In addition to electrical abnormalities and cognitive impairment, AD and TLE share pathological features such as amyloid deposition (Mackenzie & Miller, 1994), tau pathology (Tai et al., 2016; Thom et al., 2011) and hippocampal sclerosis (Davidson et al., 2011). Additionally, several transgenic animal models of AD exhibit spontaneous seizures and have increased susceptibility to epilepsy (Chan, Jones,

Bush, O'Brien, & Kwan, 2015; Palop et al., 2007; Reyes-Marin & Nunez, 2017; Westmark, Westmark, Beard, Hildebrandt, & Malter, 2008; Ziyatdinova et al., 2011; Ziyatdinova et al., 2016), suggesting the pathological hallmarks of AD may directly cause seizures.

Diseases as dysfunctional states are associated with altered gene expression, which can be detected by transcriptional analysis of the mRNA in a given tissue. However, genes do not operate in isolation, but rather interact cooperatively within and across biological pathways. Thus, it is insufficient to identify one differentially expressed group of genes in order to thoroughly characterize a disease. A more comprehensive understanding of the associated pathology requires capturing changes in biological pathways and their interaction. Viewing disease as the result of an elaborate interplay of cellular pathways - much like a network - accounts for the intricacy and complexity of human biology, as it assumes that perturbations in a single node of this network have the potential to affect the entire community or module it belongs to. This systems or network approach is proving to be powerful in biomarker discovery (Clarke et al., 2013; Huan et al., 2015; Sun, Sun, He, & Xiong, 2017; Tran et al., 2011) due to its multiple advantages over the traditional linear association model approach, which fails to fully account for the complex web of interactions of gene products and key regulators.

Weighted gene coexpression network analysis (WGCNA) is a widely used systems biology methodology that investigates the correlation between genes based on their expression level across all samples in the dataset (Zhang & Horvath, 2005). The genes (nodes) in the network are connected by an edge if the two genes have similar expression pattern i.e. their expressions rise and fall together (correlated) or when one rises the other falls (anticorrelated) (Zhang & Horvath, 2005). The WGCNA method has valuable advantages over knowledge-based networks such as protein-protein interaction (PPI) networks as it is not biased in favour of the known protein-protein interactions of the member nodes. The resultant network is constructed solely based on the pairwise expression correlation pattern of all genes. These networks are then hierarchically clustered into highly connected groups of genes called modules, and further examined through functional enrichment analysis. It has been shown previously that modularity is a conserved property of biological systems and modules of genes, proteins or metabolites have functional significance, i.e. the cellular functions are carried out by these highly connected modules of genes/proteins (Oldham et al., 2006; Oldham et al., 2008). These functional modules tend to be extremely heterogeneous, wherein the majority of the nodes have relatively few connections (edges) with other nodes, thus rendering them less relevant in the

overall function of the module, while a few "hub" nodes are highly connected and therefore are considered important regulators of the given module (Ravasz et al., 2002).

Once a healthy state and a dysfunctional state are defined in a gene coexpression network graph, its architecture becomes a comparable and quantifiable attribute that is representative of the system. The topology of these networks can then be investigated and compared in order to identify important gene regulators and capture the differential connectivity and preservation of modules, which in turn reflect the overlap in biological pathways implicated in the conditions the networks are associated with.

Recently, it has been proposed that disease phenotypes that were previously thought of as distinct entities may share common pathological mechanisms and have strong molecular relationships (Barabasi, Gulbahce, & Loscalzo, 2011). Given the correlated incidence and shared clinical symptoms between TLE and AD, we hypothesized that the common pathological features might be a result of a strong molecular relationship between the two diseases in the form of a shared set of perturbed cellular pathways and dysregulated gene modules. Since the electrophysiological and morphological symptoms common to TLE and AD impact the hippocampus in the setting of both diseases, we set out to compare the transcriptome of hippocampal tissue affected by TLE and AD. To achieve this, we employed the framework of WGCNA (Zhang & Horvath, 2005) to construct signature gene networks representing TLE and AD, and then employed network preservation statistics methods (Langfelder et al., 2011) to compare and contrast the signature gene networks by measuring the preservation of TLE modules in the AD coexpression network. Additionally, since functional gene modules have been shown to be preserved even across different species (Miller, Horvath, & Geschwind, 2010; Oldham et al., 2006), we also examined the preservation of TLE modules in a non-demented control (NDC) network to facilitate distinction of homeostatic (common to all networks) and pathology-specific (characteristic to disease state) features.

4.2. Materials and Methods

4.2.1. Data pre-processing, normalization and covariate adjustment

In an effort to increase the sample size while reducing the loss of data due to variability of probe sets in different microarray platforms, we selected and compiled three microarray datasets with a total of 50 samples from late onset AD hippocampal tissue (GSE28146, GSE5281, GSE48350) (Berchtold et al., 2013; Blalock, Buechel, Popovic, Geddes, &

Landfield, 2011; Liang et al., 2008) and three microarray datasets with a total of 87 hippocampal samples (GSE110298, GSE5281, GSE48350) (Berchtold et al., 2013; Berchtold et al., 2019; Liang et al., 2008) from non-demented individuals for the control (NDC) coexpression network (Table 4.1). These were the datasets that were generated using the same microarray platform with largest total sample size from all available sets. For the TLE gene coexpression network, we acquired a publicly available microarray dataset of 129 samples from hippocampus of patients who had been diagnosed with TLE and had undergone epilepsy resective surgery (GSE63808) (M. R. Johnson et al., 2015). The datasets used in this study are listed in Table 4.1. All expression sets were acquired from NCBI Gene Expression Omnibus via GEOquery R package (version 2.52.0) and the probe annotations were mapped to Entrez IDs (Davis & Meltzer, 2007).

Accession #	Condition	Brain region	Samples	Publication
GSE63808	**TLE**	**hippocampus**	**129**	**Johnson *et al*, 2015**
GSE5281	**AD**	**hippocampus**	**10**	**Liang *et al*, 2007**
GSE28146	**AD**	**hippocampus**	**22**	**Blalock *et al*, 2011**
GSE48350	**AD**	**hippocampus**	**19**	**Berchtold *et al*, 2013**
GSE5281	**NDC**	**hippocampus**	**13**	**Liang *et al*, 2007**
GSE48350	**NDC**	**hippocampus**	**43**	**Berchtold *et al*, 2013**
GSE110298	**NDC**	**hippocampus**	**34**	**Berchtold *et al*, 2019**

Table 4.1. List of datasets used for the Chapter 4 analyses. All raw microarray datasets were downloaded from NCBI Gene Expression Omnibus using the GEOquery R package.

Initial data visualization was facilitated by NetworkAnalyst web tool (G. Zhou et al., 2019). In the instances where multiple probes were mapped to the same gene, the average of multiple probe intensities was used to perform gene-level summarization. The expression sets were then filtered for low abundancy genes (the 5th percentile of all annotated genes with lowest relative abundance), log2 transformed and VSN normalized. The ComBat algorithm within SVA R package (version 3.32.1) was employed for batch effect correction, followed by Principal component analysis for visualization (Figure 4.1a,b) (Leek, Johnson, Parker, Jaffe, & Storey, 2012). An Empirical Bayes-moderated linear regression function (empiricalBayesLM) within WGCNA R package (version 1.67) was used for covariate (age and sex) adjustment (Langfelder & Horvath, 2008). The resultant filtered, normalized and covariate-adjusted

matrices with a total of 17821 matched probes/genes were used to generate coexpression networks for the three conditions.

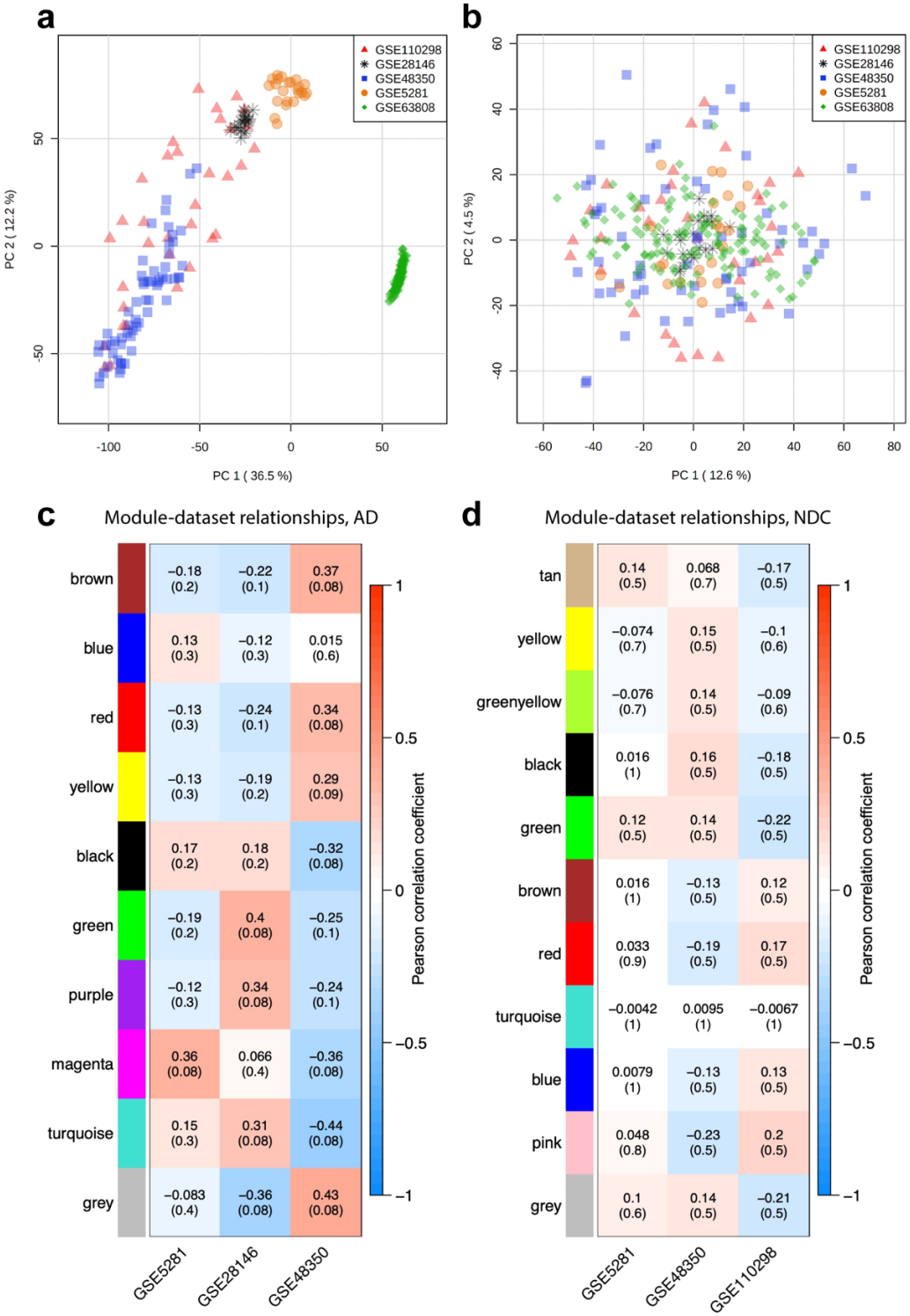

Figure 4.1. Quality control for covariates and batch effects. (a-b) Principal component analysis of expression distribution of all datasets a) before batch effect adjustment and b) after batch effect adjustment with ComBat algorithm. (c-d) Heatmap detailing the relationship between the datasets (x axis) and all detected modules (y axis) and in the c) AD and d) NDC networks. Each block in the heatmap shows the direction (red: positive, blue: negative), strength (Pearson correlation coefficient, top number) and FDR-adjusted significance (in brackets) of the Pearson correlation of the given module to each dataset that was used to generate the network.

4.2.2. Weighted gene coexpression network analysis (WGCNA)

Three weighted gene coexpression networks were constructed, one for each condition: TLE, AD and NDC. First, a sample dendrogram was created for each condition via hierarchical clustering of all samples in order to identify and remove outliers (Figure 4.2a). A correlation matrix was constructed based on pair-wise Pearson correlation coefficients of the expression level of all genes across all samples in the set, reflecting the coexpression similarity measure between all pairs of genes. A series of soft thresholding powers were then used to determine the optimal power at which the correlation matrices fit the scale-free topology model, i.e. when the characteristics of the network become independent of its size (Figure 4.2b,c). The correlation matrix reached a 90% fit to scale-free topology at ß=5 for AD and NDC datasets, and ß=7 for TLE dataset (Figure 4.2b,c). An adjacency matrix was then built for each condition by raising the correlation coefficients to the determined soft power of ß=5 for AD and NDC, and ß=7 for TLE. A correlation network representing each condition was constructed based on the respective adjacency matrix, where each node corresponds to a single gene, and the edges are determined by the adjacency value between each pair of nodes, reflecting the connection strength and distance between them. All three networks were constructed as "signed" and clustered into modules of coexpressed genes through average linkage hierarchical clustering via "dynamic tree cut" algorithm (Langfelder, Zhang, & Horvath, 2008). Given that the AD and NDC coexpression networks were generated by combining data from multiple studies, in order to capture any dataset-specific effects on the generation of specific modules, the Pearson correlation was calculated between each dataset and module in the given coexpression network (Figure 4.1c,d). The minimum module size was set to 30 genes. The modules were then functionally annotated through pathway enrichment analysis. Central hubs were determined for each module by identifying the top 10 member genes with highest intramodular connectivity and significant correlation to module eigengene – the first principal component of the expression matrix of the corresponding module.

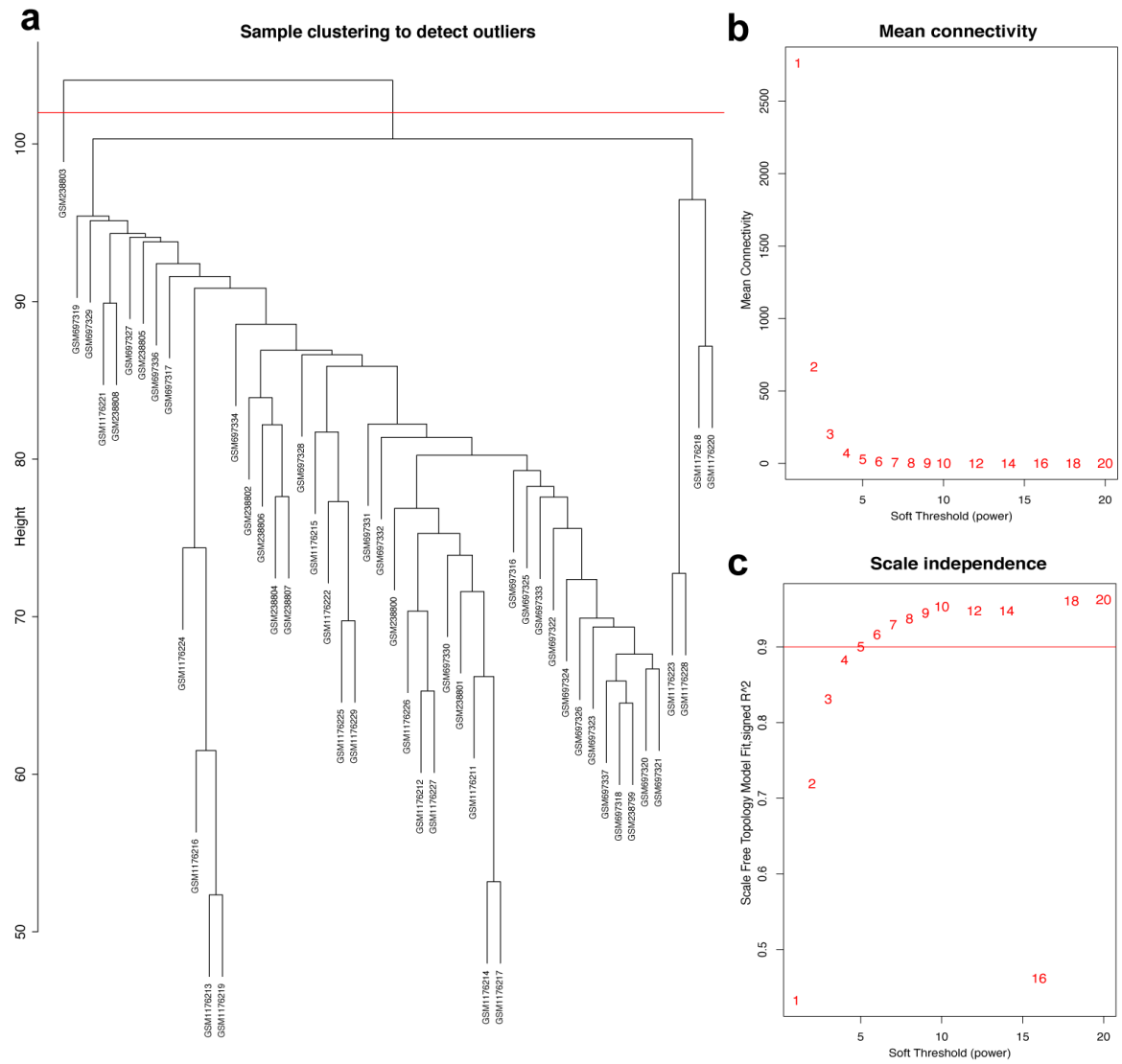

Figure 4.2. Scale-free topology model. a) clustering of AD samples and detection of outlier. b) relationship between soft threshold value ß (x-axis) and the b) average network connectivity and c) scale-free topology fit (y-axis). An R^2 value of 0.9 or 90% at ß=5 indicates that when raised to the power of ß=5, the network conforms to scale-free topology, i.e. the network connectivity becomes independent of its size.

4.2.3. Module preservation analysis

In order to understand the extent of preservation of TLE modules in the AD and NDC networks, we used two approaches. The first approach was cross-tabulation, which is a simpler method that creates a contingency table reporting the number of overlapping genes from each TLE module with each of the AD or NDC module. The significance of the overlap is calculated through Fisher's exact test. The second, more complex approach utilizes network separability, density and connectivity-based preservation statistics available within the modulePreservation function in the WGCNA R package (version 1.67) introduced by Langfelder et al and described in detail in (Langfelder et al., 2011) and (Oldham et al., 2006). This method requires adjacency

matrices of both reference (TLE) and test networks (AD and NDC) as input, however module assignment is only necessary for the reference-TLE network (Langfelder et al., 2011). The observed preservation value for each module detected in the TLE network was calculated in the AD and NDC networks. We then employed a permutation test (number of permutations=500) which randomly permutes the module assignment in the AD and NDC networks to assess if the observed value of preservation statistic is higher than what is expected by chance and assigns a permutation test p-value. The observed preservation values were then standardized with regard to the mean and variance and a significance Z score was defined for each preservation statistic. The overall significance of the observed statistics was assessed by combining multiple preservation Z statistics into a single overall measure of preservation defined as $Z_{summary}$. Thus, each module identified in the TLE network has a pair of $Z_{summary}$ scores which describe the preservation of the given module in the AD ($\boldsymbol{Z^{AD}_{summary}}$) and NDC ($\boldsymbol{Z^{NDC}_{summary}}$) networks, respectively. Modules with $Z_{summary}>10$ are considered well-preserved (Langfelder et al., 2011), thus the higher the $Z_{summary}$ score, the stronger the evidence of preservation of the given TLE module in the two test networks. In order to compare the degree of preservation of each TLE module between the AD and NDC networks, we introduce a surrogate quantifier of "differential module preservation" – $\boldsymbol{\Delta Z_{summary}}$, which is the arithmetic difference between the two preservation scores:

$$\Delta \boldsymbol{Z_{summary}} = \boldsymbol{Z^{AD}_{summary}} - \boldsymbol{Z^{NDC}_{summary}}$$

thus, the modules with a positive $\boldsymbol{\Delta Z_{summary}}$ value are more preserved (show Gain Of Preservation, GOP) and the modules with a negative $\boldsymbol{\Delta Z_{summary}}$ value are less preserved (show Loss Of Preservation, LOP) in the AD network compared to the control-NDC network.

4.2.4. Functional annotation and enrichment analysis

In order to determine the functional significance of the detected modules, a pathway enrichment analysis of the genes constituting each module was performed using the g:Profiler web tool (Reimand et al., 2016). Since the Gene Ontology database has a hierarchical order, in the instances of a large number (hundreds) of enriched pathways, we clustered the GO terms lower in hierarchy into their representative "parent" terms higher in the hierarchy using a similarity threshold of 90% (Supek et al., 2011).

4.3. Results

4.3.1. Temporal lobe epilepsy (TLE) coexpression network

After filtering, probe annotation and removal of outliers, a total of 127 samples were included in the TLE coexpression network. Hierarchical clustering identified 18 modules of highly coexpressed genes, ranging from 27 to 999 nodes in size. The modules were annotated based on the functional enrichment analysis of member genes, with the most enriched pathways in the top hierarchy levels being used as functional labels. Functional annotation of member genes from all modules rendered significantly enriched Gene Ontology terms and KEGG pathways, ranging from a few dozen to several hundreds (Figure 4.3.a). Interestingly, the largest module (Turquoise, 999 nodes) which is enriched for genes involved in synaptic signalling and neurotransmission processes in the GO biological process category, also identified "Pathways of neurodegeneration" and "Alzheimer Disease" among top significantly enriched KEGG pathways (FDR=$1.04x10^{-8}$, FDR=$6.15x10^{-7}$). This finding suggests that in TLE, the genes responsible for neurotransmission and signal transduction behave in a manner characteristic to Alzheimer's Disease pathology. A smaller module (Tan, 84 nodes) which is enriched for neurogenesis and GABAergic signalling pathways was identified as enriched for 35 terms from the human phenotype ontology database, all indicating seizure or epilepsy-related ontologies.

4.3.2. Alzheimer's Disease coexpression network

After filtering and removal of outliers, a total of 49 samples were included in the AD coexpression network. WGCNA identified 10 modules of highly coexpressed genes, ranging from 32 to 708 nodes in size (Figure 4.3.b). The largest module (also labelled as Turquoise) is enriched for neurotransmission and synaptic signalling-related processes such as "chemical synaptic transmission" (FDR=$1.1x10^{-34}$), "voltage gated channel activity" (FDR=$4.25x10^{-8}$), "ion transmembrane transport" (FDR=$1.02x10^{-21}$) and "neurotransmitter transport" (FDR=$2.18x10^{-14}$). No significant correlation ($P_{adj}<0.05$) between specific datasets and modules were detected in either AD nor NDC networks (Figure 4.1c,d).

4.3.3. Non-demented control coexpression network

After filtering and removal of outliers, a total of 84 samples were included in the NDC network. WGCNA identified 11 modules of highly coexpressed genes which were substantially larger in size (ranging from 160 to 2836 nodes) than those identified in TLE and AD networks. The two largest modules (Blue and Turquoise) were enriched for processes involved in gene expression and metabolism, respectively. Three smaller modules (Yellow, Black, Greenyellow) were enriched in synaptic signalling processes and voltage gated channel activity (Figure 4.3.c).

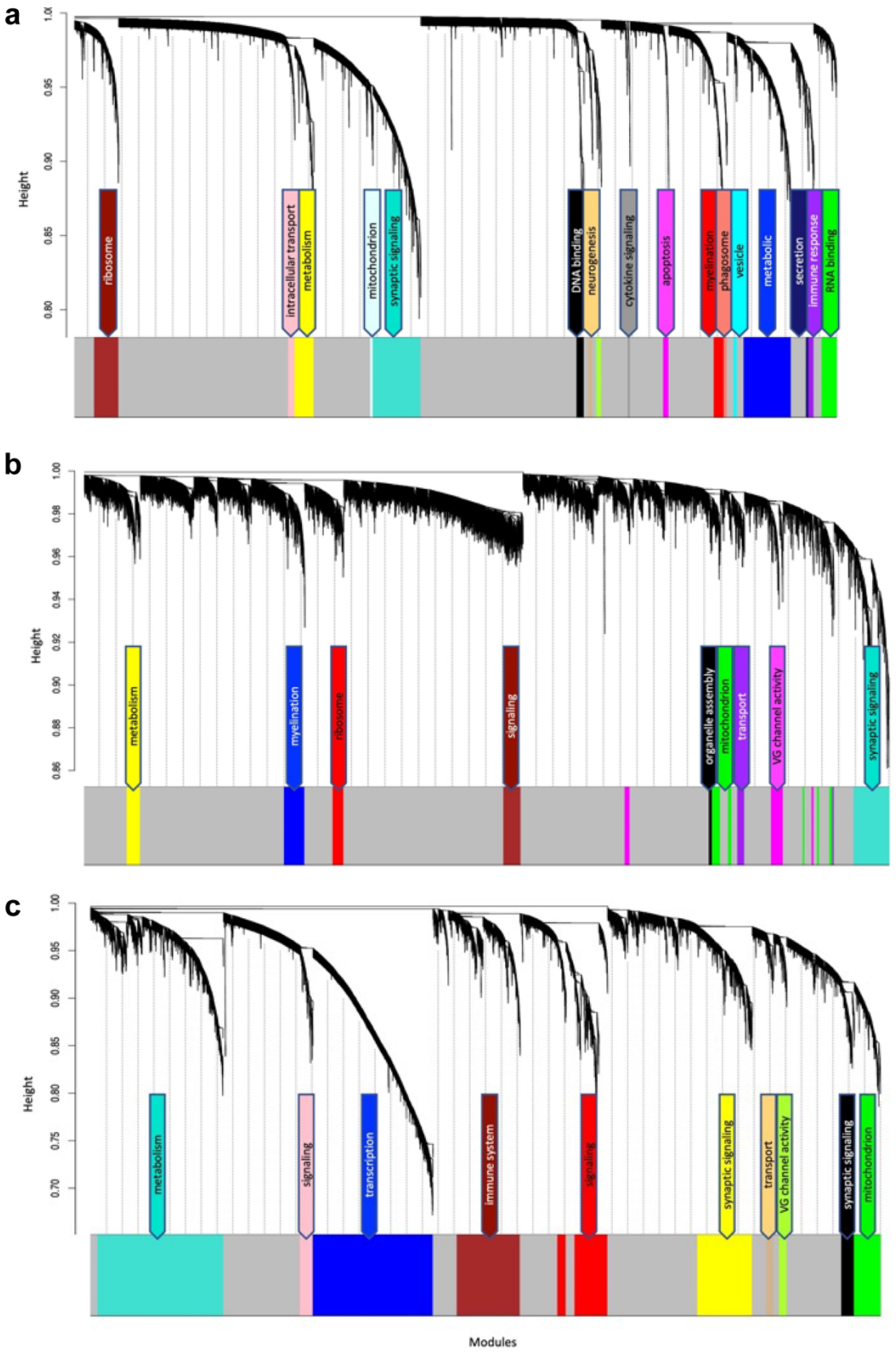

Figure 4.3. Hierarchical cluster dendrogram of a) TLE b) AD and c) NDC gene coexpression networks. Each black branch (vertical line) corresponds to one gene. The colour rows below the dendrogram indicate module membership. The modules are functionally annotated and named based on the enriched GO/KEGG pathways of the member genes. The grey module contains genes that have no specific module assignment i.e. the expression pattern of these genes does not show sufficient variability.

4.3.4. TLE modules are preserved to various degrees in AD and NDC networks

In order to capture any similarities within the module composition and network architecture of the two pathological gene networks, while allowing for discrimination between unperturbed (homeostatic) and perturbed (dysregulated) modules, two pairs of comparisons were made: [TLE vs AD] and [TLE vs NDC]. Several large modules showed significant overlap in member genes between both pairs of networks as measured by cross-tabulation of every module from TLE network with those from AD (Figure 4.4.a) and NDC (Figure 4.4.b) networks. The most significant (P≈0) overlap was observed between the two Turquoise modules in the TLE and AD networks, both of which are enriched for synaptic signalling pathways (Figure 4.5.a). The density and connectivity-based preservation scores as calculated by the modulePreservation function are shown in Figure 4.5.a for each of the TLE modules. The arithmetic difference between the two preservation scores designated as $\Delta Z_{summary}$ was used to define modules which show Gain Of Preservation (GoP) or Loss Of Preservation (LoP) in the AD network when compared to the NDC network (Figure 4.5.b). In the following sections, we characterise the overlap and preservation of TLE modules in AD and NDC networks based on the biological pathways they represent.

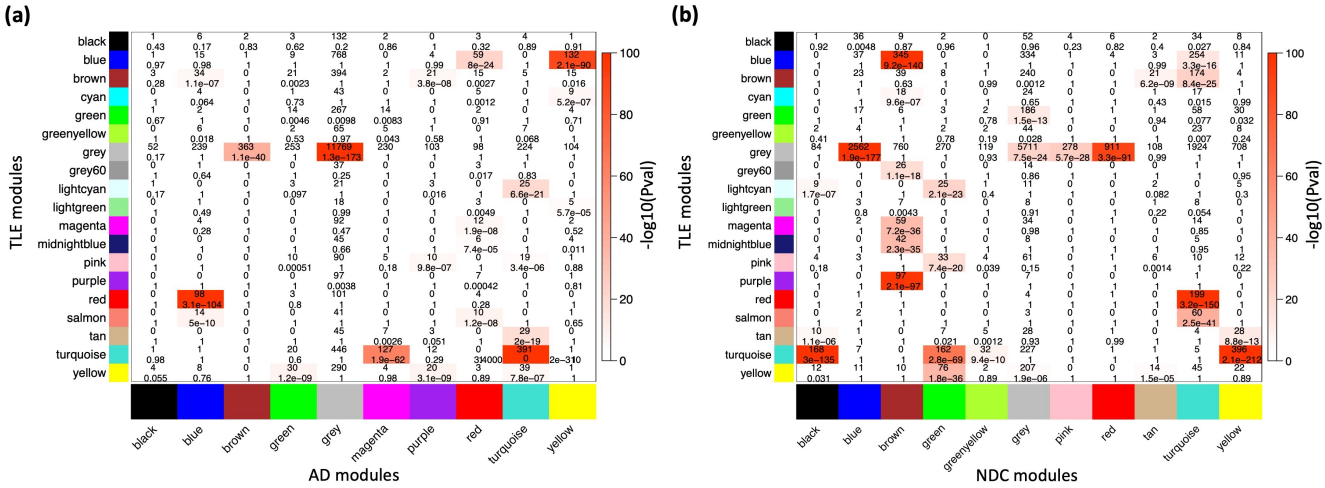

Figure 4.4. Cross-tabulation of TLE modules (in Y axis) against a) AD and b) NDC modules (in X axis). Each axis is labelled by the corresponding module colour. Each block in the table shows the number of overlapping genes in the intersection of corresponding **a)** TLE and AD and **b)** TLE and NDC modules. The table is colour-coded with -log10 of the P value associated with the Fisher exact test.

4.3.5. Synaptic signalling

The largest GOP (by ~60%, $\Delta Z_{summary}$=40.7) was observed in the Turquoise module, which functionally annotates to synaptic signalling processes. With a $Z_{summary}$ of 109.5, this module is extremely well preserved between TLE and AD coexpression networks (Figure 4.5.a). The corresponding preservation score for this module between TLE and NDC coexpression

networks is $Z_{summary}$ = 68.8. With voltage-gated sodium channel 3 subunit B (*SCN3B*) as a hub gene, this module is enriched for voltage-gated ion channel activity, synaptic signalling and neurotransmission pathways. There is significant ($p=2x10^{-310}$) overlap between the genes constituting the TLE Turquoise module with the corresponding neurotransmission-associated module in the AD network (also labelled Turquoise, Figure 3a). In the NDC network, the TLE Turquoise module appears to split into three distinct modules (Figure 4.4.b), two of which (Black and Yellow) functionally annotate to synaptic signalling pathways, while the third, Green module is enriched for mitochondrial-based processes (Figure 4.3.c). These results suggest homologous restructuring and perhaps perturbation of synaptic signalling pathways in TLE and AD-affected hippocampus compared to NDC. The WGCNA clustering algorithm identified another smaller module (Tan) in the TLE coexpression network, which functionally annotates to synaptic signalling and neurogenesis-related pathways. The Tan module shows GoP ($\Delta Z_{summary}$ =10.2) and contains a GABA receptor subunit (*GABRB3*) and an alpha subunit of VGSC (*SCN2A*) as its top regulatory hub genes. Although this module is enriched for GO terms that are similar to Turquoise module, according to the gene correlation dendrogram (Figure 4.3.a), these modules branch off from each other at a high hierarchy level, and are therefore two distinct, independent modules. There is similar overlap of genes between the TLE Tan module with corresponding neurotransmission-associated modules in both AD and NDC networks (Figure 4.4. a,b).

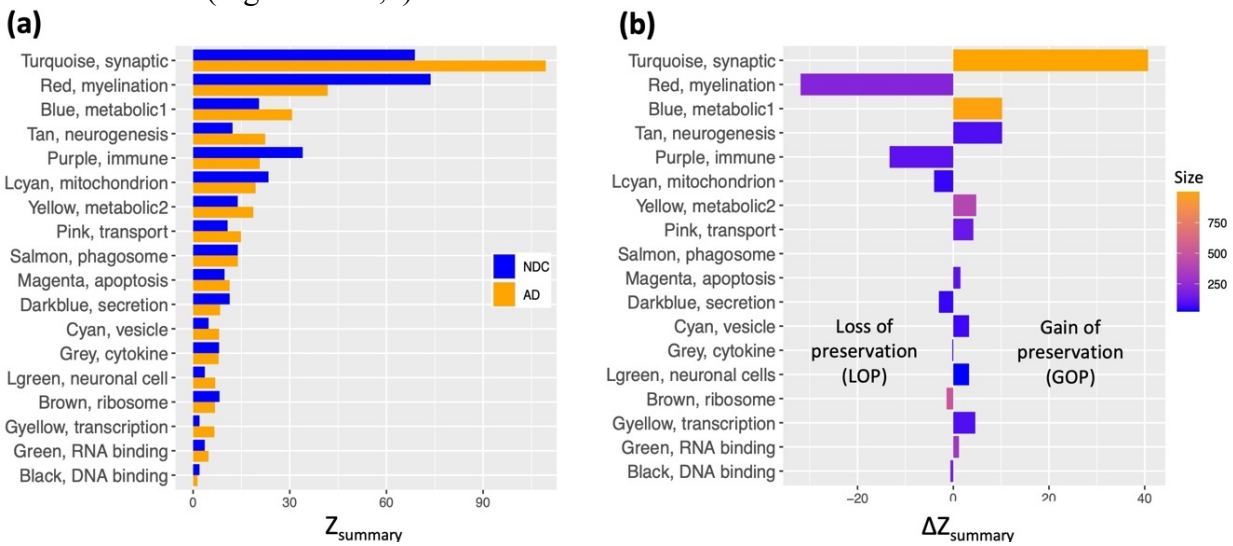

Figure 4.5. Comparison of density and connectivity-based preservation of TLE modules in AD and NDC networks. a) The overall significance of the observed preservation statistics was assessed for each TLE module (Y axis) by combining density and connectivity-based preservation Z statistics into a single overall measure of preservation defined as $Z_{summary}$ shown in pairs on X axis for NDC (blue bars) and AD (orange bars) networks. **b)** The arithmetic difference of preservation $Z_{summary}$ values, $\Delta Z_{summary}$ in X axis between NDC and AD networks for each of the TLE modules in Y axis. Positive $\Delta Z_{summary}$ indicates gain of preservation (GOP, more preserved) axnd negative $\Delta Z_{summary}$ indicates loss of preservation (LOP, less preserved) of the given TLE module in the AD network compared to NDC network.

4.3.6. Metabolism

There are two distinct TLE modules (Blue and Yellow) with member genes that are enriched for metabolic processes (Figure 4.3.a), both of which show GoP ($\Delta Z_{summary}$ =10.2 for Blue and $\Delta Z_{summary}$ =4.8 for Yellow, Figure 4.5.b). The larger, Blue module has 989 member genes, with thyroid hormone receptor interactor 6 (*TRIP6*) as its top regulatory hub gene and functionally annotates to metabolic, cellular organization, transport, and other homeostatic processes. The smaller, Yellow module functionally annotates to more specific mitochondrial functions such as "oxidative phosphorylation", "ATP synthesis coupled proton transport" and "oxidoreductase activity" as well as multiple mitochondrion organization pathways. The hub gene for this module is Acid phosphatase 1 (*ACP1*), the main function of which is hydrolysis of tyrosine and its phosphates. When cross referencing the KEGG database, the genes comprising the Yellow module rendered "Alzheimer's Disease" as one of the most enriched KEGG pathways ($P_{adj}=8.54x10^{-6}$).

Another small metabolic TLE module (Lightcyan) with 53 member genes shows LOP ($\Delta Z_{summary}$ = -4.0, Figure 4.5.b) between AD and NDC networks. The Lightcyan module is highly enriched for mitochondrial-based processes and has *YWHAG* as a central hub gene. *YWHAG* codes for the Tyrosine 3-Monooxygenase activation protein Gamma, also known as Protein Phosphatase 1, regulatory subunit 170, which belongs to a family of proteins that mediate signal transduction and are involved in many vital cellular processes such as metabolism, apoptosis and cell cycle regulation. The top enriched pathways of this module include "TCA cycle and respiratory electron transport", "mitochondrial ATP synthesis coupled electron transport", "ATP metabolic process" and other oxidative phosphorylation-related pathways.

4.3.7. Myelination

Another module of interest showing substantial LoP is the Red module, with 206 member genes and $\Delta Z_{summary}$ of -31.9 (Figure 4.5.b). This module is enriched for genes involved in myelination and axon ensheathment pathways, and as a central hub gene has NK6 homeobox 2 (*NKX6-2*), which is a transcription factor involved in axon-glial interactions at nodes of Ranvier. The Red module shows significant overlap of member genes with the corresponding myelination-associated module in the AD coexpression network (labelled Blue, Figure 4.4.a) and a large, metabolic module (labelled Turquoise, Figure 4.4.b) in the NDC coexpression network.

4.3.8. Immune system

The final TLE module of interest showing LoP ($\Delta Z_{summary}$ = -13.3) is the immune system-associated Purple module, with 107 member genes and transmembrane immune signalling adaptor (*TYROBP*) as a central regulatory hub gene. This module is enriched for immune system processes such as leukocyte activation, cytokine production and signalling, antigen processing and presentation, interferon signalling and other inflammatory pathways. With 97 out of 107 genes in common, there is significant overlap ($p=2.1x10^{-97}$) between the genes constituting the Purple module in the TLE network and the Brown immune system-associated module in the NDC network (Figure 4.3.c, 4.4.b). The same 97 genes from TLE Purple module overlap with the unassigned (Grey) module in the AD network (Figure 4.4.a), indicating that immune signalling involving these genes may be dysregulated in AD.

4.4. Discussion

The aim of this study was to characterize the shared molecular signature of AD and TLE and identify commonly dysregulated pathology-specific gene modules which could explain the correlated incidence of the two diseases. Given that the electrophysiological and morphological symptoms common to TLE and AD severely impact the hippocampus, we selected publicly available transcriptomic datasets from hippocampal tissue of relevant pathological and control states. In order to generate a reliable and robust gene coexpression signature of a disease, it is imperative to have datasets with a large number of samples. At the time of our analysis, there was no single publicly available transcriptomic dataset profiling the hippocampus of AD patients that had more than 25 samples for each group, therefore, we employed a common strategy to increase statistical power by combining several datasets together using a statistical methodology while accounting for batch effects and covariates (detailed in Methods).

According to our findings, AD and TLE show similar rewiring of synaptic transmission and metabolism-related gene networks. Perturbed synaptic transmission is not surprising, considering that circuit dysfunction and hyperexcitability are common features of both pathologies. The *SCN3B* gene which codes for a beta subunit of voltage gated sodium channel NaV1.1 was identified as the main regulatory hub gene of the synaptic transmission-associated Turquoise module identified in the TLE network, which shows the highest preservation score and largest GOP in AD coexpression network. As the most connected node of the Turquoise module, *SCN3B* is an interesting regulatory hub candidate. The beta subunits of voltage gated (VG) ion channels carry a multitude of essential functions. In addition to being VG channel

modulators, the beta subunits also function as cell adhesion molecules and regulators for voltage-gated sodium channel (VGSC) alpha subunit gene expression, due to being substrates for sequential cleavage by beta secretase (BACE1) (Wong et al., 2005). The expression of BACE1 is reportedly increased in AD pathology, resulting in abnormal VGSC beta subunit cleavage, which has been shown to result in reduced levels of functional NaV1.1 channels on the surface of GABAergic interneurons, leading to network disinhibition and higher susceptibility to seizures in mouse models of AD (B. F. Corbett et al., 2013; D. Y. Kim et al., 2007; D. Y. Kim et al., 2011).

Mutations in the genes that code for both alpha and beta subunits of VGSC are implicated in various neuropathologies (O'Malley & Isom, 2015). Pathological levels (both increase and decrease) of *SCN3B* mRNA have been implicated in multiple neurodegenerative diseases such as amyotrophic lateral sclerosis and Alzheimer's disease as well as cancer (Adachi et al., 2004; Dunckley et al., 2006; Nutini et al., 2011). Another central hub gene of this module, Ephrin type A receptor 4 (*EPHA4*), belongs to the protein-tyrosine kinase family and has been implicated in various synaptic dysfunction-related pathologies, including AD and TLE (A. K. Fu et al., 2014; Shu et al., 2016). Under homeostatic conditions, the EphA4 acts as a negative regulator of neurotransmission and synaptic plasticity in the hippocampus (Murai & Pasquale, 2011). It has been shown to become deregulated and overactivated, resulting in synaptic failure, in mouse models of AD (A. K. Fu et al., 2014) and TLE (Shu et al., 2016) pathology. In these models, blockade/knockdown of the receptor rescues the synaptic impairment. It is therefore conceivable that deregulation and downstream signalling of EphA4 is one of the shared pathological mechanisms between AD and TLE, which leads to abnormal neurogenesis and impairments in synaptic signalling.

The second notable module of interest is the neurogenesis-associated Tan module. Despite the small size of this module, the expression pattern of its 84 member genes is closely correlated in TLE and AD networks, resulting in formation of an independent module that is highly preserved and shows substantial GOP in the AD network compared to NDC. The Tan module also appears to be a seizure-associated module. Central hub genes among the top 10 most connected nodes centrally located in this module include *GABRB3* (gamma-aminobutyric acid type A receptor subunit beta3), *SCN2A* (sodium voltage-gated channel alpha subunit 2), *PRICKLE1* (Prickle planar cell polarity protein 1) and *FRMPD4* (FERM and PDZ domain containing 4). These genes have been shown to be associated with various types of seizures

and EEG abnormalities (M. A. Corbett et al., 2010; Euro, Epilepsy Phenome/Genome, & Epi, 2014; Polan et al., 2014). Notably, all 35 significantly enriched (P_{adj}<0.05) phenotypes associated with the Tan module from human phenotype ontology database implicate EEG abnormalities and epileptiform activity. These phenotypes have been observed in patients with AD and various epilepsy disorders (K. A. Vossel et al., 2012; K. A. Vossel et al., 2013; K. A. Vossel et al., 2016) and reported in animal models of AD (Bezzina et al., 2015; Drinkenburg et al., 2017; Kam, Duffy, Moretto, LaFrancois, & Scharfman, 2016; Ziyatdinova et al., 2011; Ziyatdinova et al., 2016). Epileptiform activity is one of the major clinical features shared between AD and TLE, and is thought to contribute to more rapid disease progression and cognitive decline (Volicer et al., 1995; K. A. Vossel et al., 2013; K. A. Vossel et al., 2016), therefore, further investigation of this distinct disease module has the potential of facilitating more targeted treatment options.

The second largest difference in TLE module preservation scores was observed for the Red module ($\Delta Z_{summary}$ = -31.9), which annotates to myelination and axon ensheathment processes. While a $Z_{summary}$ score of 41.8 is still indicative of very strong preservation (Langfelder et al., 2011) in the AD network, the large difference in the preservation score of the corresponding module in the NDC network ($Z_{summary}$=73.7) suggests that the operation of myelination and axon ensheathment processes is at least partially altered in the setting of AD compared to TLE and NDC. Indeed, it has been reported before that myelination-associated gene modules are severely perturbed in the prefrontal cortex of AD (B. Zhang et al., 2013). Impairment in cholesterol metabolism which is detected in AD brain (Martins et al., 2009; Sodero et al., 2012) could lead to alterations in the myelination processes, since 25% of the total cholesterol in the human body is allocated to the brain, where it is mostly localized to the plasma membranes of neurons and glia, and myelin sheaths covering the axons (Bjorkhem & Meaney, 2004). This may explain why the myelination module from TLE coexpression network is less preserved in the AD network compared to NDC.

Given the evidence of strong neuroinflammatory presence in both AD and TLE pathologies (Akiyama et al., 2000; Glass, Saijo, Winner, Marchetto, & Gage, 2010; Maroso et al., 2011; Maroso et al., 2010; Vezzani, French, Bartfai, & Baram, 2011), it is somewhat surprising that the Purple immune system-associated module is substantially less preserved between TLE and AD, compared to TLE and NDC networks. The central regulatory hub gene of the Purple module is *TYROBP*, which has been previously identified as a causal regulatory hub within a

microglia-associated module generated from prefrontal cortex samples from late onset AD patients (B. Zhang et al., 2013). Several studies investigating gene regulatory networks of AD showed disruption of normal microglial gene modules (Efthymiou & Goate, 2017; Mukherjee et al., 2019; B. Zhang et al., 2013). We therefore speculate that in the AD-affected hippocampus, there is rewiring of microglial gene networks that is distinct from TLE and NDC.

When considering the periodic increase in neuronal energy demand to sustain seizures, it is not surprising that metabolic pathways are among the primary characteristics of the molecular signature of TLE. A relatively new but growing hypothesis is that neurodegenerative disorders, including late onset AD and several types of acquired epilepsy arise from metabolic dysfunction and are aggravated by oxidative stress and mitochondrial dysfunction (Lin & Beal, 2006; Mattson, 2004). Indeed, the majority of genes and proteins associated with the term "Alzheimer's Disease" in various biological pathway databases belong to metabolic pathways (Harris et al., 2004; Joshi-Tope et al., 2005; Ogata et al., 1999; Thomas et al., 2003). A large number of these pathways were significantly enriched (FDR<0.05) in both metabolic modules (Blue and Yellow) of the TLE network and the Yellow metabolic module in the AD network. This suggests that perturbations in redox balance, oxidative phosphorylation and other mitochondrial processes are important players in epileptogenesis and should be studied further.

The results of our analysis suggest that in addition to clinical and morphological features, Alzheimer's Disease and temporal lobe epilepsy share specific defects in the molecular mechanisms that regulate excitability, synaptic signalling, neurogenesis and mitochondrial pathways. Perturbed metabolism and mitochondrial dysfunction may contribute to impairment in neurotransmission and consequently lead to the electrophysiological abnormalities and cognitive symptoms seen in both AD and epilepsy disorders. As the pathology progresses, accumulation of reactive oxygen species could increase epilepsy sensitivity and result in seizure development. On the other hand, epileptic activity may aggravate the cognitive decline and neurodegeneration in AD, thus putting the patients in a vicious cycle of debilitating symptoms and fast progression of disease. In the absence of a clear causal mechanism such as traumatic brain injury or genetic mutation, it is challenging to determine which factor is the metaphorical 'chicken' and which is the 'egg' due to the enormous variation in immune and metabolic profiles, vast variety of lifestyles, environmental circumstances and combinations of life events. As shown here, a systems level network-based approach wherein gene modules represent emergent global properties of biological function, provides a useful tool for

hypothesis generation, which then would be subject to experimental validation. We demonstrate that gene coexpression network analysis and network preservation statistics methods can be used for a holistic, hypothesis-free, systems-level examination and comparison of two pathological states, solely based on the gene coexpression network architecture of each state. Additionally, we present a list of central hub genes that have the potential of influencing the larger molecular network they regulate. The identification of pathology-related modules which are associated with the clinical features and phenotypes observed in the context of both diseases and the implication of these modules in the published epilepsy and dementia literature highlights the validity of our approach. However, further experimental evidence and pharmacological targeting of the identified regulatory hub genes and implicated cellular pathways is necessary for experimental validation.

CHAPTER 5

INVESTIGATING THE MOLECULAR AND CELLULAR MECHANISMS OF SYNERGY BETWEEN AMYLOID PATHOLOGY AND RECURRENT SEIZURES

5.1. Introduction

Epileptiform activity is more prevalent in AD patients than in the general population. In light of evidence from the familial AD mutation pedigrees and newly emerged epidemiological studies on clinical evidence, the epileptiform activity is likely underdetected and underdiagnosed in the AD patient cohort. Further, the presence of epileptiform activity predicts faster cognitive decline in AD, and it could promote disease progression through multiple mechanisms.

In previous chapters, we identified molecular mechanisms shared between AD and epileptiform disorders, leading to the proposal of a two-factor disease model for epilepsy and dementia. In this paradigm, the synergistic interaction between the two patho-mechanisms defines a distinct subpopulation of "dual-pathology" patients, characterized by faster disease progression and differing treatment outcomes. A number of recent studies have provided convincing evidence that co-occurrence of seizures and AD pathology is associated with more severe cognitive and biochemical disease profile (K. A. Vossel et al., 2016; K. A. Vossel et al., 2017). This suggests that, for the subgroup of epilepsy-prone AD patients, the accelerated cognitive deterioration is the inevitable consequence of disease progression and is likely precipitated by the synergistic interaction between AD pathology and recurrent seizures (Banote et al., 2022). The final experimental chapter of this thesis aims to characterize the molecular signature of a brain that simultaneously harbours amyloid pathology and recurrent seizures (referred to as "double pathology" throughout this chapter), in an attempt to identify the molecular mediators of synergy between amyloid pathology, recurrent seizures and cognitive decline. We utilized the 5xFAD transgenic mice coupled with the electrical amygdala kindling model of epileptogenesis to first demonstrate the already-present chronic circuit hyperexcitability in 5xFAD mice, while at the same time establishing recurrent seizure phenotype to better recapitulate the dual-pathology phenotype seen in human condition. In this experimental paradigm the amygdala-kindled 5xFAD mice represent the subpopulation of AD patients who developed recurrent seizures and are at risk of accelerated cognitive deterioration.

We then evaluated the effect of recurrent seizures on hallmark features of AD pathology – amyloid plaque load and cognitive behavioural performance. RNA sequencing and bioinformatic analysis of hippocampal tissue was conducted in order to investigate the molecular mechanisms of synergy between recurrent seizures and AD pathology as well as to identify key mediators of accelerated disease progression.

5.2. Materials and methods

5.2.1. Animals

All live animal procedures were approved by the Alfred Research Alliance Animal ethics committee (ethics number: E/1869/2018/M) and adhered to the Australian code for the care and use of animals for scientific purposes. All experiments were conducted by the researcher blinded to the genotype of mice.

Twenty-two-week-old female 5xFAD mice (N=20) and WT control littermates (N=22) were randomly assigned to experimental (kindled) and control (sham) groups (N=10-12 per group, $\sum N = 42$). All animals were housed under identical conditions, in temperature-controlled rooms with 12:12 hr dark-light cycle with *ad libitum* access to food and water.

5.2.2. Electrode implantation surgery and amygdala kindling procedure

The mice were placed under general anaesthesia and a stereotaxic surgery was performed under aseptic technique. An intradural stimulating bipolar electrode was implanted into the left amygdala (M/L: -3.1, A/P: -0.8, D/V: -4.2, relative to bregma). Epidural stainless steel screw electrodes were implanted on each side of frontal (active recording) and parietal (ground and reference) bones. All electrodes were secured to the skull with dental cement. Buprenorphine (0.05 mg/kg) and Carprofen (5mg/kg) were used as analgesic. The mice were single housed and allowed to recover for 7 days after the day of surgery, after which the kindling protocol commenced. On the 8th day post-surgery the after-discharge threshold was determined for each mouse by electrically stimulating the bipolar electrode with a burst of 1 msec biphasic square wave pulses at 60Hz frequency, starting at I=0.04 mA and incrementally increasing the current intensity (up to a maximum of 0.60 mA) until an electrographic seizure of >5 sec duration was observed. For all subsequent days, the mice were stimulated once a day at their individual ADT current intensity until each mouse experienced a total of 15 seizures. LabChart 7 software (ADInstruments) was used for controlling the stimulation and visualising the EEG data. The duration of each electrographic seizure was determined from the corresponding EEG trace. The severity of seizures was scored according to the Racine scale by two independent investigators

blinded to the genotype of mice. The animals in the sham groups were plugged to a mock EEG cable and handled in a similar manner as the kindled group, with the exception of delivering the electrical stimulation.

5.2.3. Y maze test

At least 48 hours after the last evoked seizure the mice underwent a Y maze test to assess the hippocampal-dependent spatial recognition and memory as previously described (Dellu, Mayo, Cherkaoui, Le Moal, & Simon, 1992). The maze consists of three equilaterally intersecting arms in the shape of "Y", with unique spatial cues positioned at the end of each arm. The test was conducted in two phases: during the first phase the mouse was placed in the "home" arm and allowed to freely explore only one ("familiar") of the remaining two arms for 15 minutes, while the third ("novel") arm was blocked from access. The mouse was then returned to its home cage for a 30 minute interval, and subsequently reintroduced to the Y-maze with free access to explore all three arms. Entries into the novel and familiar arms, total distance travelled, and time spent in each arm were quantified using a tracking software (TopScan Lite).

5.2.4. Tissue collection and histology

7 days after the last kindling stimulation the mice were injected with a lethal dose of pentobarbital (lethabarb) followed by transcardiac perfusion with ice-cold phosphate buffered saline (PBS). The whole brain was removed and divided into two hemispheres. The hippocampus was rapidly dissected from the left hemisphere and immediately flash-frozen in liquid nitrogen and stored at -80C until RNA extraction. The right hemisphere was immersion-fixed in 4% paraformaldehyde, dehydrated, embedded in OCT medium and frozen for immunohistochemical analysis.

5.2.5. Immunohistochemistry and microscopy

The PFA-fixed, OCT-embedded mouse brains were serially cryosectioned at 30µm thickness for immunohistochemistry. Table 1 includes all antibodies and dyes used for IHC, as well as the corresponding concentrations and further details. In order to objectively quantify the plaque load across the entire hippocampal formation, for each mouse, 5-6 equidistant coronal sections (each ~100 µm apart) were stained with 1% thioflavin S solution. Briefly, a 1% (w/v, in PBS) Thioflavin S solution was prepared fresh on the same day and filtered with 0.2 µm syringe filter. The brain sections were washed twice with PBS followed by 15-minute incubation in 1% Thio S solution, followed by consecutive 1-minute washes in 80% Ethanol and 70% Ethanol. The stained brain sections were then mounted on glass microscope slides and stored

away from light for 32 hours to allow for the mounting medium to dry. For high magnification visualization of amyloid plaques and surrounding ecosystem, as well as the morphology of plaque associated microglia and astrocytes, 3-dimentional Z-stack images were captured using either 40x or 60x oil immersion objectives on Nikon Ar1 confocal fluorescent microscope. Where indicated, orthogonal projections of Z-stacks were created, to facilitate visualization of cellular morphology and distribution.

5.2.6. Amyloid plaque area quantification

All ThioS-stained brain sections were imaged within 48 hours of staining, to prevent artefact variations in ThioS fluorescence due to oxidation. All images were captured on Nikon Ti-E widefield microscope using 20x magnification objective, with all settings and optical configuration kept identical. Using the Allen mouse brain atlas (mouse.brain-map.org, (Lein et al., 2007)), the hippocampal formation was precisely traced on an Apple iPad with Apple Pencil and using the same auto-threshold settings the total percentage of ThioS-immunoreactive area was measured for each brain section. We analysed 5-6 sections per animal, and the average % area ThioS / total area were compared between kindled 5xFAD and Sham 5xFAD groups.

Target	Reporter/antibody	Concentration or dilution factor	Catalog #
Dense core plaques	Thioflavin S	1% (w/v)	S6825
Amyloid β 1-42	Mouse anti Aß1-42	1:500	SIG-39142
APP 1-16	Mouse anti 6E10	1:1000	SIG-39320
Microglia	Goat anti Iba1	1:800	AB5076
Astrocytes	Rabbit anti GFAP	1:1000	Z0334
Vimentin	Rat anti Vim	1:500	MAB2105
Neuronal nuclei	Mouse anti NeuN	1:500	MA5-33103
All nuclei/chromatin	DAPI	1:10000	D-1306

Table 5.1. A list of primary antibodies and fluorescent dyes used for IHC labelling of brain tissue.

5.2.7. RNA sequencing, and differential expression analysis

The total RNA was extracted from the left hemisphere hippocampal tissue using Nucleo-spin RNA extraction kit (Maccerey-Nagel). A total of 42 RNA samples (4 experimental groups, n=10-12 each) were sent to BGI for library preparation and RNA sequencing, all of which

passed quality control. The transcriptome library was constructed and sequenced by BGI on DNBseq platform. After filtering and adapter trimming, ~20 million clean paired-end reads (150bp long) per sample were generated. An in-house pipeline featuring a STAR aligner (Tsyganov, Perry, Archer, & Powell, 2018) was used for mapping the raw reads to the mouse reference genome (GRCm38). The mapped reads were quantified via featureCounter, to produce a gene count matrix, which was then filtered for low abundance genes and TMM-normalized with EdgeR. A quasi-likelihood negative binomial generalized log-linear model was fitted to the TMM-normalized gene count data to perform differential expression analysis between the four experimental groups. For all pairs of comparisons, the significance threshold was set to FDR<0.05, with absolute fold change at FC>2.0.

5.2.8. Correlation network analysis by WGCNA

First, a sample dendrogram was created via hierarchical clustering of all samples in order to identify the presence of any outliers. A correlation matrix was constructed based on pair-wise Pearson correlation coefficients of the expression level of all genes across all samples in the set, reflecting the coexpression similarity measure between all pairs of genes. A series of soft thresholding powers were then used to determine the optimal power at which the correlation matrices fit the scale-free topology model, i.e. when the characteristics of the network become independent of its size. The correlation matrix reached a 90% fit to scale-free topology at ß=5. An adjacency matrix was then built by raising the correlation coefficients to the determined soft power of ß=5. A correlation network was constructed based on the respective adjacency matrix, where each node corresponds to a single gene, and the edges are determined by the adjacency value between each pair of nodes, reflecting the connection strength and distance between them. Networks were constructed as “signed” and clustered into modules of coexpressed genes through average linkage hierarchical clustering via “dynamic tree cut” algorithm (Langfelder et al., 2008). The minimum module size was set to 30 genes. Central hubs were determined for each module by identifying the top 6 member genes with highest intramodular connectivity and significant correlation to module eigengene – the first principal component of the expression matrix of the corresponding module. The correlation of modules to sample groups, behavioural data and amyloid plaque burden was assessed through Pearson correlation. The final networks were visualized in Cytoscape software version 3.6.9 (Shannon et al., 2003). In order to determine the functional significance and cell-type specific enrichment of detected modules, pathway enrichment analysis of the genes constituting each module was

performed using the EnrichR web suite (E. Y. Chen et al., 2013; Kuleshov et al., 2016; Xie et al., 2021).

5.2.9. Statistical analysis

Statistical significance was calculated using Prism 9 (GraphPad, La Jolla, CA, U.S.A.) and RStudio (2022.07.2). The normality of behavioural and imaging data was assessed by the Shapiro-Wilk test. The severity of first seizure and the number of stimulations required to elicit the first bilaterally convulsive class V seizure were compared between 5xFAD and WT groups using Mann-Whiney *U* test. Average seizure duration and total area covered by amyloid was compared between 5xFAD and WT, and kindled 5xFAD vs sham 5xFAD groups, respectively, using unpaired Student's t-test. The ratio of time spent in novel and familiar arms of Y-maze was compared between kindled and sham 5xFAD and WT groups via balanced ANOVA and Tukey's HSD test. The significance threshold for each analysis was set at $p<0.05$. Data in boxplots is presented as mean +- standard error (SEM). Statistical analyses are presented in the figure legends.

5.3. Results

5.3.1. 5xFAD mice showed hyperexcitable phenotype and impaired spatial memory

Electrographic afterdischarge was seen at comparable thresholds in all animals subjected to the kindling procedure, attesting the consistency of the implantation surgery procedure. The afterdischarge consisted of several seconds (>10 sec) of rhythmic spikes at high amplitudes and frequency of about 2-5 spikes per second. We used the behavioural severity of the first induced seizure and the number of kindling stimulations required to induce the first bilateral clonic convulsive seizure (class 5 seizure according to Racine scale) as indirect measure of hyperexcitability. More than half of 5xFAD mice (6 out of 10) had a class 5 behavioural seizure after the first kindling stimulation and after all subsequent stimulations, while an average of 8 stimulations were required to invoke a class 5 seizure in the WT group (Figure 5.1a,b). Additionally, the 5xFAD mice had on average significantly longer electrographic seizures and more severe (according to Racine scale, (Racine, 1972)) behavioural seizures (Figure 5.1c, d). The WT mice on average spent more time in the novel arm of the Y maze compared to the familiar arm, which is the normal behaviour of a mouse with intact spatial memory. In contrast, the 5xFAD mice showed no difference between the average time spent in the novel and familiar

arms of the Y maze when compared to the control group (Figure 5.1. e), suggesting impairment in hippocampal-based spatial memory.

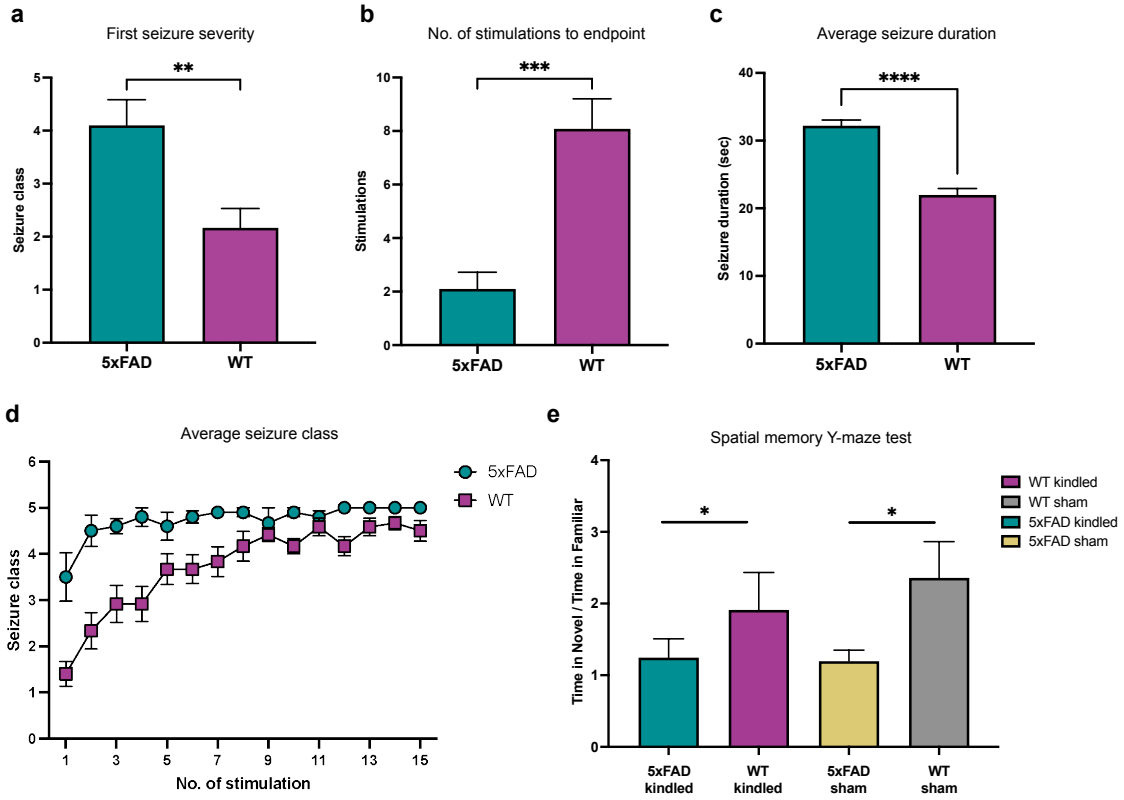

Figure 5.1. 5xFAD mice show hyperexcitable phenotype and impaired spatial memory. a. The 5xFAD mice had more severe seizures after the first stimulation compared to WT. **b.** Significantly fewer stimulations were required to induce the first bilaterally convulsive (Class 5) seizure in the 5xFAD compared to WT. **c,d.** the duration and Racine score of seizures experienced by 5xFAD mice were on average significantly higher compared to WT. **e.** The 5xFAD mice spent on average equivalent time in the novel and familiar arms of the Y-maze, while the WT group spent more time exploring the novel arm. *P<0.05, **P<0.01, ***P<0.001 and ****P< 0.0001. Box and whisker plots display the mean ± standard error of the mean (SEM).

5.3.2. Recurrent seizures lead to increased amyloid deposition.

Immunohistochemical labelling of amyloid plaques with Thioflavin S revealed widespread amyloid pathology throughout cortical regions and the entire hippocampal formation in 5xFAD mice (Figure 5.2.a,b). Notably, the Kindled 5xFAD showed a significant increase in ThioS-IR plaque area compared to shams. This effect was observed both in dorsal and ventral hippocampal sections (Figure 5.2. c,d). Moreover, the kindled 5xFAD brains showed vascular Aβ deposition in the leptomeningeal vessels, consistent with cerebral amyloid angiopathy (CAA, Figure 5.2.e). This pattern of vascular deposition was not observed in non-kindled 5xFAD mouse brain.

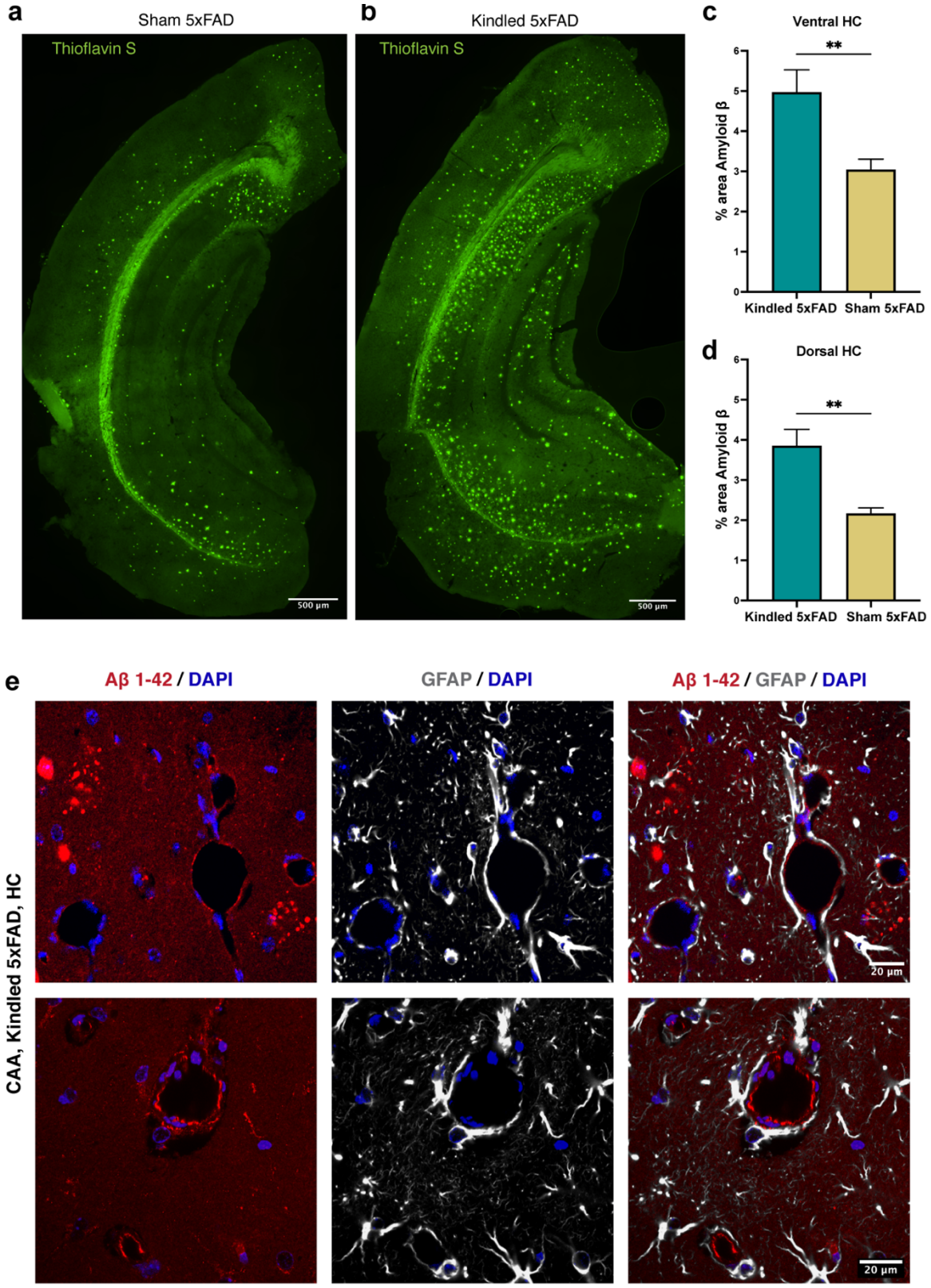

Figure 5.2. Recurrent seizures are associated with increased amyloid deposition in the hippocampus of 5xFAD mice. Thioflavin S stained brain sections of a. Sham 5xFAD and b. Kindled 5xFAD. The average ThioS-immunoreactive area fraction was compared between kindled and sham 5xFAD groups, revealing a total increase of amyloid plaque-covered area in Kindled group both in c. ventral and d. dorsal hippocampal sections. e. The Kindled 5xFAD brains showed histopathological features of cerebral amyloid angiopathy, reflected by vascular amyloid deposition.

5.3.3. Seizure-induced gene expression changes in 5xFAD mice

To explore alterations in the cellular responses to recurrent seizures in an unbiased manner, we performed RNA sequencing of hippocampal tissue from all 42 mice in the four experimental groups. Dimensionality reduction and principal component analysis showed group-specific clustering of samples and no batch effects between cohorts (Figure 5.3 a,b). Sample clustering by a principal component analysis of the top 1000 most variant genes revealed distinct clustering of 5xFAD and WT samples showing a relatively clean separation by genotype and kindling group (Figure 5.3 c). The first principal component accounted for 40.9% of the total variance and separated the mice by genotype into the 5xFAD and WT groups, while the second principal component separated the samples into kindled and sham groups (Figure 5.3 a).

Since we have a two-variable experimental design, with each variable representing the effect of the respective pathology (5xFAD – Alzheimer's Disease, kindling – epilepsy), we set up several group contrasts to delineate the singular and combined effect of each pathology.

Additionally, to capture gene expression changes caused by the interaction between the two variables, we conducted nested comparisons with interaction effect between the two pairs of experimental conditions and respective controls. Differential expression analysis identified hundreds of differentially expressed genes at FDR<0.05. The volcano plots **a-e** in **Figure 5.4** show the distribution of differentially expressed genes for each comparison group, while the pyramid plot in **Figure 5.4 f** summarizes the total number of significantly over- and under-expressed genes across all contrasts. Consistent with previous reports, almost three times as many of the DE genes were upregulated (n=424) in AD animals as were downregulated (n=116) in 5xFAD-Sham animals compared to WT controls (Figure 5.3 a). Functional enrichment analysis revealed that the downregulated genes were mostly involved in synaptic signalling and neurotransmitter synthesis/trafficking, while the upregulated genes were largely inflammatory and gliosis related (Figure 5.4 g).

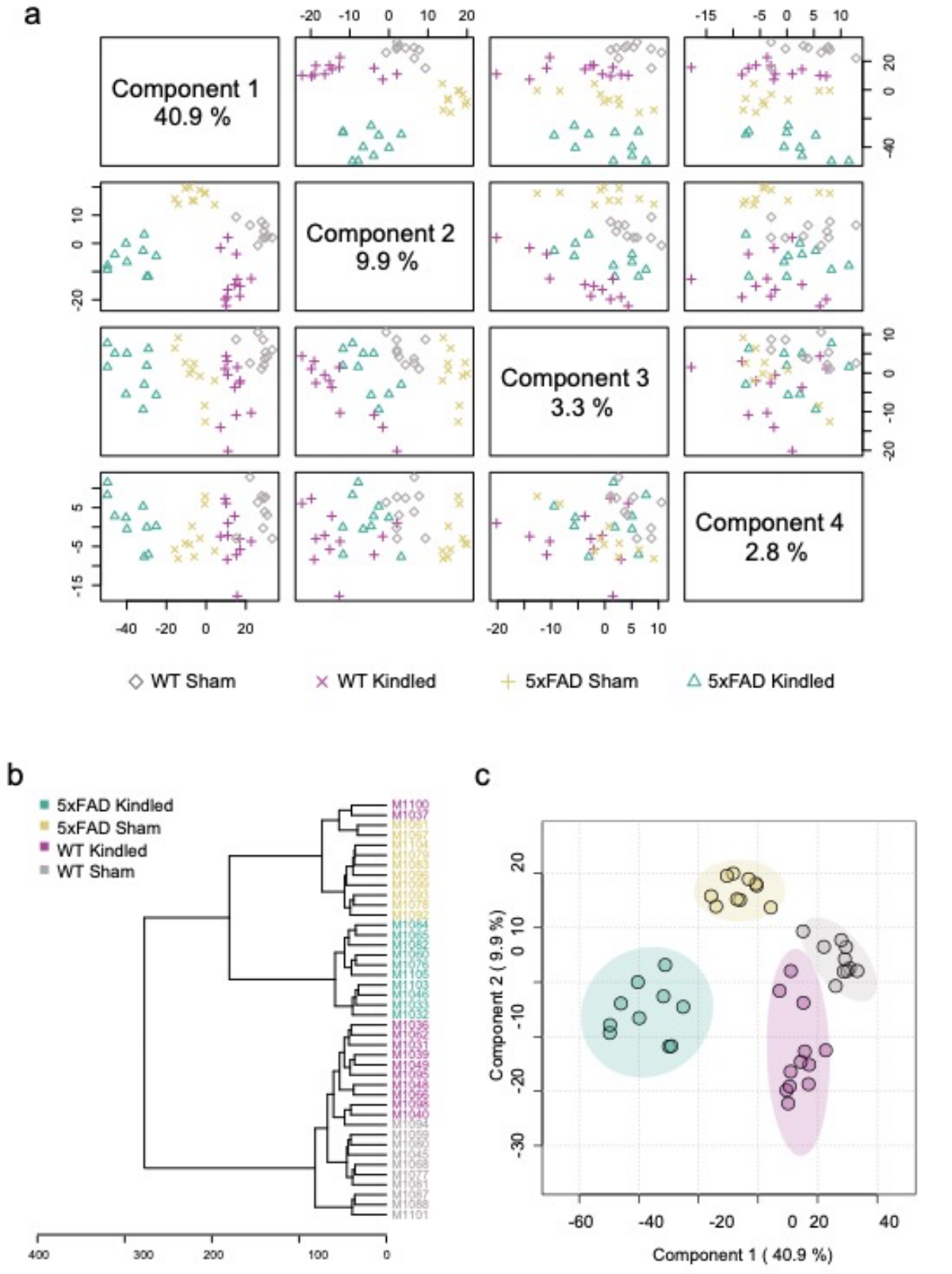

Figure 5.3. Principal component analysis of RNA-seq transcriptomics data. a. All 42 RNA-seq samples are plotted along different combinations of the top five principal components. **b.** summary PCA plot. The percent of variance explained by each principal component is displayed in the corresponding axis. **c.** sample clustering based on the top 1000 most variant genes in the dataset.

Interestingly, the overall direction of kindling-induced gene expression changes appeared to be genotype dependent: in the 5xFAD group, more than twice as many of the DE genes were upregulated (n=192) in kindled animals as were downregulated (n=77), whereas in the WT group the opposite pattern is seen, with twice as many (n=128) downregulated genes in kindled mice compared to the 65 genes that were upregulated (Figure 5.4 c). Moreover, there was a striking increase in the number of DE genes between double pathology and double control groups (Kindled 5xFAD vs Sham WT), indicating the strong likelihood of synergistic interaction between AD pathology and recurrent seizures (Figure 5.4 d).

The dramatic effect of dual pathology is also observed in the PCA plots in Figure 5.3 a and b, with all samples in the Kindled 5xFAD group always forming a well-defined distinct cluster. To identify the genes, changes in the expression of which could only be attributed to the interaction effect between the 5xFAD genotype and kindling, we performed a nested pair-wise differential expression analysis with interaction effect. A total of 291 genes were identified as significantly different according to the nested comparisons analysis, with several immediate early genes as well as ion channel receptors/subunits and astrocytic genes at the top of the list.

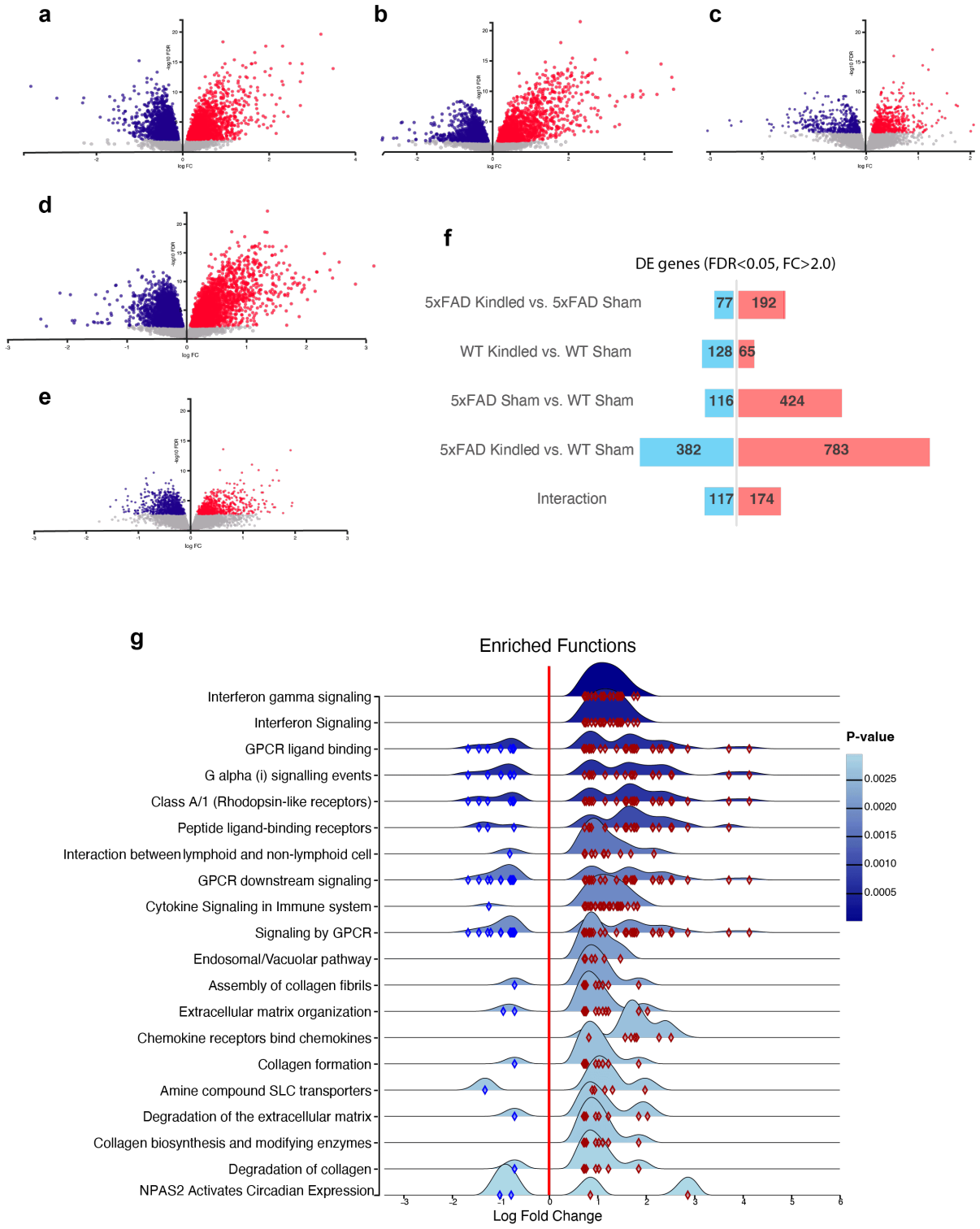

Figure 5.4. Differential expression analysis of RNA sequencing data. Volcano plots showing the gene expression distribution for the following group contrasts: **a.** 5xFAD-kindled vs 5xDAD-sham, **b.** 5xFAD-sham vs WT-sham, **c.** WT-kindled vs WT-sham, **d.** 5xFAD-kindled vs WT-Sham, **d.** interaction effect only. **f.** Numbers of significant (FDR < 0.05, FC>2) differentially expressed genes for all group contrasts. Blue represents down- and red represent up-regulated genes. **g.** Gene-Set enrichment analysis on the significant DE genes between Kindled-5xFAD and Sham-5xFAD groups.

5.3.4. Correlation Network analysis

In order to characterize the dual pathology signature in the context of molecular networks we used the WGCNA framework to construct two gene coexpression networks and define distinct transcriptional modules. First, to investigate the global emergent transcriptomic changes caused by AD pathology and recurrent seizures and examine the effect of each pathology (5xFAD-AD, kindling-epilepsy) on the co-expression modules, we constructed a gene coexpression network from filtered and normalized gene count table that included all 42 samples and 4 experimental groups involved in this study. This network will be referred to as the "global" network throughout this chapter.

Additionally, since the PCA indicated that the group separation and transcriptomic variations of the samples were mainly determined by the genotype, in an attempt to resolve the nuances in seizure-induced transcriptomic changes specific to the 5xFAD mice, which could otherwise be missed in the global coexpression network, we constructed a 5xFAD-specific coexpression network which included only the 5xFAD samples. The coexpression networks were hierarchically clustered into groups of coexpressed genes called modules (for detailed methodology description refer to section 4.2.2). Because each co-expression module groups together genes that are highly correlated, each module can be represented by a single representative expression profile called a module eigengene. Module eigengenes lead to a natural measure of similarity (membership) of all individual genes to all modules. This can be measured by kME, which is the correlation of the expression of the gene to the module eigengene. Genes with highest kME, called hub genes, are centrally located inside the module and represent the expression profile of the entire module.

To assess whether the given module was related to disease progression or either of the two experimental variables, we correlated each module eigengene to the two group contrasts and the pathologies they represent (Kindled : Sham – Epilepsy effect, 5xFAD : WT – AD effect) as well as amyloid plaque area, seizure severity measures and Y-maze data. Additionally, to determine whether the changes in the coexpression modules are driven by specific cell populations, we also interrogated the cell-type nature of each module by assessing whether it was enriched in cell-type specific markers. The resultant module correlations, cell-type specific enrichment data as well as intramodular connectivity relationships within the global and 5xFAD-specific networks were summarized in multi-layer circular heatmaps in Figure 5.5. and Figure 5.6.

5.3.5. Global transcriptomic signatures of AD pathology and recurrent seizures

Hierarchical clustering of the global coexpression network identified 12 coherent gene modules with highly correlated expression patterns. Functional annotation revealed clear ontologies for all 12 modules, and varying degrees of cell-type specific enrichment. Nine out of the 12 modules showed significant ($P<0.05$) correlation to either AD or Epilepsy traits, forming two generally defined groups: upregulated – showing strong positive correlation to seizure severity and amyloid plaque load, and downregulated – showing strong negative correlation with pathology traits.

The two most notably upregulated modules in the global network are the purple cholesterol metabolism-related module, and the turquoise immune response-related modules. The cholesterol metabolism module shows strong and highly significant correlation to both 5xFAD genotype and kindling/seizures, establishing it as the dual pathology-associated module. The central regulatory hub gene of this module is KCNIP3, also known as Calsenilin. Functional and cell-type enrichment analysis of the member genes constituting this module revealed strong enrichment in astrocytic markers and pathways involved in cholesterol synthesis and transport (Figure 5.5.b).

The highly upregulated Immune response module is comprised of 1284 genes and has Tlr2 (toll-like receptor 2) as its central regulatory hub gene. This module functionally annotates to inflammatory and immune response pathways and shows significant enrichment in microglia-specific markers such as TYROBP and TREM2. This module is highly upregulated in AD and shows strong correlation to seizure severity. To incorporate the cell-type nature and pathology associations of these notable modules into their description, we subsequently refer to the turquoise and purple modules of the global network as “AD-associated” and “AD+Epilepsy-associated” modules, respectively. Both the AD-associated AD+Epilepsy associated modules are correlated with seizure severity measures and increased amyloid plaque deposition.

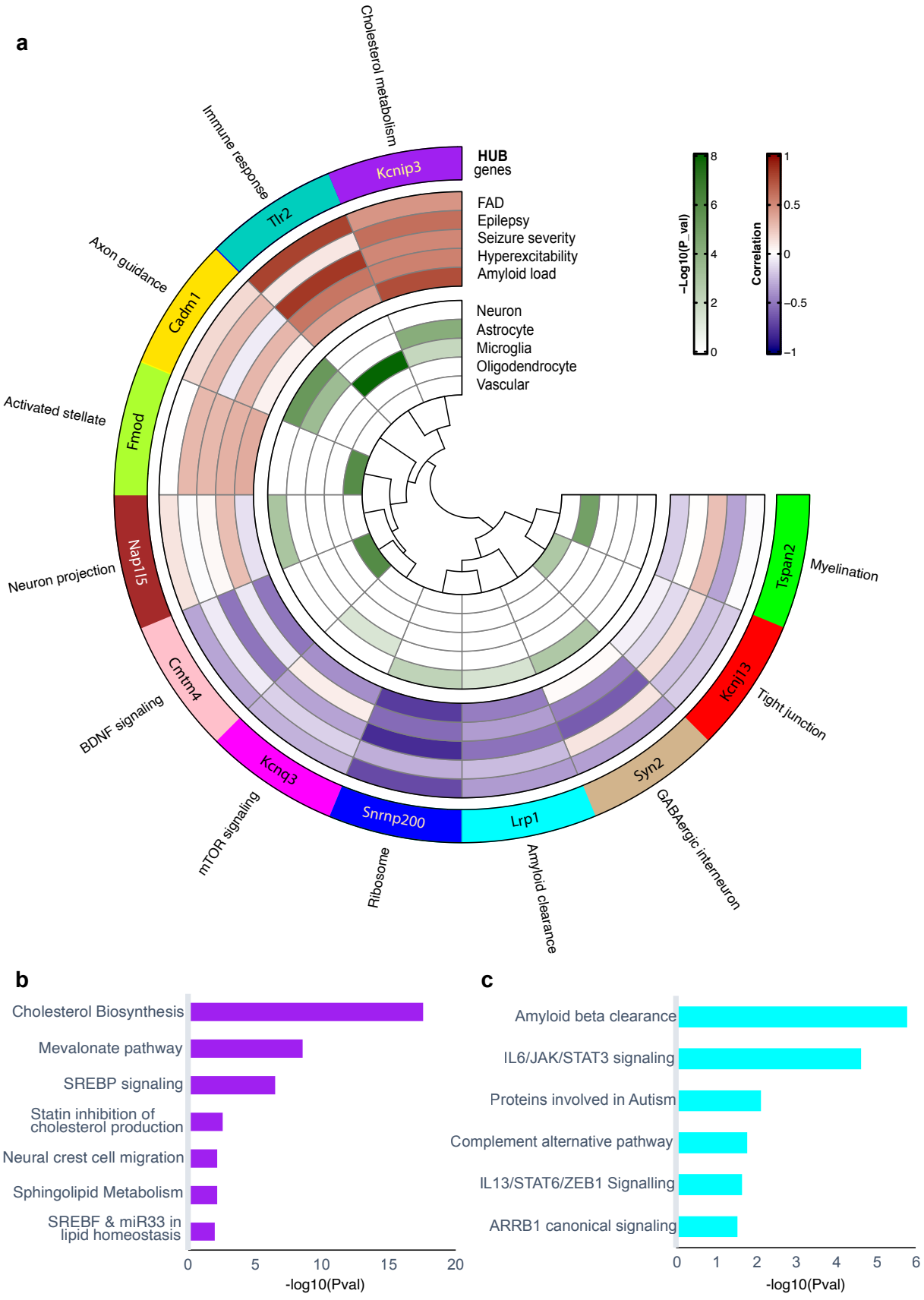
a
Cholesterol metabolism
Immune response
Axon guidance
Activated stellate
Neuron projection
BDNF signaling
mTOR signaling
Ribosome
Amyloid clearance
GABAergic interneuron
Tight junction
Myelination
Kcnip3
Tlr2
Cadm1
Fmod
Nap1l5
Cmtm4
Kcnq3
Snrnp200
Lrp1
Syn2
Kcnj13
Tspan2
HUB genes
FAD
Epilepsy
Seizure severity
Hyperexcitability
Amyloid load
Neuron
Astrocyte
Microglia
Oligodendrocyte
Vascular
−Log10(P_val)
Correlation
b
Cholesterol Biosynthesis
Mevalonate pathway
SREBP signaling
Statin inhibition of cholesterol production
Neural crest cell migration
Sphingolipid Metabolism
SREBF & miR33 in lipid homeostasis
-log10(Pval)
c
Amyloid beta clearance
IL6/JAK/STAT3 signaling
Proteins involved in Autism
Complement alternative pathway
IL13/STAT6/ZEB1 Signalling
ARRB1 canonical signaling
-log10(Pval)

Figure 5.5. The global gene co-expression network. a. WGCNA identified 12 co-expression modules labelled by colour in the outermost segment. GO analysis was used to identify the principal biology represented by each module. The central regulatory hub genes are indicated on each colour-coded segment. Pearson correlation of module eigengenes to the behavioural and histopathological outcomes shown in the red-blue heatmap segment (red, positive correlation; blue, negative correlation). Each block corresponds to either a categorical factor representing the group contrast [FAD=all5xFAD vs allWT; Epilepsy=allKindled vs allSham] or a continuous number representing the behavioural and histopathological outcome measures [seizure severity=average Racine score of behavioural seizures per animal, hyperexcitability=the number of stimulations required to elicit the first class V seizure, amyloid load=the average % area of hippocampus covered by amyloid plaques per animal]. The cell type enrichment of each module was assessed by module gene overlap with cell-type-specific marker lists of neurons, oligodendrocytes, astrocytes, microglia and vascular endothelial cells, shown in green heatmap segment. Module relatedness is shown in the central dendrogram. **b.** top significantly enriched ($p<0.05$) pathways of upregulated cholesterol metabolism module and **c.** downregulate amyloid beta clearance module.

Among the downregulated modules which are anti-correlated to AD and seizure pathologies are the blue-ribosome, cyan-amyloid clearance, tan-GABAergic interneuron and pink-BDNF signalling modules. The large blue module with over 3000 member genes is enriched in ribosomal proteins, translation and metabolic pathways. It shows strong negative correlation to all pathology traits and especially seizure severity – indicating the more severe the seizures, the more they interfere with the cellular homeostatic processes. The tan-GABAergic interneuron module is downregulated in AD, and shows strong negative correlation to seizure severity and hyperexcitability. This module is enriched in inhibitory neuronal markers and synaptic proteins and has Synapsin 2 as its central hub gene. Another downregulated module is the smaller cyan module with 93 member genes and Lrp1 (low-density lipoprotein receptor-related protein 1) as its regulatory hub. This module is enriched for pathways involved in amyloid clearance.

5.3.6. Specific transcriptomic changes in 5xFAD coexpression network

The 5xFAD-specific gene coexpression network was constructed in the same manner as the global network. WGCNA hierarchical clustering algorithm identified 17 well-defined modules of coexpressed genes representing distinct transcriptional responses to kindling-induced recurrent seizures. Analogous to the global network, 13 out of the 17 modules in the 5xFAD-specific network showed significant correlation to one or more pathology traits. Based on the direction of eigengene expression change, there are 7 upregulated, 4 relatively unchanged and 6 downregulated modules, organized in diverging order in the circular heatmap in figure 5.6. Functional enrichment analysis revealed more specific pathway annotations compared to those in the global network (Figure 5.7.).

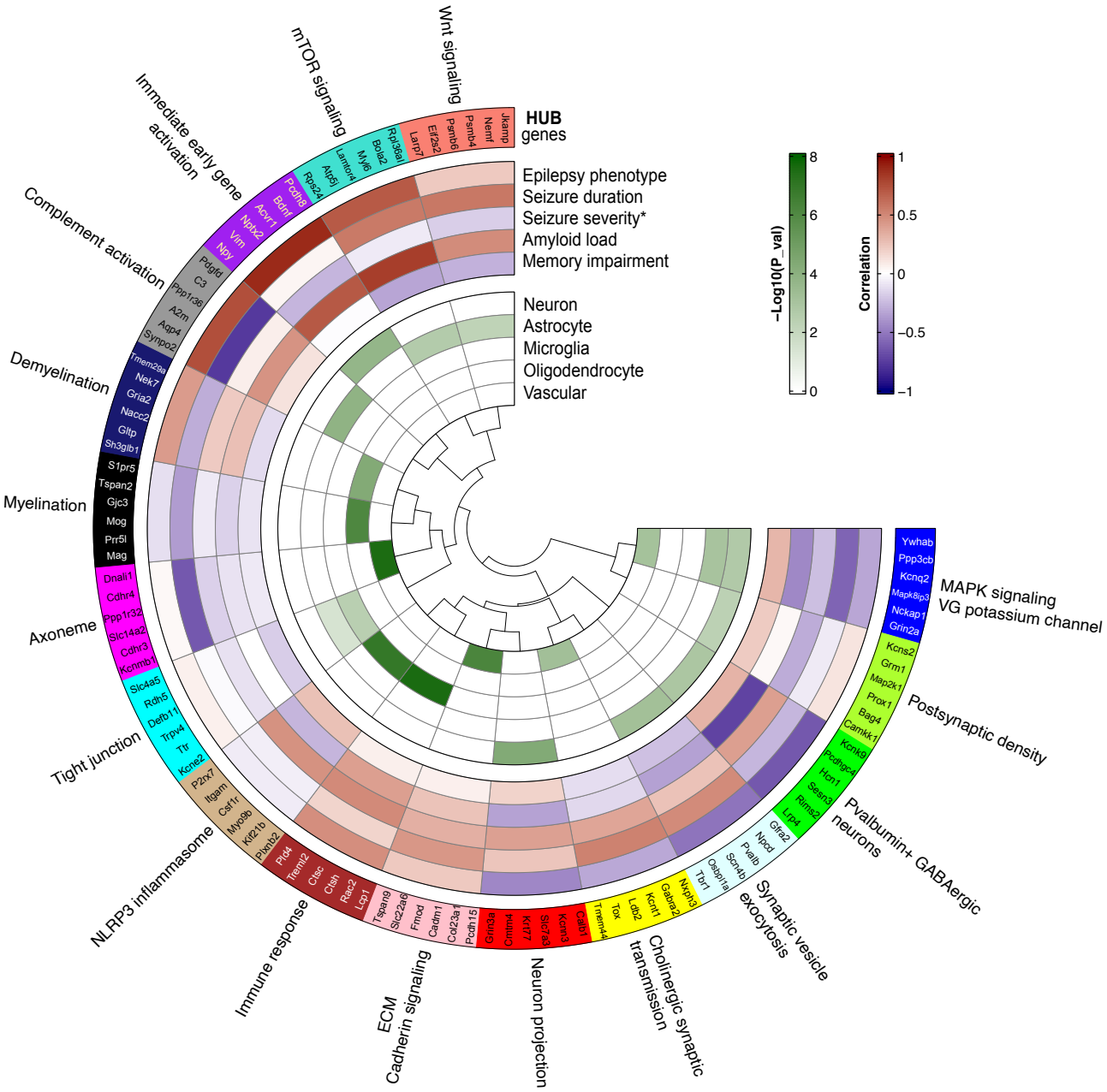

Figure 5.6. 5xFAD-specific gene co-expression network. WGCNA identified 17 co-expression modules labelled by colour in the outermost segment. GO analysis was used to identify the principal biology represented by each module. The top 6 central regulatory hub genes are indicated on each colour-coded segment. Pearson correlation of each module eigengene to the behavioural and histopathological outcomes shown in the red-blue heatmap segment (red, positive correlation; blue, negative correlation). Each block corresponds to either a categorical factor representing the group contrast [Epilepsy phenotype=Kindled5xFAD vs Sham5xFAD] or a continuous number representing the behavioural and histopathological outcome measures [seizure severity=average Racine score of behavioural seizures per animal, memory impairment = (time spent in novel/time in familiar), amyloid load=the average % area of hippocampus covered by amyloid plaques per animal]. The cell type enrichment of each module was assessed by module gene overlap with cell-type-specific marker lists of neurons, oligodendrocytes, astrocytes, microglia and vascular endothelial cells, shown in green heatmap segment. Module relatedness is shown in the central dendrogram.

The most notable upregulated modules showing highly significant correlation to increased amyloid plaque pathology and more severe seizure traits, is the purple module, with ~300 member genes (Figure 5.5.a). This module contains immediate early genes such as Pcdh8, Nptx2, BDNF as central regulatory hubs, and shows enrichment in apoptotic pathways, as well as proteins involved in Huntington's Disease and Parkinson's Disease (Figure 5.7.a). The neighbouring darkgrey-complement activation module is closely related to the purple-immediate early gene activation module, showing robust upregulation and correlation to amyloid load. This grey-complement activation module is enriched in astrocytic markers and has C3 (complement component 3) as its central hub.

Another module that is highly upregulated in kindled 5xFAD is the turquoise-mTOR signalling module. This large module shows significant positive correlation to seizure duration and amyloid plaque load and is enriched in astrocytic markers and cellular stress-related pathways such as mTOR activation, heat shock protein induction and MAPK cascades. Notably, the second most significant pathway associated with this module is "Platelet Amyloid Precursor Protein" pathway (Figure 5.7.b).

The downregulated modules (blue, greenyellow, green, lightblue, yellow, red) located on the opposite end of the heatmap show varying degrees of the generally conserved pattern, with negative correlation to epilepsy/seizure measures and amyloid plaque load. These modules are enriched in various synaptic transmission pathways and processes, as well as neuron-specific markers and are likely representing different neuronal populations.

In summary, the RNA sequencing and network analysis of gene expression data showed distinct transcriptional responses to kindling-induced recurrent seizures, with immune response modules being upregulated and synaptic transmission modules being downregulated.

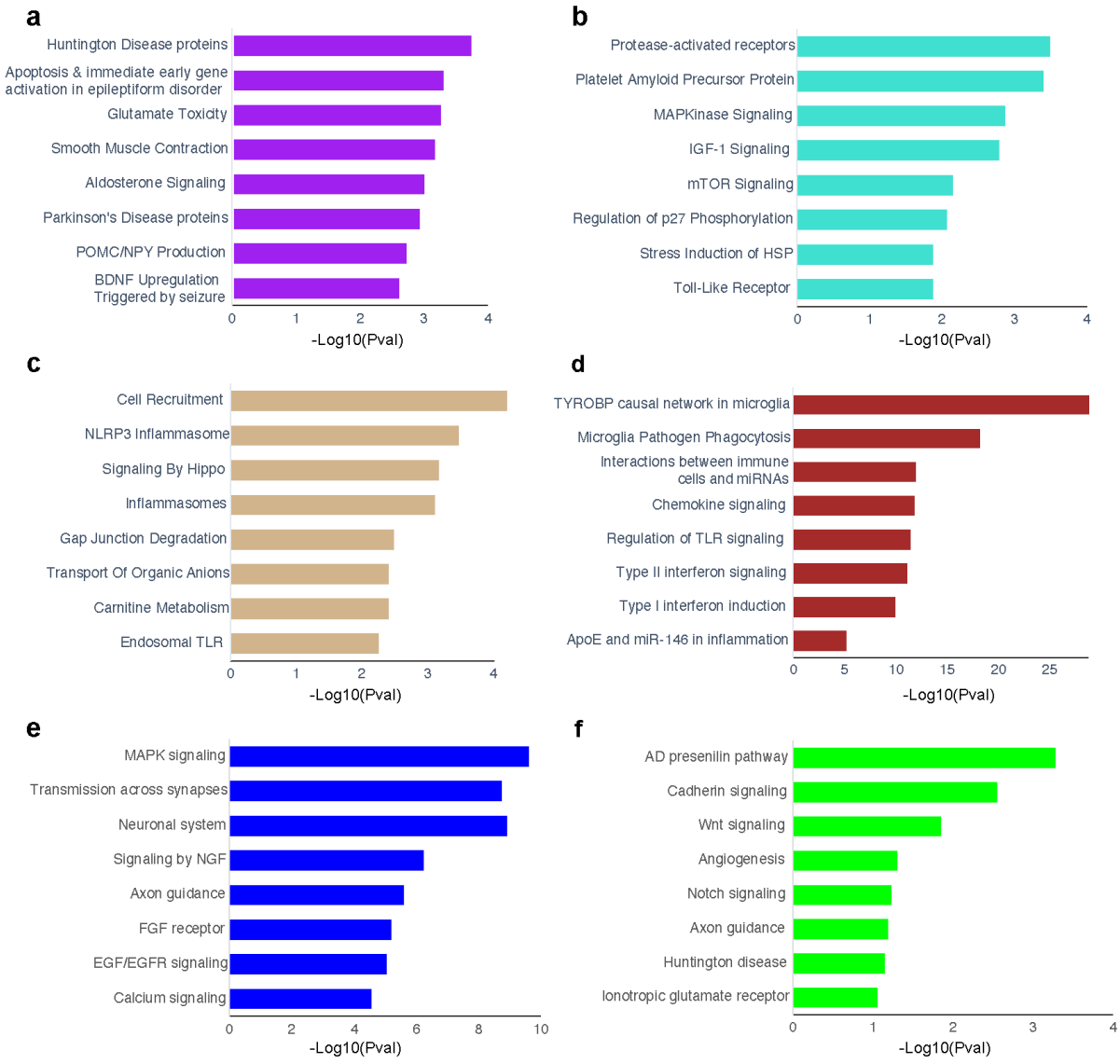

Figure 5.7. The top enriched pathways associated with corresponding 5xFAD-specific modules. a. purple-immediate early gene activation, **b.** turquoise-mTOR signalling, **c**. tan-NLRP3 inflammasome **d.** brown-immune response **e.** green-PV+ GABAergic interneurons. Bars represent the -Log10-Pvalue of significance associated with the hypergeometric test.

5.3.7. Reactive gliosis and Vim-IR astrocytes around amyloid plaques in 5xFAD

Since our transcriptomic evidence strongly suggested glial involvement in the synergistic exacerbation of pathology, we performed IHC labelling of astrocytes and microglia with GFAP and Iba1 – well-established markers of astrogliosis and microgliosis, respectively. It should be noted that the IHC experiments were carried out on the hippocampal tissue from the same brains (contralateral hemisphere) that were used for RNA -seq analysis. A pronounced increase of GFAP-immunoreactivity was observed in both Kindled and Sham 5xFAD groups compared to WT (Figure 5.8.a and 5.9), with more apparent congregation of enlarged, hypertrophic

astrocytes around amyloid plaques in kindled 5xFAD (Figure 5.9.a). The extent of GFAP immunolabelling across our experimental groups was closely correlated with GFAP mRNA expression and followed a similar pattern, from relatively low expression in Sham WT group, followed by increase in kindled WT and Sham5xFAD mice, and showed highest expression in the double pathology Kindled5xFAD group (Figure 5.8.b). To further investigate the astrocytic response to plaque formation, another reactive astrocytic marker, Vimentin, was studied. Similar to that of GFAP, Vimentin immunoreactivity was consistent with Vim mRNA expression (Figure 5.8.c), however its expression distribution followed a distinct pattern: vimentin-positive astrocytes were only located distinctly around the amyloid plaques in the Kindled-5xFAD brains, while GFAP-positive astrocytes were found throughout the brain. Many of the hypertrophic reactive astrocytes co-expressed GFAP and vimentin (Figure 5.9.a). Among the cells only expressing one of the markers, there were more single positive cells for GFAP than for vimentin. The expression of Vimentin was low in Sham 5xFAD and was colocalized with vasculature. Iba1-positive microglia were omnipresent in both kindled and sham 5xFAD tissue, however the majority of the activated microglia of characteristic amoeboid shape were seen in close proximity to amyloid plaques, making direct contact with A6E10-immunoreactive deposits.

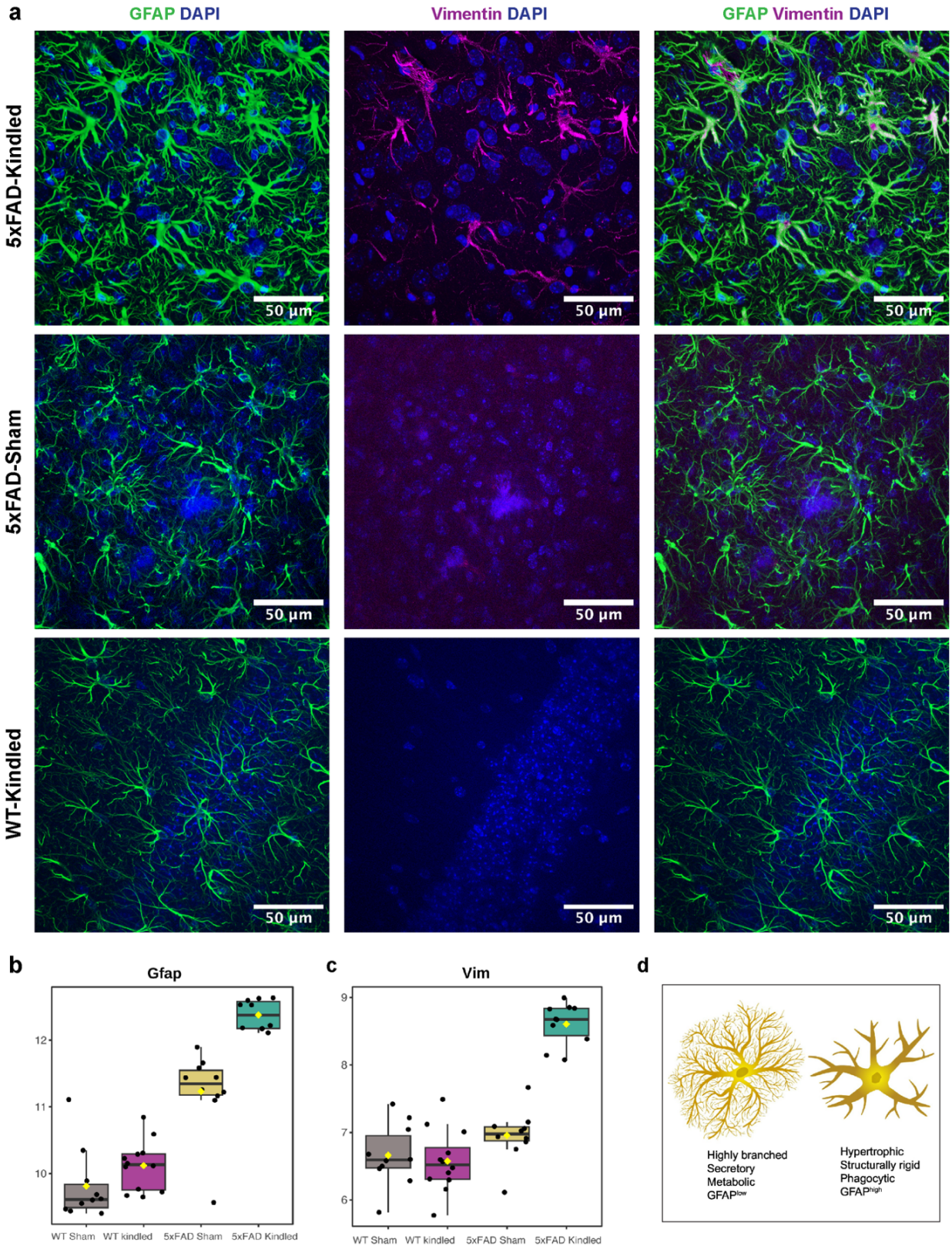

Figure 5.8. Reactive astrogliosis and hypertrophic astrocytes in Kindled 5xFAD mice. a. maximum-intensity projections of optical slices (Z-stacks) depicting the Immunohistochemical staining of Astrocytes with GFAP and Vimentin in Kindled 5xFAD, Sham 5xFAD and Kindled WT groups. The Z-stacks were captured with a 60x magnification oil-immersion objective on Nikon Ar1 confocal microscope. **b, c.** normalized mRNA expression of GFAP and Vimentin. **d.** A graphical representation of a homeostatic astrocytes seen in WT groups and a hypertrophic disease-associated Vim+ astrocyte seen in dual pathology group.

components of subpanel* **d *have been adapted from ref (Vainchtein & Molofsky, 2020) in accordance with the Creative Commons 4.0 licence regulations.*

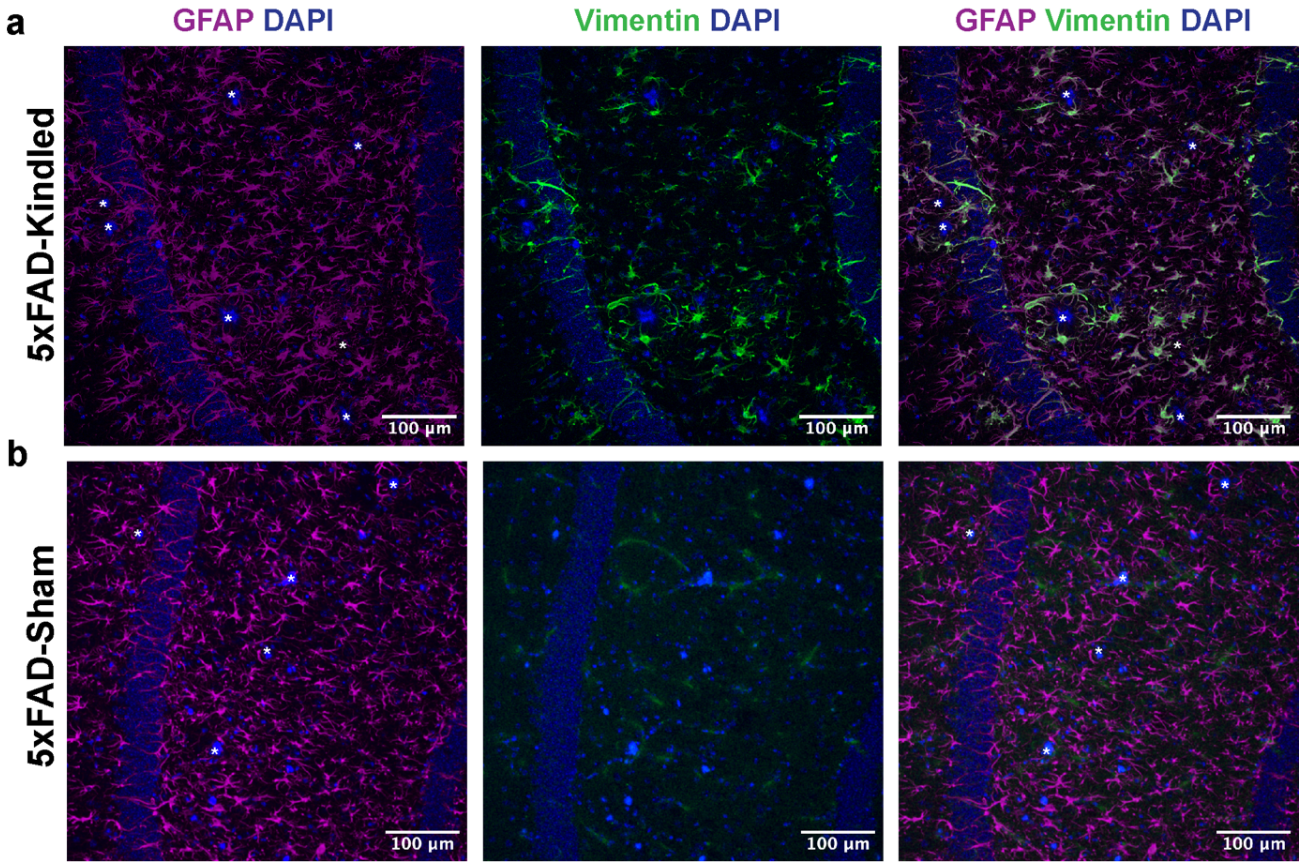

Figure 5.9. Vimentin-positive reactive astrocytes around amyloid plaques in Kindled5xFAD but not Sham-5xFAD hippocampus. a. GFAP and Vim (DAPI counterstain) immunostaining of hippocampal tissue displaying Vimentin-IR reactive astrocytes congregating around amyloid plaques in Kindled 5xFAD but not in **b.** Sham 5xFAD. Asterisks mark the centre of several large amyloid plaques.

5.4. Discussion

5.4.1. AD with seizures as a distinct pathophenotype

A recent study involving over 20,000 patients shows that seizures in AD are highly recurrent (>70% recurrence rate, within <8 months) (Vöglein et al., 2020), and are associated with a more severe cognitive and biochemical disease profile. However, only a subset of AD patients would develop seizures. Similarly, among patients with late onset epilepsy of unknown etiology (LOEU) (Costa et al.) and pathogenic (AD-like) levels of Amyloid beta 1-42 in the CSF, in the 3-year follow up, a subset (7/40, 17.5%) did indeed develop dementia/cognitive decline, while 53.8% did not. In other words, even after 3 years, more than half of the LOEU patients with pathogenic A-beta 1-42 levels did not convert to dementia patients (Costa et al.,

2019). Another study looking at CSF biomarkers in a large cohort (~18,000 individuals) of AD patients with or without seizures demonstrated that the subpopulation of AD patients who developed seizures had biochemically more pronounced disease profile compared to those without seizures (Banote et al., 2022). A strong predictor of disease severity seems to be younger age of clinical symptom presentation, where pedigrees with very early onset of FAD (<40 years old) showing very high rates (>80%) of epileptic phenotypes (Snider et al., 2005). Additionally, 84% of patients with Down's syndrome who progress to dementia also develop seizures (Aller-Alvarez et al., 2017). Together, this evidence supports the hypothesis that the dementia patients experiencing seizures represent a distinct subclass of patients, demonstrating more severe biochemical and cognitive phenotype which is likely compounded by the synergistic interaction between amyloid pathology and recurrent seizure activity.

Pre-clinical models do not always resemble the spectrum of human disease. For example, seizure frequency in patients with FAD seems to be higher than that observed in most FAD mice. Therefore, to better recapitulate the transcriptomic and neurochemical profile of human patients in a preclinical model we developed a dual pathology model by establishing a recurrent seizure phenotype in the 5xFAD mice. The results of our study are consistent with the above-mentioned clinical evidence, indicating that in addition to more severe cognitive and CSF-biochemical profile, the seizure-prone subpopulation of AD patients has a more severe histopathological phenotype, and more pronounced molecular neuroinflammatory profile.

5.4.2. Neuronal activity-dependent increase in amyloid deposition in kindled 5xFAD

Although AD is increasingly viewed as a heterogeneous syndrome, its amyloid-centric histopathology as well as fMRI signature seems to be remarkably consistent: amyloid deposits predominate in brain regions of the default mode network, which shows deactivation deficits in AD, suggesting that neuronal activity regulates amyloid-β production and deposition (Buckner et al., 2005; Palop & Mucke, 2016). Extracellular soluble Aβ aggregates into amyloid plaques in a concentration-dependent manner, and interstitial fluid Aβ concentration is closely associated with plaque growth (Bero et al., 2011; Yan et al., 2009), therefore, the size and total area of amyloid plaques can be used as an indirect measure of overall Aβ content. We compared the total percentage of area occupied by amyloid plaques between Kindled-5xFAD and Sham-5xFAD to assess whether recurrent seizures increase Aß concentration and deposition. In agreement with other reports (Gourmaud et al., 2022) we found that recurrent seizures lead to

overall increase in amyloid plaque area in the hippocampus. This is consistent with the hypothesis that neuronal activity regulates Aß production and deposition (Bero et al., 2011).

Subsequent integration of the mouse EEG, behavioural data and histopathological outcome measures with the RNAseq data from the same brain tissue into coexpression networks allowed for identification of distinct transcriptional responses to the pathology associated with 5xFAD genotype and kindling-induces recurrent seizures in the form of coherent gene coexpression modules. Interestingly, the dual pathology-associated Cholesterol Metabolism module is a better correlate/predictor of amyloid load than the AD-associated module, as it shows stronger and more significant Pearson correlation with amyloid plaque area than the AD-only module. This is not an artifact of a multiple comparison analysis, where larger modules show inflated P-values associated with the Pearson correlation coefficients (PCC) due to the large number of comparisons made. In fact, this effect is understated, because the AD-associated module is much larger, with over 1500 member genes, which would artificially increase the -log(P-value) of its correlation (PCC) to amyloid plaque number/area, yet it shows correlation that is orders of magnitude less significant (though still statistically significant) than that of the double pathology/AD+Epilepsy module. This observation reinforces the causal role of recurrent seizure activity in increasing the overall concentration of amyloid beta and plaque deposition. By combining recently developed optogenetic methodology with multi-photon live imaging, several benchmark studies have demonstrated that chronic synaptic hyperactivity is causally related to deposition of amyloid plaques (Bero et al., 2011; Yamamoto et al., 2015; Yan et al., 2009). This is also supported by the notion of neuronal activity-dependent regional vulnerability to amyloid deposition, where cortical areas of high neural activity, particularly in the default-mode network, show the largest amyloid burden (Buckner et al., 2005).

5.4.3. Distinct transcriptomic modules correlated with 5xFAD-Kindled double pathology

The initial principal component analysis (PCA) of RNAseq data indicated that the genotype of the animals had a stronger effect on sample clustering than their kindling status (Figure 5.3.a), suggesting that the hippocampal transcriptome is distinct between 5xFAD and WT animals. Therefore we constructed a second gene coexpression network that included only the 5xFAD samples. Functional enrichment analysis revealed more specific pathway annotations compared to those in the global network (Figure 5.7). Furthermore, the 5xFAD-specific coexpression network allowed for delineation of secondary small submodules within the global

pathways that represent 5xFAD-specific distinct transcriptional responses to recurrent seizures. For instance, in the Global network we detected a large and robust myelination-related module (labelled green-myelination) which is highly enriched in oligodendrocyte-specific protein markers and components of myelin sheath and shows no significant correlation to any group contrast or pathology trait (Figure 5.5a). However, in the 5xFAD-specific network, a finer split of the gene dendrogram allowed for detection of two more specific modules labelled as black-myelination and navy-demyelination. In fact, it is apparent from the intramodular connectivity dendrogram that the genes in the small navy-demyelination module constitute a distinct submodule of the larger black-myelination module. Both modules show strong enrichment in oligodendrocyte-specific protein markers and protein components of the myelin sheath, together representing the global myelination pathways, equivalent to the corresponding homologous green module in the global network.

Further examination of the enriched pathways associated with these 5xFAD-specific modules indicated that while the black module represents the homeostatic processes involved in axon ensheathment, the small navy submodule represents the pathogenic perturbations in the myelinating pathways and is associated with demyelination seen in the context of aging and neurodegenerative disorders such as multiple sclerosis. Furthermore, while the homeostatic black-myelination module shows no expression change across kindled and sham animals, the pathogenic navy-demyelination module shows a consistent trend towards upregulation in kindled-5xFAD group and is positively correlated with seizure severity and amyloid plaque load. Another example of this phenomena is seen with the immune response-related modules. In the 5xFAD-specific network the tan-NLRP3 inflammasome and brown-immune response modules show a high degree of intramodular connectivity and are both highly enriched in microglial-specific markers. Furthermore, it is apparent from the topological overlap dendrogram that the tan-NLRP3 inflammasome module is a submodule of the larger more general brown-immune response module, however, it shows a distinct correlation pattern to pathology traits, which is highly informative. While the general brown-immune response module is upregulated in the epileptic 5xFAD mice and shows positive correlation with seizure severity and amyloid load, the tan-NLRP3 inflammasome module is equally expressed in both epileptic and sham 5xFAD groups but shows positive correlation to seizure severity and memory impairment and negative correlation to amyloid load. Since the NLRP3

inflammasome activation is required for amyloid clearance (Heneka et al., 2013) it is logical that these two measures would be anticorrelated.

5.4.4. Activity-dependent elimination of synapses may be facilitated by immediate early genes and astrocytic complement activation

The results of our network analysis strongly indicate the involvement of cholesterol in the mechanism of seizure-induced synergistic exacerbation of AD pathology. The main finding from our global network analysis was the distinct dual pathology-associated cholesterol metabolism module (Figure 5.5a,b, purple) which was upregulated in the context of both AD and epilepsy pathology. Genetic variation in a cholesterol transport protein, apoE, is the most common genetic risk factor for sporadic AD, and several GWAS studies have demonstrated a link between the total brain cholesterol content and the risk of developing AD (Wood, Li, Muller, & Eckert, 2014). In the adult brain, the neurons lose the ability to produce cholesterol, and therefore rely on astrocytes to synthesise and transport cholesterol with apolipoprotein E. In a recent benchmark paper Wang et al. demonstrated that astrocytes can directly control Aβ production in neuronal membranes of APP/PS1 mice and neuronal Aβ accumulation is tightly regulated by astrocytic cholesterol synthesis and apoE transport (H. Wang et al., 2021). By transporting cholesterol into membrane apoE regulates the exposure of APP to either the non-amyloidogenic alpha secretase processing, or the amyloidogenic β and γ secretase processing (Figure 5.10). Since cholesterol interacts directly with APP and both β- and γ-secretases show higher activity in cholesterol-rich lipid rafts, the cleavage of APP and the resulting amyloid production are strongly linked to the amount of plasma membrane cholesterol and its distribution (Ikonen, 2008; Rudajev & Novotny, 2022; H. Wang et al., 2021).

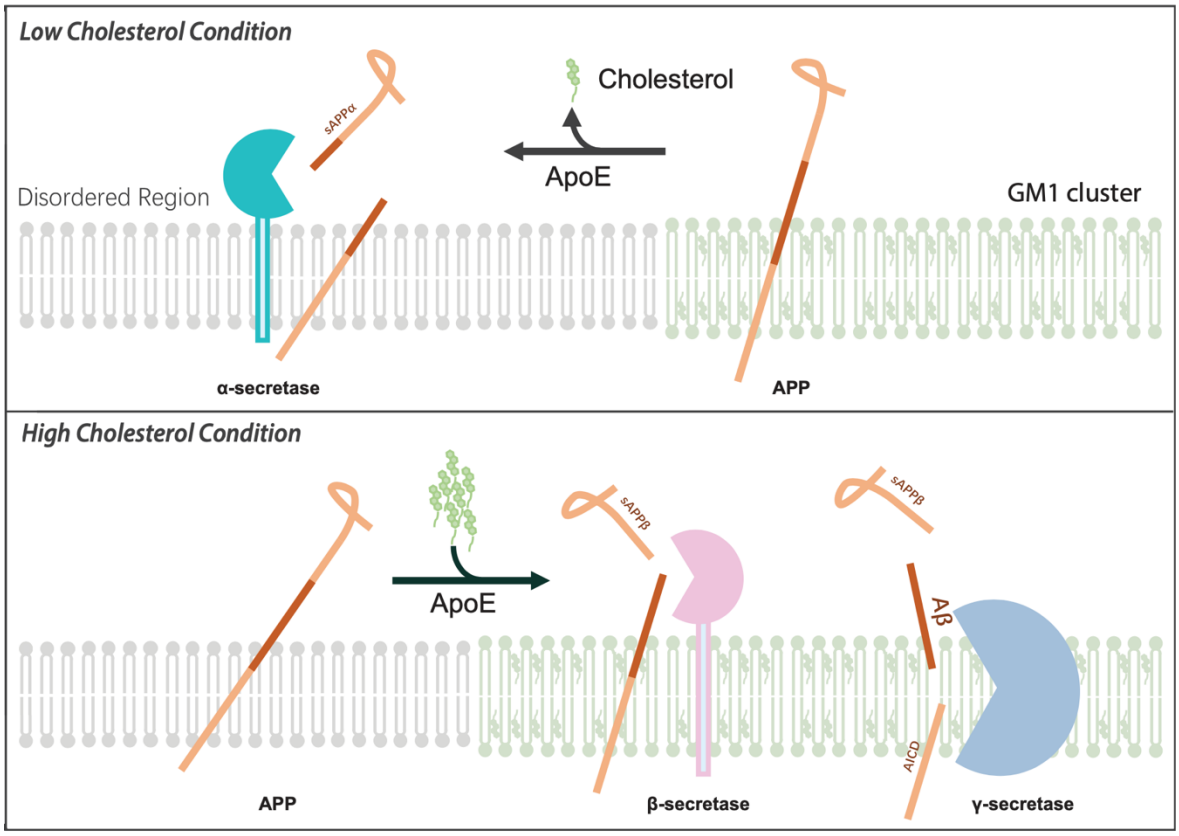

Figure 5.10. Cholesterol content of the plasma membrane controls the amyloidogenicity of APP processing. Higher levels of cholesterol increase the rigidity and permeability of the membrane, and favour the amyloidogenic processing of APP by beta- and gamma-secretases, while lower levels of cholesterol render the plasma membrane more fluid and promote the non-amyloidogenic, alpha secretase cleavage of APP. * *Diagram adapted from* ***(H. Wang et al., 2021)****, in accordance with the Creative Commons 4.0 copyright regulations.*

The central regulatory hub of cholesterol metabolism module is calsenilin or Kcnip3/KChIP3, which is dramatically overexpressed in dual pathology group, and overexpressed to a lesser degree in the 5xFAD-sham and WT-kindled groups compared to the double controls. Calsenilin is a multifunctional calcium-binding protein which has been independently identified to be: i) a binding partner of PS1/γ secretase complex ii) a calcium-dependent dynorphin gene transcription repressor that interacts with the downstream regulatory element antagonist modulator (DREAM), and iii) a pore-forming Kv4.2 channel interacting protein (Buxbaum et al., 1998; Jang et al., 2011). Consistent with our findings, increased expression of calsenilin has been reported in brains of AD patients and hAPP mice, where it is colocalized with amyloid plaques and is involved in Abeta production and apoptosis (Dong-Gyu et al., 2004). In contrast, knocking out calsenilin seems to be neuroprotective, reportedly resulting in 50% reduction of Abeta 1-40/1-42 in Kcnip3-KO mice, as well as increased long-term potentiation in CA1

(Alexander et al., 2009; Lilliehook et al., 2003). As a Kv4 channel interacting protein, calsenilin regulates neuronal membrane excitability through regulating the A-type transient current (Shibata et al., 2003). Notably, the Kcnip3 knock-out mice exhibit increased LTP in CA1 and enhanced memory in hippocampal-based fear conditioning paradigm, most likely due to reduction in A-type current (Alexander et al., 2009; Lilliehook et al., 2003; Shibata et al., 2003). Additionally, calsenilin overexpression regulates N-cadherin ε-cleavage and downstream β-catening signaling (Jang et al., 2011). Collectively, this line of evidence suggests a central role for Kcnip3 in synaptic pruning/negative regulator of LTP in the context of AD and our double pathology model.

Interestingly, the central hub of the analogous double pathology associated module in the 5xFAD-specific network is Protocadherin 8 (Pcdh8), also referred to as arcadlin, which has a similar ability to induce N-cadherin endocytosis and thus eliminate synapses. In fact, Pcdh8 is implicated in the control of dendritic spine density (Yamagata et al., 1999; Yasuda et al., 2007). Upon *cis* binding of Pcdh8 to N-cad, Pcdh8 ICD activates the MAP kinase (MAPK) TAO2β, which in turn activates MEK3, subsequently phosphorylating p38. The feedback signaling of p38 on TAO2β results in the synaptic endocytosis of N-cad and Pcdh8. Through this pathway, Pcdh8 was shown to downregulate the number of dendritic spines in rat hippocampal neurons (Takeuchi et al., 2020). The differential expression of PCDHs and their compartmental distribution define the number of synapses generated in a given region. In some cases, the formation of new synapses is favored, whereas, in other cases, there is a downregulation in the number of synapses. The expression of Pcdh8 is slightly downregulated in the 5xFAD-Sham group and shows a robust increase in kindled 5xFAD group, while remaining unchanged in kindled WT vs sham WT. This suggests that the Pcdh8-mediated reduction of dendritic spine density is a feature of 5xFAD animals only.

5.4.5. Complement-glia mediated synaptic pruning

Another notable finding of this study was the profound reactive astrogliosis seen in the near proximity to amyloid plaques. Both the transcriptomic and IHC evidence indicated the involvement of astrocytes in mediating dual pathology. In addition to robust pro-inflammatory cascade upregulation, the transcriptomic analysis identified a distinct 5xFAD-specific astrocytic module (Grey, complement activation) to be upregulated in the 5xFAD-kindled group. The top hubs of this module are astroglial markers such as C3 (complement component 3), Aquaporin 4 (Aqp4), and Synaptopodin 2 (Synpo2). Immunohistochemical evidence further

supports the conclusion that astrocytes in the hippocampus of dual pathology mice are undergoing reactive gliosis. We observed reactive Vimentin-positive astrocytes to be almost always associated with amyloid plaques. Vimentin is a type III intermediate filament, which is rarely expressed in astrocytes in the mature, healthy brain, and only by precursor cells in regions where neurogenesis occurs. However, Vimentin is upregulated in activated astrocytes undergoing reactive gliosis, and among other functions, takes part in facilitating the intracellular transport across enlarged cell volume in reactive hypertrophic astrocytes. It has been shown that cytokines released by activated microglia such as TNF-α, IL-1α and C1qa, directly polarize a subset of astrocytes towards a neurotoxic phenotype (Liddelow et al., 2017). This astrocyte subtype is characterized by increased expression of C3 as a typical marker. Several lines of evidence show that the C1q/C3/CR3-mediate classical complement activation cascade (CCC) leads to early synapse loss, and age-associated cognitive decline in mouse models of amyloidosis and tauopathy (Hong et al., 2016; Wu et al., 2019). In this pathway, the astrocytes induce the release of C1q from neurons, leading to the cleavage of astrocyte derived C3. Activated C3 fragments (C3b), in turn "tag" the synapse for elimination. The microglial C3 receptors (C3R) bind to C3b and recognize it as "eat me" tag, and proceed to phagocytose the synaptic structure (Figure 5.11d). Interestingly, APOE, a major risk factor for AD, has been shown to interact with C1q and thereby modulate CCC activity. Additionally, Neuronal Pentraxin 2 (Nptx2) – an activity dependent immediate-early gene that was dramatically upregulated in dual pathology group and constitutes a hub gene of the dual-pathology cholesterol metabolism module, has been recently established as a regulator of complement cascade (J. Zhou et al., 2022). Lastly, the resident microglia in the adult CNS phagocytose synapses when challenged by synaptotoxic Aβ, indicating that activation of the complement cascade and the subsequent initiation of microglial synapse engulfment may contribute to the synaptotoxic effects of Aβ. This is further supported by pathway enrichment analysis of the overexpressed genes in the 5xFAD-kindled group showing robust upregulation of phagocytic processes and complement pathway (Figures 5.7.d, 5.11.e).

Based on above conclusions, we propose a mechanistic paradigm potentially mediating the accelerated cognitive decline in the subpopulation of epileptic AD patients, where recurrent seizure activity dependent sustained overexpression of synaptic plasticity-regulating genes and accumulation of amyloid beta lead to progressive structural alterations in the physiology and neurochemistry of the neurons, which, in turn results in perturbations of neuronal

representations and loss of encoded information. In this synergistic paradigm (Figure 5.11), three pathways converge on the same outcome, namely widespread loss of synapses. First, excessive neuronal activity such as recurrent seizures ensure the sustained overexpression of activity-dependent immediate early genes such as KCNIP3 and Pcdh8 leading to aberrant synaptic pruning and structural degeneration of dendritic spines through endocytosis of N-cadherin (Figure 5.11.b, c). This trans-synaptic remodelling subsequently alters the intrinsic neuronal excitability by reducing the overall surface area of neurons and decreasing their total membrane capacitance (Šišková et al., 2014), rendering the network even more hyperexcitable. Additionally, the activity-driven accumulation of amyloid beta (Figure 5.11.a) leads to complement activation and phagocytic destruction of synapses by the resident activated glia (Figure 5.11.d). The resultant progressive synaptic loss quickly becomes widespread, leading to accelerated cognitive deterioration.

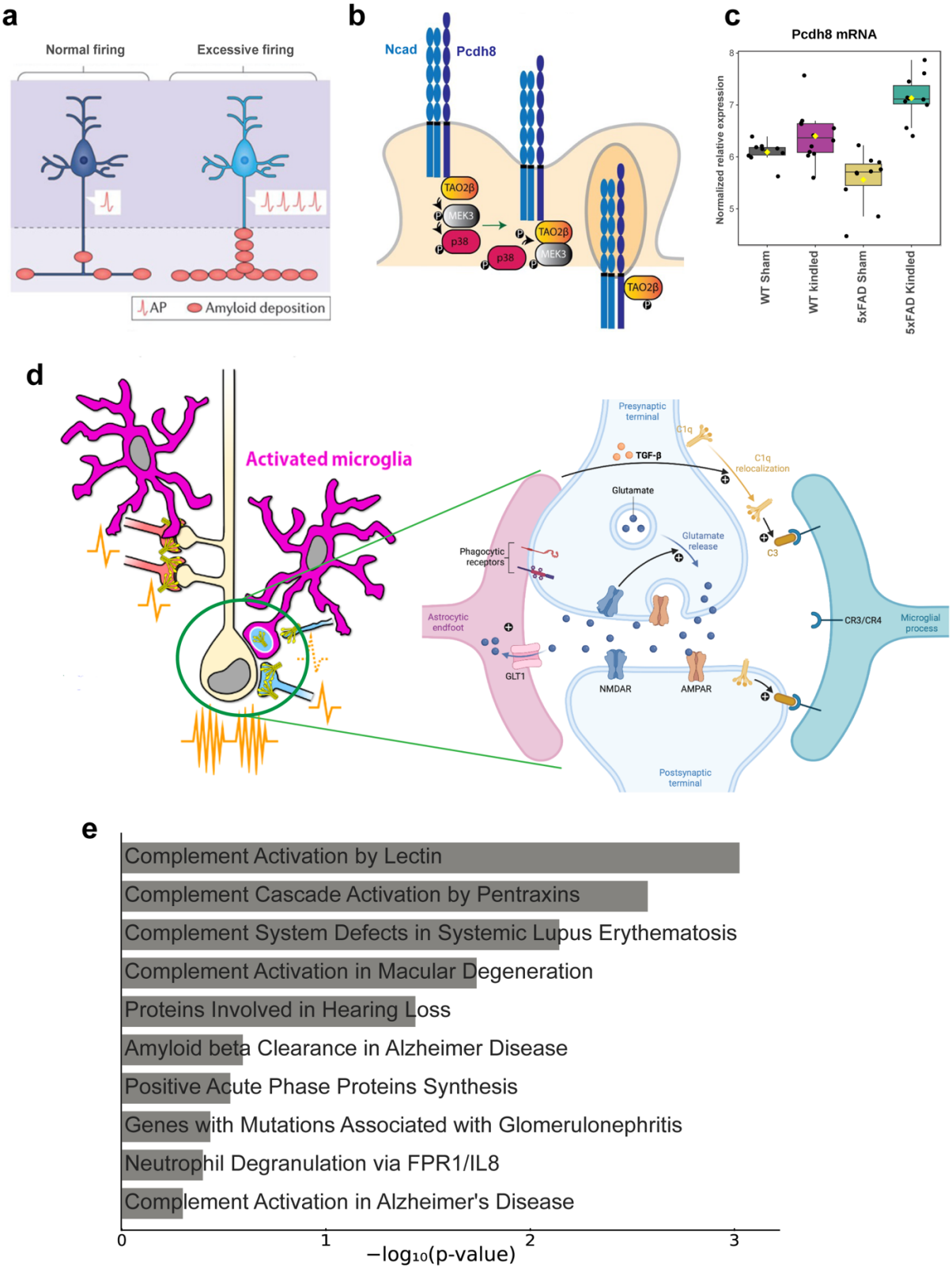

Figure 5.11. Complement-glia mediated synaptic pruning. Our hypothesized model of synaptic loss driven by the synergistic interactions between activity-dependent amyloid deposition (a), immediate-early gene overexpression (b, c), complement activation (d, e) and microglial phagocytic removal of synapses. * *components of subpanels a. and b. have been adapted from ref. (Palop & Mucke, 2016) and (Pancho, Aerts, Mitsogiannis, & Seuntjens, 2020), respectively, in accordance with Creative Commons 4.0 licence regulations.*

CHAPTER 6

GENERAL DISCUSSION

6.1. Summary of main findings and conclusions

The overarching aim of this PhD work was to better understand the molecular mechanisms underlying the bi-directional relationship between AD and epilepsy. Upon extensive review of the current literature (Chapter 1), it became increasingly evident that AD-like dementia and epilepsy syndromes are complex, multifactorial and heterogeneous diseases and therefore must be investigated through models which take into account the diversity in aetiology mechanisms and therapeutic responses. Integrative systems-level analyses have shown to facilitate more complete investigation and comprehensive understating of complex biological systems. A data-driven network-based approach was therefore selected to examine the molecular signature of the brain which presents with pathophysiology seen in AD patients and most widely used mouse models of AD, revealing robust upregulation of inflammatory pathways and immune response-related genes, and downregulation of synaptic transmission and synaptogenesis-related processes (Chapter 2). Next, we utilized a multi-omic approach to characterize the molecular signature of the brain which presents with pathophysiology seen in in two distinct models of epilepsy: the post-status epilepticus model of temporal lobe epilepsy and the GAERS model of absence epilepsy (Chapter 3). Oxidative stress pathways and dysregulated lysine catabolism defined the signature of absence seizure pathology, while dysregulation in long-term potentiation and synaptic signalling processes characterized TLE. We employed correlation network analysis to identify distinct protein-metabolite modules associated with each phenotype. The modules which positively correlated with more frequent seizures and poor cognitive performance were enriched for proteins and metabolites involved in inflammatory and cellular stress pathways as well as pathways associated with Alzheimer's Disease and different types of cardiomyopathies. The modules which positively correlated with less frequent and less severe seizures and better cognitive performance were enriched for proteins and metabolites involved in the TCA cycle, oxidative phosphorylation and other metabolic pathways. We then set out to mathematically compare the architecture of the molecular networks representing the AD and epilepsy pathologies (Chapter 4). Using publicly available transcriptomic data from hippocampal tissue of patients with temporal lobe epilepsy (TLE), late onset AD and non-AD controls, we constructed gene coexpression networks representing

all three states and employed network preservation statistics to compare the density and connectivity-based preservation of functional gene modules between TLE, AD and non-demented controls. We identified two synaptic signalling-associated modules and two metabolic modules showing substantial gain of preservation between AD and TLE, indicating that the pathways underlying synaptic function were similarly perturbed in the context of both pathologies.

One of the predictions of network medicine is the so-called "local hypothesis" which implies that, gene products implicated in the same disease have a high probability of interacting with each other. Likewise, genes associated with diseases that show similar phenotypes such as AD and TLE also tend to interact with each other. Our results from Chapters 2, 3 and 4 support this notion. Moreover, as detailed in Chapter 4, upon mathematical comparison of the architectures of the molecular networks representing the two pathologies, we found that the pathways underlying synaptic reorganization and signalling were similarly dysregulated in the context of both pathologies. The results from these first three experimental chapters and additional review of most recent clinical evidence involving patients with AD/dementia, epilepsy or dual diagnoses informed the rationale and experimental design of the fourth and final study described in Chapter 5. We hypothesized that due to profound commonalities in the molecular signature of AD and epilepsy in the form of highly preserved pathology-associated gene modules, when coincided, the two pathomechanisms act as agonists for one another, resulting in synergistic exacerbation of pathology and accelerated disease progression. To test this hypothesis, we induced a recurrent seizure phenotype in a transgenic FAD mouse, thus establishing a dual pathology model to recapitulate the human condition (kindled 5xFAD mice represent the subpopulation of AD patients who developed recurrent seizures). We found that recurrent seizures exacerbated the amyloid plaque pathology and induced profound reactive gliosis in the hippocampus of Kindled 5xFAD mice. Transcriptomic analysis revealed a dramatic change in gene expression profile when the two pathologies coincided. The massive increase in the number of dysregulated genes in dual pathology group compared to both single pathology controls indicated the presence of a significant interaction effect between amyloid pathology and recurrent seizures. This distinct dual pathology transcriptome is characterized by exacerbated neuroinflammatory profile, reactive gliosis and downregulation of synaptic proteins and signalling mechanisms. These results lend support to our proposed two-factor disease model for dementia and seizures, where the synergistic interaction between the two

patho-mechanisms defines a distinct subpopulation of "dual-pathology" patients, characterized by faster disease progression and cognitive deterioration due to more severe histopathological and molecular phenotype. Subsequently, we employed an integrative network-based approach in an attempt to identify the potential mediators of synergy. Our results indicated the complement cascade and activity-dependent IEGs to have central roles in dual pathology, leading to the conclusion that complement-mediated synaptic pruning might mediate the synergistic acceleration in cognitive decline seen in the seizure-prone subpopulation of AD patients.

Based on above conclusions, we proposed a mechanistic paradigm (Figure 5.11), where recurrent seizure activity dependent sustained overexpression of synaptic plasticity-regulating genes and accumulation of amyloid beta lead to progressive structural alterations in the physiology and neurochemistry of the neurons, which, in turn results in perturbations of neuronal representations and loss of encoded information.

The model builds on three sets of observations:

- **Increased neuronal firing leads to increased Aβ concentration**
- **Sustained seizure activity induces robust overexpression of synaptic plasticity-related immediate-early genes**
- **Both Aβ and IEG can induce complement pathway activation**

In this synergistic paradigm, three pathways converge on the same outcome: widespread loss of synapses: first, excessive neuronal activity such as recurrent seizures ensure the sustained overexpression of activity-dependent immediate early genes such as KCNIP3, Pcdh8 and Nptx2, leading to aberrant synaptic pruning and structural degeneration of dendritic spines through endocytosis of N-cadherin and potentially other CAM signalling pathways. This trans-synaptic remodelling subsequently alters the intrinsic neuronal excitability by reducing the overall surface area of neurons and decreasing their total membrane capacitance (Šišková et al., 2014), rendering the network even more hyperexcitable. Additionally, the activity-driven accumulation of amyloid beta and IEG overexpression lead to complement activation and phagocytic destruction of synapses by the resident activated glia. Thus, a synergistic positive feedback loop emerges between neuronal hyperactivity, amyloid beta accumulation and synaptic degeneration. Each of the three elements in this positive feedback loop have been

recently experimentally demonstrated by other research groups (Zhilin Wang et al., 2020; Xiao et al., 2021; J. Zhou et al., 2022).

6.2. Translational implications

Since epileptiform activity can occur before memory impairments and even before histological changes such as white matter atrophy and hippocampal sclerosis, these electrographic "biomarkers" can be used in the diagnosis of epileptic AD. Moreover, since epileptiform activity contributes towards and predicts faster disease progression and worse clinical outcomes, targeting this activity with antiepileptic drugs may help attenuate the potential damage it may cause during the progression of the disease.

The expression of immediate-early genes discussed in this study seems to be an all-or-none response, where a "strong enough" signal, namely a long lasting seizure, is required for their expression (Christensen et al., 2010). Consequently, the overexpression of IEGs and complement activation may serve as additional specific biomarkers that might help delineate patients with AD experiencing seizures from those without.

In conclusion, this work demonstrated the utility of data-driven systems-level investigation of complex pathomechanisms and key elements that control them. Future studies involving quantification of synaptic density in the dual pathology model would be instrumental in experimental validation of our hypothesized synergistic mechanism-model, and provide novel substrates for direct pharmacological intervention specific to seizure-prone patients of Alzheimer's Disease.

6.3. Limitations and concluding remarks

A complex interaction between numerous internal and external factors such as genomic makeup, presence of specific genetic variants, environmental and metabolic factors, injury and infection associated immune responses, determine the state and the specific electrical properties of the given circuit. The complexity of this system is difficult to conceptualize, but a simpler way to determine the likelihood of the given circuit to sustain a seizure can be described in terms of overall excitability of circuits, and the excitatory-to-inhibitory balance. Normal neuronal function in the brain depends on the dynamic and extremely precise equilibrium between excitatory and inhibitory inputs. Any disruption of this delicate balance may result in abnormal electrical activity, resulting in seizures. Any changes in these factors -

structural (altered dendritic spine density) or molecular (changes in the number of neurotransmitter transporters or receptors) that alter the intrinsic excitability of neurons have the potential of changing the excitatory to inhibitory balance, thus rendering the network more excitable, resulting in hyperexcitability, or less excitable – providing seizure resistance. It is important to delineate the excitability of which neurons (excitatory or inhibitory) is being influenced, as this will determine the overall direction the network will be shifting towards (more excitatory input or more inhibitory input). Our gene expression studies show downregulation of both excitatory and inhibitory synaptic proteins, thereby indicating a total loss of synapses, without providing additional information regarding the excitatory or inhibitory nature of these lost synapses. Future studies leveraging single-cell spatial transcriptomics paired with super-resolution microscopy techniques will be instrumental in elucidating which specific neuronal populations are more vulnerable to this synergistic activity-driven loss of synapses, which could inform the design of therapeutic interventions.

BIBLIOGRAPHY

Abramov, E., Dolev, I., Fogel, H., Ciccotosto, G. D., Ruff, E., & Slutsky, I. (2009). Amyloid-beta as a positive endogenous regulator of release probability at hippocampal synapses. *Nat Neurosci, 12*(12), 1567-1576. doi:10.1038/nn.2433

Adachi, K., Toyota, M., Sasaki, Y., Yamashita, T., Ishida, S., Ohe-Toyota, M., . . . Tokino, T. (2004). Identification of SCN3B as a novel p53-inducible proapoptotic gene. *Oncogene, 23*(47), 7791-7798. doi:10.1038/sj.onc.1208067

Akiyama, H., Barger, S., Barnum, S., Bradt, B., Bauer, J., Cole, G. M., . . . Wyss-Coray, T. (2000). Inflammation and Alzheimer's disease. *Neurobiol Aging, 21*(3), 383-421. Retrieved from https://www.ncbi.nlm.nih.gov/pubmed/10858586

https://www.ncbi.nlm.nih.gov/pmc/articles/PMC3887148/pdf/nihms542954.pdf

Alexander, J. C., McDermott, C. M., Tunur, T., Rands, V., Stelly, C., Karhson, D., . . . Schrader, L. A. (2009). The role of calsenilin/DREAM/KChIP3 in contextual fear conditioning. *Learn Mem, 16*(3), 167-177. doi:10.1101/lm.1261709

Aller-Alvarez, J. S., Menéndez-González, M., Ribacoba-Montero, R., Salvado, M., Vega, V., Suárez-Moro, R., . . . Álvarez-Sabin, J. (2017). Myoclonic epilepsy in Down syndrome and Alzheimer disease. *Neurologia, 32*(2), 69-73. doi:10.1016/j.nrl.2014.12.008

Alzheimer, A., Forstl, H., & Levy, R. (1991). On certain peculiar diseases of old age. *Hist Psychiatry, 2*(5 Pt 1), 71-101. doi:10.1177/0957154X9100200505

Amatniek, J. C., Hauser, W. A., DelCastillo-Castaneda, C., Jacobs, D. M., Marder, K., Bell, K., . . . Stern, Y. (2006). Incidence and predictors of seizures in patients with Alzheimer's disease. *Epilepsia, 47*(5), 867-872. doi:10.1111/j.1528-1167.2006.00554.x

Banote, R. K., Håkansson, S., Zetterberg, H., & Zelano, J. (2022). CSF biomarkers in patients with epilepsy in Alzheimer's disease: a nation-wide study. *Brain Commun, 4*(4), fcac210. doi:10.1093/braincomms/fcac210

Barabási, A.-L., & Oltvai, Z. N. (2004). Network biology: understanding the cell's functional organization. *Nature Reviews Genetics, 5*(2), 101-113. doi:10.1038/nrg1272

Barabasi, A. L., Gulbahce, N., & Loscalzo, J. (2011). Network medicine: a network-based approach to human disease. *Nat Rev Genet, 12*(1), 56-68. doi:10.1038/nrg2918

Beghi, E., Giussani, G., Nichols, E., Abd-Allah, F., Abdela, J., Abdelalim, A., . . . Murray, C. J. L. (2019). Global, regional, and national burden of epilepsy, 1990–2016: a systematic analysis for the Global Burden of Disease Study 2016. *The Lancet Neurology, 18*(4), 357-375. doi:https://doi.org/10.1016/S1474-4422(18)30454-X

Bell, D., Berchuck, A., Birrer, M., Chien, J., Cramer, D. W., Dao, F., . . . Data coordination, c. (2011). Integrated genomic analyses of ovarian carcinoma. *Nature, 474*(7353), 609-615. doi:10.1038/nature10166

Benjamini, Y., & Hochberg, Y. (1995). Controlling the False Discovery Rate: A Practical and Powerful Approach to Multiple Testing. *Journal of the Royal Statistical Society. Series B (Methodological), 57*(1), 289-300. doi:10.2307/2346101

Berchtold, N. C., Coleman, P. D., Cribbs, D. H., Rogers, J., Gillen, D. L., & Cotman, C. W. (2013). Synaptic genes are extensively downregulated across multiple brain regions in normal human aging and Alzheimer's disease. *Neurobiol Aging, 34*(6), 1653-1661. doi:10.1016/j.neurobiolaging.2012.11.024

Berchtold, N. C., Prieto, G. A., Phelan, M., Gillen, D. L., Baldi, P., Bennett, D. A., . . . Cotman, C. W. (2019). Hippocampal gene expression patterns linked to late-life physical activity oppose age and AD-related transcriptional decline. *Neurobiol Aging, 78*, 142-154. doi:10.1016/j.neurobiolaging.2019.02.012

Bero, A. W., Yan, P., Roh, J. H., Cirrito, J. R., Stewart, F. R., Raichle, M. E., . . . Holtzman, D. M. (2011). Neuronal activity regulates the regional vulnerability to amyloid-β deposition. *Nat Neurosci, 14*(6), 750-756. doi:10.1038/nn.2801

Bezzina, C., Verret, L., Juan, C., Remaud, J., Halley, H., Rampon, C., & Dahan, L. (2015). Early onset of hypersynchronous network activity and expression of a marker of chronic seizures in the Tg2576 mouse model of Alzheimer's disease. *PLoS One, 10*(3). doi:10.1371/journal.pone.0119910

Bhandare, A. M., Kapoor, K., Powell, K. L., Braine, E., Casillas-Espinosa, P., O'Brien, T. J., . . . Pilowsky, P. M. (2017). Inhibition of microglial activation with minocycline at the intrathecal level attenuates sympathoexcitatory and proarrhythmogenic changes in rats with chronic temporal lobe epilepsy. *Neuroscience, 350*, 23-38. doi:10.1016/j.neuroscience.2017.03.012

Bjorkhem, I., & Meaney, S. (2004). Brain cholesterol: long secret life behind a barrier. *Arterioscler Thromb Vasc Biol, 24*(5), 806-815. doi:10.1161/01.ATV.0000120374.59826.1b

Blalock, E. M., Buechel, H. M., Popovic, J., Geddes, J. W., & Landfield, P. W. (2011). Microarray analyses of laser-captured hippocampus reveal distinct gray and white matter signatures associated with incipient Alzheimer's disease. *J Chem Neuroanat, 42*(2), 118-126. doi:10.1016/j.jchemneu.2011.06.007

Block, M. L., Zecca, L., & Hong, J. S. (2007). Microglia-mediated neurotoxicity: uncovering the molecular mechanisms. *Nat Rev Neurosci, 8*(1), 57-69. doi:10.1038/nrn2038

Brady, R., Wong, K., Robinson, D., Mychasiuk, R., McDonald, S., D'Cunha, R., . . . Shultz, S. (2019). Bone Health in Rats With Temporal Lobe Epilepsy in the Absence of Anti-Epileptic Drugs. *Frontiers in Pharmacology, 10*, 1278-1278. Retrieved from HTTP://unimelb.hosted.exlibrisgroup.com/sfxlcl41?sid=Entrez%3APubMed&id=pmid%3A31749702

https://www.ncbi.nlm.nih.gov/pmc/articles/PMC6842946/pdf/fphar-10-01278.pdf

Breitner, J. C. (1996). The role of anti-inflammatory drugs in the prevention and treatment of Alzheimer's disease. *Annu Rev Med, 47*, 401-411. doi:10.1146/annurev.med.47.1.401

Breitner, J. C., Welsh, K. A., Helms, M. J., Gaskell, P. C., Gau, B. A., Roses, A. D., . . . Saunders, A. M. (1995). Delayed onset of Alzheimer's disease with nonsteroidal anti-inflammatory and histamine H2 blocking drugs. *Neurobiol Aging, 16*(4), 523-530. doi:10.1016/0197-4580(95)00049-k

Buckner, R. L., Snyder, A. Z., Shannon, B. J., LaRossa, G., Sachs, R., Fotenos, A. F., . . . Mintun, M. A. (2005). Molecular, Structural, and Functional Characterization of Alzheimer's Disease: Evidence for a Relationship between Default Activity, Amyloid, and Memory. *The Journal of Neuroscience, 25*(34), 7709-7717. doi:10.1523/jneurosci.2177-05.2005

Buxbaum, J. D., Choi, E. K., Luo, Y., Lilliehook, C., Crowley, A. C., Merriam, D. E., & Wasco, W. (1998). Calsenilin: a calcium-binding protein that interacts with the presenilins and regulates the levels of a presenilin fragment. *Nat Med, 4*(10), 1177-1181. doi:10.1038/2673

Canevari, L., Abramov, A. Y., & Duchen, M. R. (2004). Toxicity of amyloid beta peptide: tales of calcium, mitochondria, and oxidative stress. *Neurochem Res, 29*(3), 637-650. doi:10.1023/b:nere.0000014834.06405.af

Cappellano, G., Carecchio, M., Fleetwood, T., Magistrelli, L., Cantello, R., Dianzani, U., & Comi, C. (2013). Immunity and inflammation in neurodegenerative diseases. *Am J*

Neurodegener Dis, 2(2), 89-107. Retrieved from https://www.ncbi.nlm.nih.gov/pubmed/23844334

Cardin, J. A., Carlen, M., Meletis, K., Knoblich, U., Zhang, F., Deisseroth, K., . . . Moore, C. I. (2009). Driving fast-spiking cells induces gamma rhythm and controls sensory responses. *Nature, 459*(7247), 663-667. doi:10.1038/nature08002

Casillas Espinosa, P., Hicks, A., Jeffreys, A., Snutch, T., O'Brien, T., & Powell, K. (2015). Z944, a Novel Selective T-Type Calcium Channel Antagonist Delays the Progression of Seizures in the Amygdala Kindling Model. *PLoS One, 10*(8), e0130012. Retrieved from http://sfx.unimelb.hosted.exlibrisgroup.com/sfxlcl41/?sid=Entrez%3APubMed&id=pmid%3A26274319

http://www.ncbi.nlm.nih.gov/pmc/articles/PMC4537250/pdf/pone.0130012.pdf

https://www.ncbi.nlm.nih.gov/pmc/articles/PMC4537250/pdf/pone.0130012.pdf

Casillas-Espinosa, P. M., Anderson, A., Harutyunyan, A., Li, C., Lee, J., Braine, E. L., . . . O'Brien, T. J. (2023). Disease-modifying effects of sodium selenate in a model of drug-resistant, temporal lobe epilepsy. *eLife, 12*. doi:10.7554/eLife.78877

Casillas-Espinosa, P. M., Powell, K. L., Zhu, M., Campbell, C. R., Maia, J. M., Ren, Z., . . . Petrovski, S. (2017). Evaluating whole genome sequence data from the Genetic Absence Epilepsy Rat from Strasbourg and its related non-epileptic strain. *PLoS One, 12*(7). doi:http://dx.doi.org/10.1371/journal.pone.0179924

Casillas-Espinosa, P. M., Sargsyan, A., Melkonian, D., & O'Brien, T. J. (2019). A universal automated tool for reliable detection of seizures in rodent models of acquired and genetic epilepsy. *Epilepsia, 60*(4), 783-791. doi:https://doi.org/10.1111/epi.14691

Casillas-Espinosa, P. M., Shultz, S. R., Braine, E. L., Jones, N. C., Snutch, T. P., Powell, K. L., & O'Brien, T. J. (2019). Disease-modifying effects of a novel T-type calcium channel antagonist, Z944, in a model of temporal lobe epilepsy. *Prog Neurobiol*, 101677. doi:10.1016/j.pneurobio.2019.101677

Chan, J., Jones, N. C., Bush, A. I., O'Brien, T. J., & Kwan, P. (2015). A mouse model of Alzheimer's disease displays increased susceptibility to kindling and seizure-associated death. *Epilepsia, 56*(6), e73-77. doi:10.1111/epi.12993

Chen, C.-H., Ferreira, J. C. B., Gross, E. R., & Mochly-Rosen, D. (2014). Targeting aldehyde dehydrogenase 2: new therapeutic opportunities. *Physiological reviews, 94*(1), 1-34. doi:10.1152/physrev.00017.2013

Chen, E. Y., Tan, C. M., Kou, Y., Duan, Q., Wang, Z., Meirelles, G. V., . . . Ma'ayan, A. (2013). Enrichr: interactive and collaborative HTML5 gene list enrichment analysis tool. *BMC Bioinformatics, 14*, 128. doi:10.1186/1471-2105-14-128

Chen, S., Frederickson, R. C., & Brunden, K. R. (1996). Neuroglial-mediated immunoinflammatory responses in Alzheimer's disease: complement activation and therapeutic approaches. *Neurobiol Aging, 17*(5), 781-787. doi:10.1016/0197-4580(96)00103-0

Chen, Y., Zhu, J., Lum, P. Y., Yang, X., Pinto, S., MacNeil, D. J., . . . Schadt, E. E. (2008). Variations in DNA elucidate molecular networks that cause disease. *Nature, 452*, 429. doi:10.1038/nature06757

https://www.nature.com/articles/nature06757#supplementary-information

Christensen, K. V., Leffers, H., Watson, W. P., Sánchez, C., Kallunki, P., & Egebjerg, J. (2010). Levetiracetam attenuates hippocampal expression of synaptic plasticity-related

immediate early and late response genes in amygdala-kindled rats. *BMC Neuroscience, 11*(1), 9. doi:10.1186/1471-2202-11-9

Ciriello, G., Gatza, Michael L., Beck, Andrew H., Wilkerson, Matthew D., Rhie, Suhn K., Pastore, A., . . . Perou, C. M. (2015). Comprehensive Molecular Portraits of Invasive Lobular Breast Cancer. *Cell, 163*(2), 506-519. doi:https://doi.org/10.1016/j.cell.2015.09.033

Clarke, C., Madden, S. F., Doolan, P., Aherne, S. T., Joyce, H., O'Driscoll, L., . . . Clynes, M. (2013). Correlating transcriptional networks to breast cancer survival: a large-scale coexpression analysis. *Carcinogenesis, 34*(10), 2300-2308. doi:10.1093/carcin/bgt208

Clough, E., & Barrett, T. (2016). The Gene Expression Omnibus Database. *Methods Mol Biol, 1418*, 93-110. doi:10.1007/978-1-4939-3578-9_5

Coenen, A. M. L., & van Luijtelaar, E. L. J. M. (2003). Genetic Animal Models for Absence Epilepsy: A Review of the WAG/Rij Strain of Rats. *Behavior Genetics, 33*(6), 635-655. doi:10.1023/A:1026179013847

Condello, C., Yuan, P., Schain, A., & Grutzendler, J. (2015). Microglia constitute a barrier that prevents neurotoxic protofibrillar Aβ42 hotspots around plaques. *Nat Commun, 6*, 6176. doi:10.1038/ncomms7176

Corbett, B. F., Leiser, S. C., Ling, H. P., Nagy, R., Breysse, N., Zhang, X., . . . Chin, J. (2013). Sodium channel cleavage is associated with aberrant neuronal activity and cognitive deficits in a mouse model of Alzheimer's disease. *J Neurosci, 33*(16), 7020-7026. doi:10.1523/JNEUROSCI.2325-12.2013

Corbett, B. F., You, J. C., Zhang, X., Pyfer, M. S., Tosi, U., Iascone, D. M., . . . Chin, J. (2017). ΔFosB Regulates Gene Expression and Cognitive Dysfunction in a Mouse Model of Alzheimer's Disease. *Cell Reports, 20*(2), 344-355. doi:10.1016/j.celrep.2017.06.040

Corbett, M. A., Bahlo, M., Jolly, L., Afawi, Z., Gardner, A. E., Oliver, K. L., . . . Gecz, J. (2010). A focal epilepsy and intellectual disability syndrome is due to a mutation in TBC1D24. *Am J Hum Genet, 87*(3), 371-375. doi:10.1016/j.ajhg.2010.08.001

Costa, C., Romoli, M., Liguori, C., Farotti, L., Eusebi, P., Bedetti, C., . . . Calabresi, P. (2019). Alzheimer's disease and late-onset epilepsy of unknown origin: two faces of beta amyloid pathology. *Neurobiology of Aging, 73*, 61-67. doi:https://doi.org/10.1016/j.neurobiolaging.2018.09.006

Creek, D. J., Jankevics, A., Breitling, R., Watson, D. G., Barrett, M. P., & Burgess, K. E. V. (2011). Toward Global Metabolomics Analysis with Hydrophilic Interaction Liquid Chromatography–Mass Spectrometry: Improved Metabolite Identification by Retention Time Prediction. *Analytical Chemistry, 83*(22), 8703-8710. doi:10.1021/ac2021823

Creek, D. J., Jankevics, A., Burgess, K. E., Breitling, R., & Barrett, M. P. (2012). IDEOM: an Excel interface for analysis of LC-MS-based metabolomics data. *Bioinformatics, 28*(7), 1048-1049. doi:10.1093/bioinformatics/bts069

Crunelli, V., & Leresche, N. (2002). Childhood absence epilepsy: Genes, channels, neurons and networks. *Nature Reviews Neuroscience, 3*(5), 371-382. doi:10.1038/nrn811

Danış, Ö., Demir, S., Günel, A., Aker, R. G., Gülçebi, M., Onat, F., & Ogan, A. (2011). Changes in intracellular protein expression in cortex, thalamus and hippocampus in a genetic rat model of absence epilepsy. *Brain Research Bulletin, 84*(6), 381-388. doi:https://doi.org/10.1016/j.brainresbull.2011.02.002

Danober, L., Deransart, C., Depaulis, A., Vergnes, M., & Marescaux, C. (1998). Pathophysiological mechanisms of genetic absence epilepsy in the rat. *Progress in Neurobiology, 55*(1), 27-57. doi:https://doi.org/10.1016/S0301-0082(97)00091-9

Davidson, Y. S., Raby, S., Foulds, P. G., Robinson, A., Thompson, J. C., Sikkink, S., . . . Mann, D. M. (2011). TDP-43 pathological changes in early onset familial and sporadic Alzheimer's disease, late onset Alzheimer's disease and Down's syndrome: association with age, hippocampal sclerosis and clinical phenotype. *Acta Neuropathol, 122*(6), 703-713. doi:10.1007/s00401-011-0879-y

Davis, S., & Meltzer, P. S. (2007). GEOquery: a bridge between the Gene Expression Omnibus (GEO) and BioConductor. *Bioinformatics, 23*(14), 1846-1847. doi:10.1093/bioinformatics/btm254

Dejakaisaya, H., Harutyunyan, A., Kwan, P., & Jones, N. C. (2021). Altered metabolic pathways in a transgenic mouse model suggest mechanistic role of amyloid precursor protein overexpression in Alzheimer's disease. *Metabolomics, 17*(5), 42. doi:10.1007/s11306-021-01793-4

Dellu, F., Mayo, W., Cherkaoui, J., Le Moal, M., & Simon, H. (1992). A two-trial memory task with automated recording: study in young and aged rats. *Brain Research, 588*(1), 132-139. doi:https://doi.org/10.1016/0006-8993(92)91352-F

Depaulis, A., & Charpier, S. (2018). Pathophysiology of absence epilepsy: Insights from genetic models. *Neuroscience Letters, 667*, 53-65. doi:https://doi.org/10.1016/j.neulet.2017.02.035

Devinsky, O., Kim, A., Friedman, D., Bedigian, A., Moffatt, E., & Tseng, Z. H. (2018). Incidence of cardiac fibrosis in SUDEP and control cases. *Neurology, 91*(1), e55-e61. doi:10.1212/wnl.0000000000005740

Devinsky, O., Schein, A., & Najjar, S. (2013). Epilepsy Associated with Systemic Autoimmune Disorders: Epilepsy and Systemic Autoimmune Disorders. *Epilepsy Currents, 13*(2), 62-68. doi:10.5698/1535-7597-13.2.62

Devinsky, O., Vezzani, A., O'Brien, T. J., Jette, N., Scheffer, I. E., de Curtis, M., & Perucca, P. (2018). Epilepsy. *Nature Reviews Disease Primers, 4*(1), 18024. doi:10.1038/nrdp.2018.24

Dong-Gyu, J., Joo-Yong, L., Yeon-Mi, H., Sungmin, S., Inhee, M.-J., Jae-Young, K., & Yong-Keun, J. (2004). Induction of pro-apoptotic calsenilin/DREAM/KChIP3 in Alzheimer's disease and cultured neurons after amyloid-β exposure. *Journal of Neurochemistry, 88*(3), 604-611. doi:https://doi.org/10.1111/j.1471-4159.2004.02159.x

Drinkenburg, W. H., Maher, M. P., Raeymaekers, L., Ravula, S., Ameriks, M. K., Savall, B. M., . . . Ahnaou, A. (2017). Cortical hyper-excitability-related seizures in APP/PS1 transgenic mice are attenuated by selective TARP-gamma8 AMPA receptor modulation. *Neurodegenerative Diseases, 17*, 918. Retrieved from http://www.embase.com/search/results?subaction=viewrecord&from=export&id=L615511089

Dun, C., Zhang, Y., Yin, J., Su, B., Peng, X., & Liu, L. (2022). Bi-directional associations of epilepsy with dementia and Alzheimer's disease: a systematic review and meta-analysis of longitudinal studies. *Age and Ageing, 51*(3). doi:10.1093/ageing/afac010

Dunckley, T., Beach, T. G., Ramsey, K. E., Grover, A., Mastroeni, D., Walker, D. G., . . . Stephan, D. A. (2006). Gene expression correlates of neurofibrillary tangles in Alzheimer's disease. *Neurobiol Aging, 27*(10), 1359-1371. doi:10.1016/j.neurobiolaging.2005.08.013

Efthymiou, A. G., & Goate, A. M. (2017). Late onset Alzheimer's disease genetics implicates microglial pathways in disease risk. *Mol Neurodegener, 12*(1), 43. doi:10.1186/s13024-017-0184-x

Euro, E.-R. E. S. C., Epilepsy Phenome/Genome, P., & Epi, K. C. (2014). De novo mutations in synaptic transmission genes including DNM1 cause epileptic encephalopathies. *Am J Hum Genet, 95*(4), 360-370. doi:10.1016/j.ajhg.2014.08.013

Fabregat, A., Jupe, S., Matthews, L., Sidiropoulos, K., Gillespie, M., Garapati, P., . . . D'Eustachio, P. (2018). The Reactome Pathway Knowledgebase. *Nucleic Acids Res, 46*(D1), D649-D655. doi:10.1093/nar/gkx1132

Fisher, R. S., Cross, J. H., French, J. A., Higurashi, N., Hirsch, E., Jansen, F. E., . . . Zuberi, S. M. (2017). Operational classification of seizure types by the International League Against Epilepsy: Position Paper of the ILAE Commission for Classification and Terminology. *Epilepsia, 58*(4), 522-530. doi:10.1111/epi.13670

Forman, M. S., Mufson, E. J., Leurgans, S., Pratico, D., Joyce, S., Leight, S., . . . Trojanowski, J. Q. (2007). Cortical biochemistry in MCI and Alzheimer disease: lack of correlation with clinical diagnosis. *Neurology, 68*(10), 757-763. doi:10.1212/01.wnl.0000256373.39415.b1

Fu, A. K., Hung, K. W., Huang, H., Gu, S., Shen, Y., Cheng, E. Y., . . . Ip, N. Y. (2014). Blockade of EphA4 signaling ameliorates hippocampal synaptic dysfunctions in mouse models of Alzheimer's disease. *Proc Natl Acad Sci U S A, 111*(27), 9959-9964. doi:10.1073/pnas.1405803111

Fu, C. H., Iascone, D. M., Petrof, I., Hazra, A., Zhang, X., Pyfer, M. S., . . . Chin, J. (2019). Early Seizure Activity Accelerates Depletion of Hippocampal Neural Stem Cells and Impairs Spatial Discrimination in an Alzheimer's Disease Model. *Cell Reports, 27*(13), 3741-3751.e3744. doi:10.1016/j.celrep.2019.05.101

Fukumoto, H., Cheung, B. S., Hyman, B. T., & Irizarry, M. C. (2002). Beta-secretase protein and activity are increased in the neocortex in Alzheimer disease. *Arch Neurol, 59*(9), 1381-1389. doi:10.1001/archneur.59.9.1381

Gibney, E. R., & Nolan, C. M. (2010). Epigenetics and gene expression. *Heredity, 105*(1), 4-13. doi:10.1038/hdy.2010.54

Gilchrist, L. (1963). CARDIOMYOPATHY, TEMPORAL LOBE EPILEPSY AND PREGNANCY. *Proc R Soc Med, 56*(10), 923.

Glass, C. K., Saijo, K., Winner, B., Marchetto, M. C., & Gage, F. H. (2010). Mechanisms underlying inflammation in neurodegeneration. *Cell, 140*(6), 918-934. doi:10.1016/j.cell.2010.02.016

Gourmaud, S., Shou, H., Irwin, D. J., Sansalone, K., Jacobs, L. M., Lucas, T. H., . . . Talos, D. M. (2020). Alzheimer-like amyloid and tau alterations associated with cognitive deficit in temporal lobe epilepsy. *Brain, 143*(1), 191-209. doi:10.1093/brain/awz381

Gourmaud, S., Stewart, D. A., Irwin, D. J., Roberts, N., Barbour, A. J., Eberwine, G., . . . Jensen, F. E. (2022). The role of mTORC1 activation in seizure-induced exacerbation of Alzheimer's disease. *Brain, 145*(1), 324-339. doi:10.1093/brain/awab268

Goytain, A., & Ng, T. (2020). NanoString nCounter Technology: High-Throughput RNA Validation. *Methods Mol Biol, 2079*, 125-139. doi:10.1007/978-1-4939-9904-0_10

Grimes, T., Potter, S. S., & Datta, S. (2019). Integrating gene regulatory pathways into differential network analysis of gene expression data. *Scientific reports, 9*(1), 5479. doi:10.1038/s41598-019-41918-3

Grundke-Iqbal, I., Iqbal, K., Tung, Y. C., Quinlan, M., Wisniewski, H. M., & Binder, L. I. (1986). Abnormal phosphorylation of the microtubule-associated protein tau (tau) in Alzheimer cytoskeletal pathology. *Proc Natl Acad Sci U S A, 83*(13), 4913-4917. doi:10.1073/pnas.83.13.4913

Habeych, M. E., Falcone, T., Dagar, A., Ford, L., & Castilla-Puentes, R. (2021). Dementia, Subtype of Seizures, and the Risk of New Onset Seizures: A Cohort Study. *J Alzheimers Dis, 81*(3), 973-980. doi:10.3233/jad-210028

Habib, N., McCabe, C., Medina, S., Varshavsky, M., Kitsberg, D., Dvir-Szternfeld, R., . . . Schwartz, M. (2020). Disease-associated astrocytes in Alzheimer's disease and aging. *Nature Neuroscience, 23*(6), 701-706. doi:10.1038/s41593-020-0624-8

Han, Z., Xue, W., Tao, L., & Zhu, F. (2019). Identification of Key Long Non-Coding RNAs in the Pathology of Alzheimer's Disease and their Functions Based on Genome-Wide Associations Study, Microarray, and RNA-seq Data. *J Alzheimers Dis, 68*(1), 339-355. doi:10.3233/jad-181051

Hardy, J. A., & Higgins, G. A. (1992). Alzheimer's disease: the amyloid cascade hypothesis. *Science, 256*(5054), 184-185. Retrieved from https://www.ncbi.nlm.nih.gov/pubmed/1566067

https://science.sciencemag.org/content/256/5054/184.long

Harris, M. A., Clark, J., Ireland, A., Lomax, J., Ashburner, M., Foulger, R., . . . Gene Ontology, C. (2004). The Gene Ontology (GO) database and informatics resource. *Nucleic Acids Res, 32*(Database issue), D258-261. doi:10.1093/nar/gkh036

Harutyunyan, A., Chong, D., Li, R., Shah, A. D., Ali, Z., Huang, C., . . . Casillas-Espinosa, P. M. (2022). An Integrated Multi-Omic Network Analysis Identifies Seizure-Associated Dysregulated Pathways in the GAERS Model of Absence Epilepsy. *Int J Mol Sci, 23*(11). doi:10.3390/ijms23116063

Harutyunyan, A., Jones, N. C., Kwan, P., & Anderson, A. (2022). Network Preservation Analysis Reveals Dysregulated Synaptic Modules and Regulatory Hubs Shared Between Alzheimer's Disease and Temporal Lobe Epilepsy. *Frontiers in Genetics, 13*. doi:10.3389/fgene.2022.821343

Hauser, W. A., & Annegers, J. F. (1991). Risk factors for epilepsy. *Epilepsy Res Suppl, 4*, 45-52. Retrieved from https://www.ncbi.nlm.nih.gov/pubmed/1815610

Hauser, W. A., Morris, M. L., Heston, L. L., & Anderson, V. E. (1986). Seizures and myoclonus in patients with Alzheimer's disease. *Neurology, 36*(9), 1226-1230. Retrieved from https://www.ncbi.nlm.nih.gov/pubmed/3092131

Hazra, A., Corbett, B. F., You, J. C., Aschmies, S., Zhao, L., Li, K., . . . Chin, J. (2016). Corticothalamic network dysfunction and behavioral deficits in a mouse model of Alzheimer's disease. *Neurobiology of Aging, 44*, 96-107. doi:10.1016/j.neurobiolaging.2016.04.016

Heneka, M. T., Carson, M. J., El Khoury, J., Landreth, G. E., Brosseron, F., Feinstein, D. L., . . . Kummer, M. P. (2015). Neuroinflammation in Alzheimer's disease. *Lancet Neurol, 14*(4), 388-405. doi:10.1016/S1474-4422(15)70016-5

Heneka, M. T., Kummer, M. P., Stutz, A., Delekate, A., Schwartz, S., Vieira-Saecker, A., . . . Golenbock, D. T. (2013). NLRP3 is activated in Alzheimer's disease and contributes to pathology in APP/PS1 mice. *Nature, 493*(7434), 674-678. doi:10.1038/nature11729

Hermann, B., Seidenberg, M., & Jones, J. (2008). The neurobehavioural comorbidities of epilepsy: can a natural history be developed? *Lancet neurology, 7*(2), 151-160. Retrieved from http://sfx.unimelb.hosted.exlibrisgroup.com/sfxlcl41/?sid=Entrez%3APubMed&id=pmid%3A18207113

http://ac.els-cdn.com.ezp.lib.unimelb.edu.au/S1474442208700188/1-s2.0-S1474442208700188-main.pdf?_tid=d4398bf6-85f2-11e6-8a43-00000aacb35d&acdnat=1475119047_62dce0913f56eeb7f9e7ed1aac87cc39

Hermann, B. P., Seidenberg, M., Bell, B., Woodard, A., Rutecki, P., & Sheth, R. (2000). Comorbid psychiatric symptoms in temporal lobe epilepsy: association with chronicity of epilepsy and impact on quality of life. *Epilepsy & behavior, 1*(3), 184-190. Retrieved from http://sfx.unimelb.hosted.exlibrisgroup.com/sfxlcl41?sid=Entrez%3APubMed&id=pmid%3A12609152

Hesdorffer, D. C., Hauser, W. A., Annegers, J. F., Kokmen, E., & Rocca, W. A. (1996). Dementia and adult-onset unprovoked seizures. *Neurology, 46*(3), 727-730. Retrieved from https://www.ncbi.nlm.nih.gov/pubmed/8618673

Hoeijmakers, W. A., Bartfai, R., & Stunnenberg, H. G. (2013). Transcriptome analysis using RNA-Seq. *Methods Mol Biol, 923*, 221-239. doi:10.1007/978-1-62703-026-7_15

Hong, S., Beja-Glasser, V. F., Nfonoyim, B. M., Frouin, A., Li, S., Ramakrishnan, S., . . . Stevens, B. (2016). Complement and microglia mediate early synapse loss in Alzheimer mouse models. *Science, 352*(6286), 712-716. doi:10.1126/science.aad8373

Horgan, R. P., & Kenny, L. C. (2011). 'Omic' technologies: genomics, transcriptomics, proteomics and metabolomics. *The Obstetrician & Gynaecologist, 13*(3), 189-195. doi:https://doi.org/10.1576/toag.13.3.189.27672

Horvath, A. A., Papp, A., Zsuffa, J., Szucs, A., Luckl, J., Radai, F., . . . Kamondi, A. (2021). Subclinical epileptiform activity accelerates the progression of Alzheimer's disease: A long-term EEG study. *Clinical Neurophysiology, 132*(8), 1982-1989. doi:https://doi.org/10.1016/j.clinph.2021.03.050

Huan, T., Meng, Q., Saleh, M. A., Norlander, A. E., Joehanes, R., Zhu, J., . . . Levy, D. (2015). Integrative network analysis reveals molecular mechanisms of blood pressure regulation. *Mol Syst Biol, 11*(1), 799. doi:10.15252/msb.20145399

Huang, L., Fu, C., Li, J., & Peng, S. (2022). Late-onset epilepsy and the risk of dementia: a systematic review and meta-analysis. *Aging Clinical and Experimental Research, 34*(8), 1771-1779. doi:10.1007/s40520-022-02118-8

Ikonen, E. (2008). Cellular cholesterol trafficking and compartmentalization. *Nature Reviews Molecular Cell Biology, 9*(2), 125-138. doi:10.1038/nrm2336

Jackson, J. E. (1991). *A user's guide to principal components*. New York: Wiley.

Jang, C., Choi, J.-K., Na, Y.-J., Jang, B., Wasco, W., Buxbaum, J., . . . Choi, E.-K. (2011). Calsenilin regulates presenilin 1/ -secretase-mediated N-cadherin -cleavage and -catenin signaling. *FASEB journal : official publication of the Federation of American Societies for Experimental Biology, 25*, 4174-4183. doi:10.1096/fj.11-185926

Jassal, B., Matthews, L., Viteri, G., Gong, C., Lorente, P., Fabregat, A., . . . D'Eustachio, P. (2020). The reactome pathway knowledgebase. *Nucleic Acids Res, 48*(D1), D498-D503. doi:10.1093/nar/gkz1031

Jassal, B., Matthews, L., Viteri, G., Gong, C., Lorente, P., Fabregat, A., . . . D'Eustachio, P. (2020). The reactome pathway knowledgebase. *Nucleic Acids Research, 48*(D1), D498-D503. doi:10.1093/nar/gkz1031

Jaturapatporn, D., Isaac, M. G., McCleery, J., & Tabet, N. (2012). Aspirin, steroidal and non-steroidal anti-inflammatory drugs for the treatment of Alzheimer's disease. *Cochrane Database Syst Rev*(2), CD006378. doi:10.1002/14651858.CD006378.pub2

Johnson, M. R., Behmoaras, J., Bottolo, L., Krishnan, M. L., Pernhorst, K., Santoscoy, P. L. M., . . . Petretto, E. (2015). Systems genetics identifies Sestrin 3 as a regulator of a proconvulsant gene network in human epileptic hippocampus. *Nat Commun, 6*, 6031. doi:10.1038/ncomms7031

Johnson, M. R., Behmoaras, J., Bottolo, L., Krishnan, M. L., Pernhorst, K., Santoscoy, P. L. M., . . . Petretto, E. (2015). Systems genetics identifies Sestrin 3 as a regulator of a

proconvulsant gene network in human epileptic hippocampus. *Nature Communications, 6*, 6031. doi:10.1038/ncomms7031

https://www.nature.com/articles/ncomms7031#supplementary-information

Johnstone, V. P., Wright, D. K., Wong, K., O'Brien, T. J., Rajan, R., & Shultz, S. R. (2015). Experimental Traumatic Brain Injury Results in Long-Term Recovery of Functional Responsiveness in Sensory Cortex but Persisting Structural Changes and Sensorimotor, Cognitive, and Emotional Deficits. *J Neurotrauma, 32*(17), 1333-1346. doi:10.1089/neu.2014.3785

Jones, N. C., Salzberg, M. R., Kumar, G., Couper, A., Morris, M. J., & O'Brien, T. J. (2008). Elevated anxiety and depressive-like behavior in a rat model of genetic generalized epilepsy suggesting common causation. *Exp Neurol, 209*(1), 254-260. doi:10.1016/j.expneurol.2007.09.026

Joshi-Tope, G., Gillespie, M., Vastrik, I., D'Eustachio, P., Schmidt, E., de Bono, B., . . . Stein, L. (2005). Reactome: a knowledgebase of biological pathways. *Nucleic Acids Res, 33*(Database issue), D428-432. doi:10.1093/nar/gki072

Kam, K., Duffy, A. M., Moretto, J., LaFrancois, J. J., & Scharfman, H. E. (2016). Interictal spikes during sleep are an early defect in the Tg2576 mouse model of beta-amyloid neuropathology. *Sci Rep, 6*, 20119. doi:10.1038/srep20119

Kamenetz, F., Tomita, T., Hsieh, H., Seabrook, G., Borchelt, D., Iwatsubo, T., . . . Malinow, R. (2003). APP processing and synaptic function. *Neuron, 37*(6), 925-937. doi:10.1016/s0896-6273(03)00124-7

Kim, D. Y., Carey, B. W., Wang, H., Ingano, L. A., Binshtok, A. M., Wertz, M. H., . . . Kovacs, D. M. (2007). BACE1 regulates voltage-gated sodium channels and neuronal activity. *Nat Cell Biol, 9*(7), 755-764. doi:10.1038/ncb1602

Kim, D. Y., Gersbacher, M. T., Inquimbert, P., & Kovacs, D. M. (2011). Reduced sodium channel Na(v)1.1 levels in BACE1-null mice. *J Biol Chem, 286*(10), 8106-8116. doi:10.1074/jbc.M110.134692

Kim, T., Vidal, G. S., Djurisic, M., William, C. M., Birnbaum, M. E., Garcia, K. C., . . . Shatz, C. J. (2013). Human LilrB2 is a β-amyloid receptor and its murine homolog PirB regulates synaptic plasticity in an Alzheimer's model. *Science, 341*(6152), 1399-1404. doi:10.1126/science.1242077

Koschutzki, D., & Schreiber, F. (2008). Centrality analysis methods for biological networks and their application to gene regulatory networks. *Gene Regul Syst Bio, 2*, 193-201. doi:10.4137/grsb.s702

Kuleshov, M. V., Jones, M. R., Rouillard, A. D., Fernandez, N. F., Duan, Q., Wang, Z., . . . Ma'ayan, A. (2016). Enrichr: a comprehensive gene set enrichment analysis web server 2016 update. *Nucleic Acids Res, 44*(W1), W90-97. doi:10.1093/nar/gkw377

Kwan, P., Schachter, S. C., & Brodie, M. J. (2011). Drug-resistant epilepsy. *N Engl J Med, 365*(10), 919-926. doi:10.1056/NEJMra1004418

Langfelder, P., & Horvath, S. (2007). Eigengene networks for studying the relationships between co-expression modules. *BMC Syst Biol, 1*, 54. doi:10.1186/1752-0509-1-54

Langfelder, P., & Horvath, S. (2008). WGCNA: an R package for weighted correlation network analysis. *BMC Bioinformatics, 9*, 559. doi:10.1186/1471-2105-9-559

Langfelder, P., Luo, R., Oldham, M. C., & Horvath, S. (2011). Is my network module preserved and reproducible? *PLoS Comput Biol, 7*(1), e1001057. doi:10.1371/journal.pcbi.1001057

Langfelder, P., Zhang, B., & Horvath, S. (2008). Defining clusters from a hierarchical cluster tree: the Dynamic Tree Cut package for R. *Bioinformatics, 24*(5), 719-720. doi:10.1093/bioinformatics/btm563

Leandro, J., & Houten, S. M. (2020). The lysine degradation pathway: Subcellular compartmentalization and enzyme deficiencies. *Molecular Genetics and Metabolism, 131*(1), 14-22. doi:https://doi.org/10.1016/j.ymgme.2020.07.010

Lee, H. K., Hsu, A. K., Sajdak, J., Qin, J., & Pavlidis, P. (2004). Coexpression analysis of human genes across many microarray data sets. *Genome Res, 14*(6), 1085-1094. doi:10.1101/gr.1910904

Leek, J. T., Johnson, W. E., Parker, H. S., Jaffe, A. E., & Storey, J. D. (2012). The sva package for removing batch effects and other unwanted variation in high-throughput experiments. *Bioinformatics, 28*(6), 882-883. doi:10.1093/bioinformatics/bts034

Lehmann, B. D., Bauer, J. A., Chen, X., Sanders, M. E., Chakravarthy, A. B., Shyr, Y., & Pietenpol, J. A. (2011). Identification of human triple-negative breast cancer subtypes and preclinical models for selection of targeted therapies. *J Clin Invest, 121*(7), 2750-2767. doi:10.1172/JCI45014

Lei, M., Xu, H., Li, Z., Wang, Z., O'Malley, T. T., Zhang, D., . . . Li, S. (2016). Soluble Aβ oligomers impair hippocampal LTP by disrupting glutamatergic/GABAergic balance. *Neurobiology of Disease, 85*, 111-121. doi:10.1016/j.nbd.2015.10.019

Lein, E. S., Hawrylycz, M. J., Ao, N., Ayres, M., Bensinger, A., Bernard, A., . . . Jones, A. R. (2007). Genome-wide atlas of gene expression in the adult mouse brain. *Nature, 445*(7124), 168-176. doi:10.1038/nature05453

Liang, W. S., Reiman, E. M., Valla, J., Dunckley, T., Beach, T. G., Grover, A., . . . Stephan, D. A. (2008). Alzheimer's disease is associated with reduced expression of energy metabolism genes in posterior cingulate neurons. *Proc Natl Acad Sci U S A, 105*(11), 4441-4446. doi:10.1073/pnas.0709259105

Liddelow, S. A., Guttenplan, K. A., Clarke, L. E., Bennett, F. C., Bohlen, C. J., Schirmer, L., . . . Barres, B. A. (2017). Neurotoxic reactive astrocytes are induced by activated microglia. *Nature, 541*(7638), 481-487. doi:10.1038/nature21029

Lilliehook, C., Bozdagi, O., Yao, J., Gomez-Ramirez, M., Zaidi, N. F., Wasco, W., . . . Buxbaum, J. D. (2003). Altered Abeta formation and long-term potentiation in a calsenilin knock-out. *J Neurosci, 23*(27), 9097-9106. doi:10.1523/jneurosci.23-27-09097.2003

Lin, M. T., & Beal, M. F. (2006). Mitochondrial dysfunction and oxidative stress in neurodegenerative diseases. *Nature, 443*(7113), 787-795. doi:10.1038/nature05292

Liu, C.-S., & Tsai, C.-S. (2002). Enhanced Lipid Peroxidation in Epileptics With Null Genotype of Glutathione S-Transferase M1 and Intractable Seizure. *The Japanese Journal of Pharmacology, 90*(3), 291-294. doi:10.1254/jjp.90.291

Liu, S., Liu, Y., Hao, W., Wolf, L., Kiliaan, A. J., Penke, B., . . . Fassbender, K. (2012). TLR2 is a primary receptor for Alzheimer's amyloid beta peptide to trigger neuroinflammatory activation. *J Immunol, 188*(3), 1098-1107. doi:10.4049/jimmunol.1101121

Lu, D., & Thum, T. (2019). RNA-based diagnostic and therapeutic strategies for cardiovascular disease. *Nat Rev Cardiol, 16*(11), 661-674. doi:10.1038/s41569-019-0218-x

Mackenzie, I. R., & Miller, L. A. (1994). Senile plaques in temporal lobe epilepsy. *Acta Neuropathol, 87*(5), 504-510. doi:10.1007/bf00294177

Marescaux, C., Vergnes, M., & Depaulis, A. (1992). GENETIC ABSENCE EPILEPSY IN RATS FROM STRASBOURG - A REVIEW. *J. Neural Transm.-Gen. Sect.*, 37-69.

Marks, W. N., Cavanagh, M. E., Greba, Q., Cain, S. M., Snutch, T. P., & Howland, J. G. (2016). The Genetic Absence Epilepsy Rats from Strasbourg model of absence epilepsy exhibits alterations in fear conditioning and latent inhibition consistent with psychiatric comorbidities in humans. *European Journal of Neuroscience, 43*(1), 25-40. doi:10.1111/ejn.13110

Maroso, M., Balosso, S., Ravizza, T., Iori, V., Wright, C. I., French, J., & Vezzani, A. (2011). Interleukin-1beta biosynthesis inhibition reduces acute seizures and drug resistant chronic epileptic activity in mice. *Neurotherapeutics, 8*(2), 304-315. doi:10.1007/s13311-011-0039-z

Maroso, M., Balosso, S., Ravizza, T., Liu, J., Aronica, E., Iyer, A. M., . . . Vezzani, A. (2010). Toll-like receptor 4 and high-mobility group box-1 are involved in ictogenesis and can be targeted to reduce seizures. *Nat Med, 16*(4), 413-419. doi:10.1038/nm.2127

Martins, I. J., Berger, T., Sharman, M. J., Verdile, G., Fuller, S. J., & Martins, R. N. (2009). Cholesterol metabolism and transport in the pathogenesis of Alzheimer's disease. *J Neurochem, 111*(6), 1275-1308. doi:10.1111/j.1471-4159.2009.06408.x

Mathur, R., Ince, P. G., Minett, T., Garwood, C. J., Shaw, P. J., Matthews, F. E., . . . Wharton, S. B. (2015). A reduced astrocyte response to β-amyloid plaques in the ageing brain associates with cognitive impairment. *PLoS One, 10*(2), e0118463. doi:10.1371/journal.pone.0118463

Mattson, M. P. (2004). Pathways towards and away from Alzheimer's disease. *Nature, 430*(7000), 631-639. doi:10.1038/nature02621

McAreavey, M. J., Ballinger, B. R., & Fenton, G. W. (1992). Epileptic seizures in elderly patients with dementia. *Epilepsia, 33*(4), 657-660. Retrieved from https://www.ncbi.nlm.nih.gov/pubmed/1628580

https://onlinelibrary.wiley.com/doi/abs/10.1111/j.1528-1157.1992.tb02343.x?sid=nlm%3Apubmed

Meister, A. (1988). Glutathione metabolism and its selective modification. *J Biol Chem, 263*(33), 17205-17208. Retrieved from https://www.ncbi.nlm.nih.gov/pubmed/3053703

Mihaly, Z., Kormos, M., Lanczky, A., Dank, M., Budczies, J., Szasz, M. A., & Gyorffy, B. (2013). A meta-analysis of gene expression-based biomarkers predicting outcome after tamoxifen treatment in breast cancer. *Breast Cancer Res Treat, 140*(2), 219-232. doi:10.1007/s10549-013-2622-y

Miller, J. A., Horvath, S., & Geschwind, D. H. (2010). Divergence of human and mouse brain transcriptome highlights Alzheimer disease pathways. *Proc Natl Acad Sci U S A, 107*(28), 12698-12703. doi:10.1073/pnas.0914257107

Minkeviciene, R., Rheims, S., Dobszay, M. B., Zilberter, M., Hartikainen, J., Fulop, L., . . . Tanila, H. (2009). Amyloid beta-induced neuronal hyperexcitability triggers progressive epilepsy. *J Neurosci, 29*(11), 3453-3462. doi:10.1523/JNEUROSCI.5215-08.2009

Miranda, D. D. C., & Brucki, S. M. D. (2014). Epilepsy in patients with Alzheimer's disease: A systematic review. *Dement Neuropsychol, 8*(1), 66-71. doi:10.1590/S1980-57642014DN81000010

Mucke, L., Masliah, E., Yu, G. Q., Mallory, M., Rockenstein, E. M., Tatsuno, G., . . . McConlogue, L. (2000). High-level neuronal expression of abeta 1-42 in wild-type human amyloid protein precursor transgenic mice: synaptotoxicity without plaque formation. *J Neurosci, 20*(11), 4050-4058. Retrieved from https://www.ncbi.nlm.nih.gov/pubmed/10818140

Mukherjee, S., Klaus, C., Pricop-Jeckstadt, M., Miller, J. A., & Struebing, F. L. (2019). A Microglial Signature Directing Human Aging and Neurodegeneration-Related Gene Networks. *Front Neurosci, 13*, 2. doi:10.3389/fnins.2019.00002

Mullen, S. A., Berkovic, S. F., & the, I. G. C. (2018). Genetic generalized epilepsies. *Epilepsia, 59*(6), 1148-1153. doi:https://doi.org/10.1111/epi.14042

Murai, K. K., & Pasquale, E. B. (2011). Eph receptors and ephrins in neuron-astrocyte communication at synapses. *GLIA, 59*(11), 1567-1578. doi:10.1002/glia.21226

Naggar, I., Lazar, J., Kamran, H., Orman, R., & Stewart, M. (2014). Relation of autonomic and cardiac abnormalities to ventricular fibrillation in a rat model of epilepsy. *Epilepsy Res, 108*(1), 44-56. doi:10.1016/j.eplepsyres.2013.10.018

Nagrath, S., Sequist, L. V., Maheswaran, S., Bell, D. W., Irimia, D., Ulkus, L., . . . Toner, M. (2007). Isolation of rare circulating tumour cells in cancer patients by microchip technology. *Nature, 450*(7173), 1235-1239. doi:10.1038/nature06385

Nutini, M., Spalloni, A., Florenzano, F., Westenbroek, R. E., Marini, C., Catterall, W. A., . . . Longone, P. (2011). Increased expression of the beta3 subunit of voltage-gated Na+ channels in the spinal cord of the SOD1G93A mouse. *Mol Cell Neurosci, 47*(2), 108-118. doi:10.1016/j.mcn.2011.03.005

O'Malley, H. A., & Isom, L. L. (2015). Sodium channel beta subunits: emerging targets in channelopathies. *Annu Rev Physiol, 77*, 481-504. doi:10.1146/annurev-physiol-021014-071846

Oakley, A. (2011). Glutathione transferases: a structural perspective. *Drug Metabolism Reviews, 43*(2), 138-151. doi:10.3109/03602532.2011.558093

Ogata, H., Goto, S., Sato, K., Fujibuchi, W., Bono, H., & Kanehisa, M. (1999). KEGG: Kyoto Encyclopedia of Genes and Genomes. *Nucleic Acids Res, 27*(1), 29-34. doi:10.1093/nar/27.1.29

Oldham, M. C., Horvath, S., & Geschwind, D. H. (2006). Conservation and evolution of gene coexpression networks in human and chimpanzee brains. *Proc Natl Acad Sci U S A, 103*(47), 17973-17978. doi:10.1073/pnas.0605938103

Oldham, M. C., Konopka, G., Iwamoto, K., Langfelder, P., Kato, T., Horvath, S., & Geschwind, D. H. (2008). Functional organization of the transcriptome in human brain. *Nat Neurosci, 11*(11), 1271-1282. doi:10.1038/nn.2207

Oliver, K. L., Lukic, V., Thorne, N. P., Berkovic, S. F., Scheffer, I. E., & Bahlo, M. (2014). Harnessing gene expression networks to prioritize candidate epileptic encephalopathy genes. *PLoS One, 9*(7), e102079-e102079. doi:10.1371/journal.pone.0102079

Olsen, M., Aguilar, X., Sehlin, D., Fang, X. T., Antoni, G., Erlandsson, A., & Syvänen, S. (2018). Astroglial Responses to Amyloid-Beta Progression in a Mouse Model of Alzheimer's Disease. *Molecular Imaging and Biology, 20*(4), 605-614. doi:10.1007/s11307-017-1153-z

Palop, J. J., Chin, J., Roberson, E. D., Wang, J., Thwin, M. T., Bien-Ly, N., . . . Mucke, L. (2007). Aberrant excitatory neuronal activity and compensatory remodeling of inhibitory hippocampal circuits in mouse models of Alzheimer's disease. *Neuron, 55*(5), 697-711. doi:10.1016/j.neuron.2007.07.025

Palop, J. J., & Mucke, L. (2010). Amyloid-beta-induced neuronal dysfunction in Alzheimer's disease: from synapses toward neural networks. *Nat Neurosci, 13*(7), 812-818. doi:10.1038/nn.2583

Palop, J. J., & Mucke, L. (2016). Network abnormalities and interneuron dysfunction in Alzheimer disease. *Nat Rev Neurosci, 17*(12), 777-792. doi:10.1038/nrn.2016.141

Pancho, A., Aerts, T., Mitsogiannis, M. D., & Seuntjens, E. (2020). Protocadherins at the Crossroad of Signaling Pathways. *Frontiers in Molecular Neuroscience, 13*. doi:10.3389/fnmol.2020.00117

Pang, X., Zhao, Y., Wang, J., Zhou, Q., Xu, L., Kang, . . . Du, G. H. (2017). The Bioinformatic Analysis of the Dysregulated Genes and MicroRNAs in Entorhinal Cortex, Hippocampus, and Blood for Alzheimer's Disease. *Biomed Res Int, 2017*, 9084507. doi:10.1155/2017/9084507

Pang, Z., Chong, J., Zhou, G., de Lima Morais, D. A., Chang, L., Barrette, M., . . . Xia, J. (2021). MetaboAnalyst 5.0: narrowing the gap between raw spectra and functional insights. *Nucleic Acids Res*. doi:10.1093/nar/gkab382

Papazoglou, A., Soos, J., Lundt, A., Wormuth, C., Ginde, V. R., Muller, R., . . . Weiergraber, M. (2016). Gender-Specific Hippocampal Dysrhythmia and Aberrant Hippocampal and Cortical Excitability in the APPswePS1dE9 Model of Alzheimer's Disease. *Neural Plast, 2016*, 7167358. doi:10.1155/2016/7167358

Patel, M. (2018). A Metabolic Paradigm for Epilepsy. *Epilepsy Currents, 18*(5), 318-322. doi:10.5698/1535-7597.18.5.318

Pearson-Smith, J. N., & Patel, M. (2017). Metabolic Dysfunction and Oxidative Stress in Epilepsy. *International Journal of Molecular Sciences, 18*(11), 2365. doi:http://dx.doi.org/10.3390/ijms18112365

Penninx, B. W., Kritchevsky, S. B., Yaffe, K., Newman, A. B., Simonsick, E. M., Rubin, S., . . . Pahor, M. (2003). Inflammatory markers and depressed mood in older persons: results from the Health, Aging and Body Composition study. *Biol Psychiatry, 54*(5), 566-572. doi:10.1016/s0006-3223(02)01811-5

Perea, G., Gómez, R., Mederos, S., Covelo, A., Ballesteros, J. J., Schlosser, L., . . . Araque, A. (2016). Activity-dependent switch of GABAergic inhibition into glutamatergic excitation in astrocyte-neuron networks. *eLife, 5*, e20362. doi:10.7554/eLife.20362

Perucca, P., Bahlo, M., & Berkovic, S. F. (2020). The Genetics of Epilepsy. *Annual Review of Genomics and Human Genetics, 21*, 16.11-16.26. doi:10.1146/annurev-genom-120219-074937

Polan, M. B., Pastore, M. T., Steingass, K., Hashimoto, S., Thrush, D. L., Pyatt, R., . . . McBride, K. L. (2014). Neurodevelopmental disorders among individuals with duplication of 4p13 to 4p12 containing a GABAA receptor subunit gene cluster. *Eur J Hum Genet, 22*(1), 105-109. doi:10.1038/ejhg.2013.99

Powell, K. L., Tang, H., Ng, C., Guillemain, I., Dieuset, G., Dezsi, G., . . . Jones, N. C. (2014). Seizure expression, behavior, and brain morphology differences in colonies of Genetic Absence Epilepsy Rats from Strasbourg. *Epilepsia, 55*(12), 1959-1968. doi:https://doi.org/10.1111/epi.12840

Racine, R. J. (1972). Modification of seizure activity by electrical stimulation. II. Motor seizure. *Electroencephalogr Clin Neurophysiol, 32*(3), 281-294. Retrieved from http://www.ncbi.nlm.nih.gov/pubmed/4110397

http://www.sciencedirect.com/science/article/pii/0013469472901770

Ravasz, E., Somera, A. L., Mongru, D. A., Oltvai, Z. N., & Barabasi, A. L. (2002). Hierarchical organization of modularity in metabolic networks. *Science, 297*(5586), 1551-1555. doi:10.1126/science.1073374

Raz, T., Causey, M., Jones, D. R., Kieu, A., Letovsky, S., Lipson, D., . . . Milos, P. M. (2011). RNA sequencing and quantitation using the Helicos Genetic Analysis System. *Methods Mol Biol, 733*, 37-49. doi:10.1007/978-1-61779-089-8_3

Reid, C. A., Berkovic, S. F., & Petrou, S. (2009). Mechanisms of human inherited epilepsies. *Prog Neurobiol, 87*(1), 41-57. doi:10.1016/j.pneurobio.2008.09.016

Reid, C. A., Jackson, G. D., Berkovic, S. F., & Petrou, S. (2010). New therapeutic opportunities in epilepsy: a genetic perspective. *Pharmacol Ther, 128*(2), 274-280. doi:10.1016/j.pharmthera.2010.07.003

Reimand, J., Arak, T., Adler, P., Kolberg, L., Reisberg, S., Peterson, H., & Vilo, J. (2016). g:Profiler-a web server for functional interpretation of gene lists (2016 update). *Nucleic Acids Res, 44*(W1), W83-89. doi:10.1093/nar/gkw199

Reimand, J., Isserlin, R., Voisin, V., Kucera, M., Tannus-Lopes, C., Rostamianfar, A., . . . Bader, G. D. (2019). Pathway enrichment analysis and visualization of omics data using g:Profiler, GSEA, Cytoscape and EnrichmentMap. *Nat Protoc, 14*(2), 482-517. doi:10.1038/s41596-018-0103-9

Reyes-Marin, K. E., & Nunez, A. (2017). Seizure susceptibility in the APP/PS1 mouse model of Alzheimer's disease and relationship with amyloid beta plaques. *Brain Res, 1677*, 93-100. doi:10.1016/j.brainres.2017.09.026

Ritchie, M. E., Phipson, B., Wu, D., Hu, Y., Law, C. W., Shi, W., & Smyth, G. K. (2015). limma powers differential expression analyses for RNA-sequencing and microarray studies. *Nucleic Acids Research, 43*(7), e47-e47. doi:10.1093/nar/gkv007

Romoli, M., Sen, A., Parnetti, L., Calabresi, P., & Costa, C. (2021). Amyloid-β: a potential link between epilepsy and cognitive decline. *Nature Reviews Neurology, 17*(8), 469-485. doi:10.1038/s41582-021-00505-9

Rudajev, V., & Novotny, J. (2022). Cholesterol as a key player in amyloid β-mediated toxicity in Alzheimer's disease. *Front Mol Neurosci, 15*, 937056. doi:10.3389/fnmol.2022.937056

Rui Li, L. M., Xin Yuan, Mohsen Radfar, Peter Marendy, Wei Ni, Terence J. O'Brien, Pablo Casillas-Espinosa. (2021). *Spike wave discharges detection in animal models and epilepsy patients with genetic generalised epilepsy with absence seizures*. Paper presented at the International Epilepsy Congress.

Sarkisova, K. Y., Midzianovskaia, I. S., & Kulikov, M. A. (2003). Depressive-like behavioral alterations and c-fos expression in the dopaminergic brain regions in WAG/Rij rats with genetic absence epilepsy. *Behav Brain Res, 144*(1-2), 211-226. Retrieved from http://www.ncbi.nlm.nih.gov/pubmed/12946611

http://ac.els-cdn.com/S0166432803000901/1-s2.0-S0166432803000901-main.pdf?_tid=03ec1e1a-25fd-11e5-8e9f-00000aab0f02&acdnat=1436420612_bfc172069b343a6cc5a41903943fe75a

Saunders, A. M., Strittmatter, W. J., Schmechel, D., George-Hyslop, P. H., Pericak-Vance, M. A., Joo, S. H., . . . et al. (1993). Association of apolipoprotein E allele epsilon 4 with late-onset familial and sporadic Alzheimer's disease. *Neurology, 43*(8), 1467-1472. doi:10.1212/wnl.43.8.1467

Schadt, E. E. (2009). Molecular networks as sensors and drivers of common human diseases. *Nature, 461*(7261), 218-223. doi:10.1038/nature08454

Schadt, E. E., Friend, S. H., & Shaywitz, D. A. (2009). A network view of disease and compound screening. *Nature Reviews Drug Discovery, 8*, 286. doi:10.1038/nrd2826

Scharfman, H. E. (2012). Alzheimer's disease and epilepsy: insight from animal models. *Future Neurol, 7*(2), 177-192. doi:10.2217/fnl.12.8

Scheffer, I. E., Berkovic, S., Capovilla, G., Connolly, M. B., French, J., Guilhoto, L., . . . Zuberi, S. M. (2017). ILAE classification of the epilepsies: Position paper of the ILAE

Commission for Classification and Terminology. *Epilepsia, 58*(4), 512-521. doi:10.1111/epi.13709
Scheltema, R. A., Jankevics, A., Jansen, R. C., Swertz, M. A., & Breitling, R. (2011). PeakML/mzMatch: a file format, Java library, R library, and tool-chain for mass spectrometry data analysis. *Anal Chem, 83*(7), 2786-2793. doi:10.1021/ac2000994
Schnier, C., Duncan, S., Wilkinson, T., Mbizvo, G. K., & Chin, R. F. M. (2020). A nationwide, retrospective, data-linkage, cohort study of epilepsy and incident dementia. *Neurology, 95*(12), e1686-e1693. doi:10.1212/wnl.0000000000010358
Selkoe, D. J. (2002). Alzheimer's disease is a synaptic failure. *Science, 298*(5594), 789-791. doi:10.1126/science.1074069
Shankar, G. M., Bloodgood, B. L., Townsend, M., Walsh, D. M., Selkoe, D. J., & Sabatini, B. L. (2007). Natural oligomers of the Alzheimer amyloid-beta protein induce reversible synapse loss by modulating an NMDA-type glutamate receptor-dependent signaling pathway. *J Neurosci, 27*(11), 2866-2875. doi:10.1523/JNEUROSCI.4970-06.2007
Shannon, P., Markiel, A., Ozier, O., Baliga, N. S., Wang, J. T., Ramage, D., . . . Ideker, T. (2003). Cytoscape: a software environment for integrated models of biomolecular interaction networks. *Genome Res, 13*(11), 2498-2504. doi:10.1101/gr.1239303
Sharma, A. K., Reams, R. Y., Jordan, W. H., Miller, M. A., Thacker, H. L., & Snyder, P. W. (2007). Mesial temporal lobe epilepsy: pathogenesis, induced rodent models and lesions. *Toxicol Pathol, 35*(7), 984-999. doi:10.1080/01926230701748305
Shibata, R., Misonou, H., Campomanes, C. R., Anderson, A. E., Schrader, L. A., Doliveira, L. C., . . . Trimmer, J. S. (2003). A Fundamental Role for KChIPs in Determining the Molecular Properties and Trafficking of Kv4.2 Potassium Channels *. *Journal of Biological Chemistry, 278*(38), 36445-36454. doi:10.1074/jbc.M306142200
Shu, Y., Xiao, B., Wu, Q., Liu, T., Du, Y., Tang, H., . . . Li, Y. (2016). The Ephrin-A5/EphA4 Interaction Modulates Neurogenesis and Angiogenesis by the p-Akt and p-ERK Pathways in a Mouse Model of TLE. *Mol Neurobiol, 53*(1), 561-576. doi:10.1007/s12035-014-9020-2
Šišková, Z., Justus, D., Kaneko, H., Friedrichs, D., Henneberg, N., Beutel, T., . . . Remy, S. (2014). Dendritic structural degeneration is functionally linked to cellular hyperexcitability in a mouse model of Alzheimer's disease. *Neuron, 84*(5), 1023-1033. doi:10.1016/j.neuron.2014.10.024
Snead, O. C., 3rd. (1995). Basic mechanisms of generalized absence seizures. *Ann Neurol, 37*(2), 146-157. doi:10.1002/ana.410370204
Snider, B. J., Norton, J., Coats, M. A., Chakraverty, S., Hou, C. E., Jervis, R., . . . Morris, J. C. (2005). Novel presenilin 1 mutation (S170F) causing Alzheimer disease with Lewy bodies in the third decade of life. *Arch Neurol, 62*(12), 1821-1830. doi:10.1001/archneur.62.12.1821
Sodero, A. O., Vriens, J., Ghosh, D., Stegner, D., Brachet, A., Pallotto, M., . . . Dotti, C. G. (2012). Cholesterol loss during glutamate-mediated excitotoxicity. *EMBO Journal, 31*(7), 1764-1773. doi:10.1038/emboj.2012.31
Söllvander, S., Nikitidou, E., Brolin, R., Söderberg, L., Sehlin, D., Lannfelt, L., & Erlandsson, A. (2016). Accumulation of amyloid-β by astrocytes result in enlarged endosomes and microvesicle-induced apoptosis of neurons. *Molecular Neurodegeneration, 11*(1), 38. doi:10.1186/s13024-016-0098-z
Stewart, W. F., Kawas, C., Corrada, M., & Metter, E. J. (1997). Risk of Alzheimer's disease and duration of NSAID use. *Neurology, 48*(3), 626-632. Retrieved from https://www.ncbi.nlm.nih.gov/pubmed/9065537

Stoessel, D., Nowell, C., Jones, A., Ferrins, L., Ellis, K., Riley, J., . . . Avery, V. (2016). Metabolomics and lipidomics reveal perturbation of sphingolipid metabolism by a novel anti-trypanosomal 3-(oxazolo [4, 5-b] pyridine-2-yl) anilide. *Metabolomics, 12*(7), 126.

Stöllberger, C., Wegner, C., & Finsterer, J. (2011). Seizure-associated Takotsubo cardiomyopathy. *Epilepsia, 52*(11), e160-167. doi:10.1111/j.1528-1167.2011.03185.x

Strittmatter, W. J., Saunders, A. M., Schmechel, D., Pericak-Vance, M., Enghild, J., Salvesen, G. S., & Roses, A. D. (1993). Apolipoprotein E: high-avidity binding to beta-amyloid and increased frequency of type 4 allele in late-onset familial Alzheimer disease. *Proc Natl Acad Sci U S A, 90*(5), 1977-1981. doi:10.1073/pnas.90.5.1977

Subramanian, A., Tamayo, P., Mootha, V. K., Mukherjee, S., Ebert, B. L., Gillette, M. A., . . . Mesirov, J. P. (2005). Gene set enrichment analysis: a knowledge-based approach for interpreting genome-wide expression profiles. *Proc Natl Acad Sci U S A, 102*(43), 15545-15550. doi:10.1073/pnas.0506580102

Sun, M., Sun, T., He, Z., & Xiong, B. (2017). Identification of two novel biomarkers of rectal carcinoma progression and prognosis via co-expression network analysis. *Oncotarget, 8*(41), 69594-69609. doi:10.18632/oncotarget.18646

Supek, F., Bosnjak, M., Skunca, N., & Smuc, T. (2011). REVIGO summarizes and visualizes long lists of gene ontology terms. *PLoS One, 6*(7), e21800. doi:10.1371/journal.pone.0021800

Surges, R., & Sander, J. W. (2012). Sudden unexpected death in epilepsy: mechanisms, prevalence, and prevention. *Curr Opin Neurol, 25*(2), 201-207. doi:10.1097/WCO.0b013e3283506714

Tai, X. Y., Koepp, M., Duncan, J. S., Fox, N., Thompson, P., Baxendale, S., . . . Thom, M. (2016). Hyperphosphorylated tau in patients with refractory epilepsy correlates with cognitive decline: a study of temporal lobe resections. *Brain, 139*(Pt 9), 2441-2455. doi:10.1093/brain/aww187

Takeuchi, C., Ishikawa, M., Sawano, T., Shin, Y., Mizuta, N., Hasegawa, S., . . . Tanaka, H. (2020). Dendritic Spine Density is Increased in Arcadlin-deleted Mouse Hippocampus. *Neuroscience, 442*, 296-310. doi:10.1016/j.neuroscience.2020.06.037

Tanila, H., Gureviciene, I., Ishchenko, I., Jin, N., Ziyatdinova, S., Lipponen, A., & Gurevicius, K. (2019). Nonconvulsive epileptic discharges in alzheimer model mice: Characterization and treatment options. *Neuropsychobiology, 77*(3), 131. doi:10.1159/000496817

Tejera, D., Mercan, D., Sanchez-Caro, J. M., Hanan, M., Greenberg, D., Soreq, H., . . . Heneka, M. T. (2019). Systemic inflammation impairs microglial Abeta clearance through NLRP3 inflammasome. *EMBO J, 38*(17), e101064. doi:10.15252/embj.2018101064

Tellez Zenteno, J., Patten, S., Jetté, N., Williams, J., & Wiebe, S. (2007). Psychiatric comorbidity in epilepsy: a population-based analysis. *Epilepsia, 48*(12), 2336-2344. Retrieved from http://sfx.unimelb.hosted.exlibrisgroup.com/sfxlcl41/?sid=Entrez%3APubMed&id=pmid%3A17662062

http://onlinelibrary.wiley.com/store/10.1111/j.1528-1167.2007.01222.x/asset/j.1528-1167.2007.01222.x.pdf?v=1&t=ito0nwgz&s=8252e572843f3d72048241804f30f36a066b0421

https://onlinelibrary.wiley.com/doi/pdf/10.1111/j.1528-1167.2007.01222.x

Terry, R. D., Masliah, E., Salmon, D. P., Butters, N., DeTeresa, R., Hill, R., . . . Katzman, R. (1991). Physical basis of cognitive alterations in Alzheimer's disease: synapse loss is

the major correlate of cognitive impairment. *Ann Neurol, 30*(4), 572-580. doi:10.1002/ana.410300410

Thom, M., Liu, J. Y., Thompson, P., Phadke, R., Narkiewicz, M., Martinian, L., . . . Sisodiya, S. M. (2011). Neurofibrillary tangle pathology and Braak staging in chronic epilepsy in relation to traumatic brain injury and hippocampal sclerosis: a post-mortem study. *Brain, 134*(Pt 10), 2969-2981. doi:10.1093/brain/awr209

Thomas, P. D., Kejariwal, A., Campbell, M. J., Mi, H., Diemer, K., Guo, N., . . . Doremieux, O. (2003). PANTHER: a browsable database of gene products organized by biological function, using curated protein family and subfamily classification. *Nucleic Acids Res, 31*(1), 334-341. doi:10.1093/nar/gkg115

Thomson, K. E., Metcalf, C. S., Newell, T. G., Huff, J., Edwards, S. F., West, P. J., & Wilcox, K. S. (2020). Evaluation of subchronic administration of antiseizure drugs in spontaneously seizing rats. *Epilepsia, 61*(6), 1301-1311. doi:10.1111/epi.16531

Townsend, D. M., & Tew, K. D. (2003). The role of glutathione-S-transferase in anti-cancer drug resistance. *Oncogene, 22*(47), 7369-7375. doi:10.1038/sj.onc.1206940

Tran, L. M., Zhang, B., Zhang, Z., Zhang, C., Xie, T., Lamb, J. R., . . . Zhu, J. (2011). Inferring causal genomic alterations in breast cancer using gene expression data. *BMC Syst Biol, 5*, 121. doi:10.1186/1752-0509-5-121

Tsyganov, K., Perry, A., Archer, S., & Powell, D. (2018). MonashBioinformaticsPlatform/RNAsik-pipe: JOSS ready. doi:10.5281/ZENODO.1403976

Vainchtein, I. D., & Molofsky, A. V. (2020). Astrocytes and Microglia: In Sickness and in Health. *Trends Neurosci, 43*(3), 144-154. doi:10.1016/j.tins.2020.01.003

van Dyck, C. H., Swanson, C. J., Aisen, P., Bateman, R. J., Chen, C., Gee, M., . . . Iwatsubo, T. (2022). Lecanemab in Early Alzheimer's Disease. *New England Journal of Medicine, 388*(1), 9-21. doi:10.1056/NEJMoa2212948

van Karnebeek, C. D. M., Hartmann, H., Jaggumantri, S., Bok, L. A., Cheng, B., Connolly, M., . . . Stockler, S. (2012). Lysine restricted diet for pyridoxine-dependent epilepsy: First evidence and future trials. *Molecular Genetics and Metabolism, 107*(3), 335-344. doi:https://doi.org/10.1016/j.ymgme.2012.09.006

Venegas, C., Kumar, S., Franklin, B. S., Dierkes, T., Brinkschulte, R., Tejera, D., . . . Heneka, M. T. (2017). Microglia-derived ASC specks cross-seed amyloid-beta in Alzheimer's disease. *Nature, 552*(7685), 355-361. doi:10.1038/nature25158

Vergnes, M., Marescaux, C., Micheletti, G., Reis, J., Depaulis, A., Rumbach, L., & Warter, J. M. (1982). Spontaneous paroxysmal electroclinical patterns in rat: A model of generalized non-convulsive epilepsy. *Neuroscience Letters, 33*(1), 97-101. doi:https://doi.org/10.1016/0304-3940(82)90136-7

Verret, L., Mann, E. O., Hang, G. B., Barth, A. M., Cobos, I., Ho, K., . . . Palop, J. J. (2012). Inhibitory interneuron deficit links altered network activity and cognitive dysfunction in Alzheimer model. *Cell, 149*(3), 708-721. doi:10.1016/j.cell.2012.02.046

Vezzani, A., Conti, M., De Luigi, A., Ravizza, T., Moneta, D., Marchesi, F., & De Simoni, M. G. (1999). Interleukin-1beta immunoreactivity and microglia are enhanced in the rat hippocampus by focal kainate application: functional evidence for enhancement of electrographic seizures. *J Neurosci, 19*(12), 5054-5065. Retrieved from https://www.ncbi.nlm.nih.gov/pubmed/10366638

Vezzani, A., French, J., Bartfai, T., & Baram, T. Z. (2011). The role of inflammation in epilepsy. *Nat Rev Neurol, 7*(1), 31-40. doi:10.1038/nrneurol.2010.178

Vezzani, A., & Viviani, B. (2015). Neuromodulatory properties of inflammatory cytokines and their impact on neuronal excitability. *Neuropharmacology, 96*(Pt A), 70-82. doi:10.1016/j.neuropharm.2014.10.027

Vöglein, J., Ricard, I., Noachtar, S., Kukull, W. A., Dieterich, M., Levin, J., & Danek, A. (2020). Seizures in Alzheimer's disease are highly recurrent and associated with a poor disease course. *J Neurol, 267*(10), 2941-2948. doi:10.1007/s00415-020-09937-7

Volicer, L., Smith, S., & Volicer, B. J. (1995). Effect of seizures on progression of dementia of the Alzheimer type. *Dementia, 6*(5), 258-263. Retrieved from https://www.ncbi.nlm.nih.gov/pubmed/8528372

Vossel, K., Ranasinghe, K. G., Beagle, A. J., La, A., Ah Pook, K., Castro, M., . . . Kirsch, H. E. (2021). Effect of Levetiracetam on Cognition in Patients With Alzheimer Disease With and Without Epileptiform Activity: A Randomized Clinical Trial. *JAMA Neurol, 78*(11), 1345-1354. doi:10.1001/jamaneurol.2021.3310

Vossel, K. A., Beagle, A., Hegde, M., Mantle, M., Kirsch, H., Garcia, P., . . . Mucke, L. (2012). Subclinical epileptiform activity in Alzheimer's disease. *Alzheimer's and Dementia, 8*(4), P395-P396. doi:10.1016/j.jalz.2012.05.1087

Vossel, K. A., Beagle, A. J., Rabinovici, G. D., Shu, H., Lee, S. E., Naasan, G., . . . Mucke, L. (2013). Seizures and epileptiform activity in the early stages of Alzheimer disease. *JAMA Neurol, 70*(9), 1158-1166. doi:10.1001/jamaneurol.2013.136

Vossel, K. A., Ranasinghe, K. G., Beagle, A. J., Mizuiri, D., Honma, S. M., Dowling, A. F., . . . Nagarajan, S. S. (2016). Incidence and impact of subclinical epileptiform activity in Alzheimer's disease. *Ann Neurol, 80*(6), 858-870. doi:10.1002/ana.24794

Vossel, K. A., Tartaglia, M. C., Nygaard, H. B., Zeman, A. Z., & Miller, B. L. (2017). Epileptic activity in Alzheimer's disease: causes and clinical relevance. *Lancet Neurol, 16*(4), 311-322. doi:10.1016/S1474-4422(17)30044-3

Walsh, D. M., Klyubin, I., Fadeeva, J. V., Cullen, W. K., Anwyl, R., Wolfe, M. S., . . . Selkoe, D. J. (2002). Naturally secreted oligomers of amyloid beta protein potently inhibit hippocampal long-term potentiation in vivo. *Nature, 416*(6880), 535-539. doi:10.1038/416535a

Wang, H., Kulas, J. A., Wang, C., Holtzman, D. M., Ferris, H. A., & Hansen, S. B. (2021). Regulation of beta-amyloid production in neurons by astrocyte-derived cholesterol. *Proceedings of the National Academy of Sciences, 118*(33), e2102191118. doi:doi:10.1073/pnas.2102191118

Wang, Y., Dye, C. A., Sohal, V., Long, J. E., Estrada, R. C., Roztocil, T., . . . Rubenstein, J. L. (2010). Dlx5 and Dlx6 regulate the development of parvalbumin-expressing cortical interneurons. *J Neurosci, 30*(15), 5334-5345. doi:10.1523/JNEUROSCI.5963-09.2010

Wang, Z., Gerstein, M., & Snyder, M. (2009). RNA-Seq: a revolutionary tool for transcriptomics. *Nat Rev Genet, 10*(1), 57-63. doi:10.1038/nrg2484

Wang, Z., Jin, T., Le, Q., Liu, C., Wang, X., Wang, F., & Ma, L. (2020). Retrieval-Driven Hippocampal NPTX2 Plasticity Facilitates the Extinction of Cocaine-Associated Context Memory. *Biological Psychiatry, 87*(11), 979-991. doi:10.1016/j.biopsych.2019.10.009

Westmark, C. J., Westmark, P. R., Beard, A. M., Hildebrandt, S. M., & Malter, J. S. (2008). Seizure susceptibility and mortality in mice that over-express amyloid precursor protein. *Int J Clin Exp Pathol, 1*(2), 157-168. Retrieved from https://www.ncbi.nlm.nih.gov/pubmed/18784809

https://www.ncbi.nlm.nih.gov/pmc/articles/PMC2480559/pdf/ijcep0001-0157.pdf

Wisniewski, H. M., Narang, H. K., & Terry, R. D. (1976). Neurofibrillary tangles of paired helical filaments. *J Neurol Sci, 27*(2), 173-181. doi:10.1016/0022-510x(76)90059-9

Wofford, J. L., Loehr, L. R., & Schwartz, E. (1996). Acute cognitive impairment in elderly ED patients: etiologies and outcomes. *Am J Emerg Med, 14*(7), 649-653. doi:10.1016/S0735-6757(96)90080-7

Wong, H. K., Sakurai, T., Oyama, F., Kaneko, K., Wada, K., Miyazaki, H., . . . Nukina, N. (2005). beta Subunits of voltage-gated sodium channels are novel substrates of beta-site amyloid precursor protein-cleaving enzyme (BACE1) and gamma-secretase. *J Biol Chem, 280*(24), 23009-23017. doi:10.1074/jbc.M414648200

Wood, W. G., Li, L., Muller, W. E., & Eckert, G. P. (2014). Cholesterol as a causative factor in Alzheimer's disease: a debatable hypothesis. *J Neurochem, 129*(4), 559-572. doi:10.1111/jnc.12637

World Health Organisation. (2019). *Epilepsy: A Public Health Imperative*.

Wu, T., Dejanovic, B., Gandham, V. D., Gogineni, A., Edmonds, R., Schauer, S., . . . Hanson, J. E. (2019). Complement C3 Is Activated in Human AD Brain and Is Required for Neurodegeneration in Mouse Models of Amyloidosis and Tauopathy. *Cell Reports, 28*(8), 2111-2123.e2116. doi:10.1016/j.celrep.2019.07.060

Xiao, M.-F., Roh, S.-E., Zhou, J., Chien, C.-C., Lucey, B. P., Craig, M. T., . . . Worley, P. F. (2021). A biomarker-authenticated model of schizophrenia implicating NPTX2 loss of function. *Science Advances, 7*(48), eabf6935. doi:doi:10.1126/sciadv.abf6935

Xie, Z., Bailey, A., Kuleshov, M. V., Clarke, D. J. B., Evangelista, J. E., Jenkins, S. L., . . . Ma'ayan, A. (2021). Gene Set Knowledge Discovery with Enrichr. *Curr Protoc, 1*(3), e90. doi:10.1002/cpz1.90

Yamagata, K., Andreasson, K. I., Sugiura, H., Maru, E., Dominique, M., Irie, Y., . . . Worley, P. F. (1999). Arcadlin is a neural activity-regulated cadherin involved in long term potentiation. *J Biol Chem, 274*(27), 19473-11979. doi:10.1074/jbc.274.27.19473

Yamamoto, K., Tanei, Z. I., Hashimoto, T., Wakabayashi, T., Okuno, H., Naka, Y., . . . Iwatsubo, T. (2015). Chronic Optogenetic Activation Augments Aβ Pathology in a Mouse Model of Alzheimer Disease. *Cell Reports, 11*(6), 859-865. doi:10.1016/j.celrep.2015.04.017

Yan, P., Bero, A. W., Cirrito, J. R., Xiao, Q., Hu, X., Wang, Y., . . . Lee, J. M. (2009). Characterizing the appearance and growth of amyloid plaques in APP/PS1 mice. *J Neurosci, 29*(34), 10706-10714. doi:10.1523/jneurosci.2637-09.2009

Yasuda, S., Tanaka, H., Sugiura, H., Okamura, K., Sakaguchi, T., Tran, U., . . . Yamagata, K. (2007). Activity-induced protocadherin arcadlin regulates dendritic spine number by triggering N-cadherin endocytosis via TAO2beta and p38 MAP kinases. *Neuron, 56*(3), 456-471. doi:10.1016/j.neuron.2007.08.020

Yuce-Dursun, B., Danis, O., Demir, S., Ogan, A., & Onat, F. (2014). Proteomic changes in the cortex membrane fraction of genetic absence epilepsy rats from Strasbourg. *Journal of Integrative Neuroscience, 13*(04), 633-644. doi:10.1142/S021963521450023X

Zhang, B., Gaiteri, C., Bodea, L.-G., Wang, Z., McElwee, J., Podtelezhnikov, Alexei A., . . . Emilsson, V. (2013). Integrated Systems Approach Identifies Genetic Nodes and Networks in Late-Onset Alzheimer's Disease. *Cell, 153*(3), 707-720. doi:https://doi.org/10.1016/j.cell.2013.03.030

Zhang, B., Gaiteri, C., Bodea, L. G., Wang, Z., McElwee, J., Podtelezhnikov, A. A., . . . Emilsson, V. (2013). Integrated systems approach identifies genetic nodes and networks in late-onset Alzheimer's disease. *Cell, 153*(3), 707-720. doi:10.1016/j.cell.2013.03.030

Zhang, B., & Horvath, S. (2005). A general framework for weighted gene co-expression network analysis. *Stat Appl Genet Mol Biol, 4*, Article17. doi:10.2202/1544-6115.1128

Zhao, B., Shen, L. X., Ou, Y. N., Ma, Y. H., Dong, Q., Tan, L., & Yu, J. T. (2021). Risk of seizures and subclinical epileptiform activity in patients with dementia: A systematic review and meta-analysis. *Ageing Research Reviews, 72*. doi:10.1016/j.arr.2021.101478

Zhao, N., Chen, H., Zhang, W., Yao, J., Tu, Q., Yu, X., & Sun, X. (2022). Bidirectional influences between seizures and dementia: A systematic review and meta-analysis. *International Journal of Geriatric Psychiatry, 37*(7). doi:10.1002/gps.5723

Zhou, G., Soufan, O., Ewald, J., Hancock, R. E. W., Basu, N., & Xia, J. (2019). NetworkAnalyst 3.0: a visual analytics platform for comprehensive gene expression profiling and meta-analysis. *Nucleic Acids Res, 47*(W1), W234-W241. doi:10.1093/nar/gkz240

Zhou, J., Wade, S. D., Graykowski, D., Xiao, M.-F., Zhao, B., Giannini, L. A., . . . Dejanovic, B. (2022). Neuronal pentraxin Nptx2 regulates complement activity in the brain. *bioRxiv*, 2022.2009.2022.509106. doi:10.1101/2022.09.22.509106

Ziyatdinova, S., Gurevicius, K., Kutchiashvili, N., Bolkvadze, T., Nissinen, J., Tanila, H., & Pitkanen, A. (2011). Spontaneous epileptiform discharges in a mouse model of Alzheimer's disease are suppressed by antiepileptic drugs that block sodium channels. *Epilepsy Res, 94*(1-2), 75-85. doi:10.1016/j.eplepsyres.2011.01.003

Ziyatdinova, S., Ronnback, A., Gurevicius, K., Miszczuk, D., Graff, C., Winblad, B., . . . Tanila, H. (2016). Increased Epileptiform EEG Activity and Decreased Seizure Threshold in Arctic APP Transgenic Mouse Model of Alzheimer's Disease. *Curr Alzheimer Res, 13*(7), 817-830. Retrieved from http://docserver.ingentaconnect.com/deliver/connect/ben/15672050/v13n7/s11.pdf?expires=1574399256&id=0000&titleid=10320&checksum=F0868EFF13F3DABB73702BDA926646AF